Transonic Flow Calculations

Antony Jameson

Princeton University
MAE Report #1651

March 22, 2014

Note

This text is based on lectures given at the CIME Third Session, on Numerical Methods in Fluid Dynamics, held at Como, July 4-12, 1983. It has been typed with great patience by Lori Marchesano.

1 Introduction

In these lectures I shall attempt to survey some of the principal recent developments in computational aerodynamics. Prior to 1960 computational methods were hardly used in aerodynamic analysis, although they were already widely used for structural analysis. The NACA 6 series of airfoils had been developed during the forties, using hand computation to perform the Theodorsen method for conformal mapping [1]. The primary tool for the development of aerodynamic configurations was the wind tunnel. Shapes were tested and modifications selected in the light of pressure and force measurements together with flow visualization techniques. In much the same way that Michelangelo, della Porta and Fontana could design the dome of St. Peters through a good physical understanding of stress paths, so could experienced aerodynamicists arrive at efficient shapes through testing guided by good physical insight. Notable examples of the power of this method include the achievement of the Wright brothers in leaving the ground (after first building a wind tunnel), and more recently Whitcomb's discovery of the area rule for transonic flow, followed by his development of aftloaded supercritical airfoils and winglets [2, 3, 4]. The process was expensive. More than 20000 hours of wind tunnel testing were expended in the development of some modern designs, such as the F 111 or Boeing 747.

By 1960 it began to be recognized that computers had become powerful enough to make it worth while to attempt calculations of aerodynamic properties of at least isolated components of an airplane. Efficient flight can

be achieved only by establishing highly coherent flows. Consequently there are many important applications where it is not necessary to solve the full Navier Stokes equations, and useful predictions can be made with simplified mathematical models. Since the work of Prandtl, it has been recognized that in flows at the large Reynolds numbers typical in most flight regimes, viscous effects are important chiefly in thin shear layers-adjacent to the surface. While these boundary layers play a critical role in determining whether the flow will separate, and how much circulation will be generated around a lifting surface, the equations of inviscid flow are a good approximation in the bulk of the flow field. The Reynolds numbers for a large airplane (or the order of 30 million) are such that laminar flow in the boundary layer becomes unstable, with the result that the flow will be turbulent over most of the surface of the airplane. On the other hand, many useful predictions can be made under the assumption that the flow is inviscid. It then follows from Kelvin's Theorem that in the absence of discontinuities an initially irrotational flow remains irrotational. This allows us to simplify the equations further by representing the velocity as the gradient of a potential. Initial attempts concentrated on incompressible potential flows. During the sixties the boundary integral method was developed into a powerful tool for the analysis of flows over complex configurations.

In the seventies the battleground of computational aerodynamics switched to the prediction of transonic flows. The reason for this is that to a first approximation, cruising efficiency is proportional to

$$ML/D$$

where M is the Mach number (speed divided by the speed of sound), L is the lift, and D is the drag. As long as the speed is well below the speed of sound, the lift to drag ratio does not vary much with speed, so it pays to increase the speed until the effects of compressibility start to cause a radical change in the flow. This occurs when embedded pockets of supersonic flow appear, generally terminating in shockwaves. A typical transonic flow pattern over a wing is illustrated in Figure 1.1. As-the Mach number is increased the shock waves become strong enough to cause a sharp increase in drag, and finally the pressure rise through the shock waves becomes so large that the boundary layer separates. An unsteady buffeting flow may then develop. This causes violent vibrations which cannot be tolerated even by the pilots of military aircraft. The most efficient cruising speed is usually in the transonic regime just at the onset of drag rise, and the prediction of aerodynamic properties in steady transonic flow has therefore been the key challenge. Unsteady flow is inherent in certain other models of flight (the flight of bats, insects, and helicopters, for example), but for airplanes it is important primarily for the analysis of extreme situations such as wing flutter.

In these lectures I shall therefore concentrate on the calculation of steady transonic flows. Some of the principal difficulties of the problem are:

1. The equations of gas dynamics are nonlinear.

2. Solutions In the transonic range will ordinarily be discontinuous. Cathleen Morawetz has shown that shock free solutions are isolated points [5]. Thus we may expect to find shock waves. The solutions will also generally contain contact surfaces in the form of vortex sheets (shed both by wings in three-dimensional flow, and also by profiles in two-dimensional flow in the event that shock waves of differing strength produce different amounts of entropy on the upper and lower surfaces).

3. There are regions of the flow in the neighborhood, for example, of stagnation points, the wing trailing edge or the wing tip, where the derivatives may become very large or even unbounded, leading to large discretization errors.

4. The equations are to be solved in an unbounded domain.

5. We are generally interested in calculating flows over bodies of extreme geometric complexity (including cases where the domain is multiply connected).

Section 2 reviews the mathematical models appropriate to the prediction of aerodynamic flows in various flight regimes. In the subsequent sections methods for solving the corresponding equations are examined in ascending order of complexity.

2 Choice of a Mathematical Model

The equations for flow of a gas in thermodynamic equilibrium are the Navier Stokes equations. Let ρ, u, v, E and p be the density, Cartesian velocity components, total energy and pressure, and let x and y be Cartesian Coordinates. Then for a two dimensional flow these equations can be written as

$$\frac{\partial w}{\partial t} + \frac{\partial f}{\partial x} + \frac{\partial g}{\partial y} = \frac{\partial R}{\partial x} + \frac{\partial S}{\partial y} \tag{2.1}$$

where w is the vector of dependent variables, and f and g are the convective flux vectors

$$w = \begin{bmatrix} \rho \\ \rho u \\ \rho \\ \rho E \end{bmatrix}, \quad f = \begin{bmatrix} \rho u \\ \rho u^2 + p \\ \rho uv \\ \rho uH \end{bmatrix} \quad g = \begin{bmatrix} \rho v \\ \rho vu \\ \rho v^2 + p \\ \rho vH \end{bmatrix} \tag{2.2}$$

Here H is the enthalpy

$$H = E + \frac{p}{\rho}$$

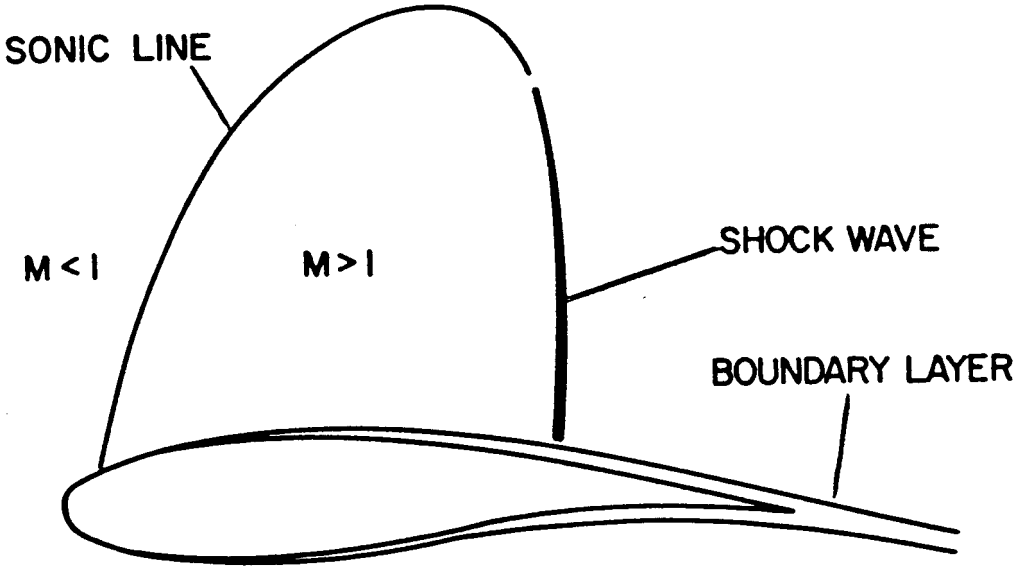

TRANSONIC FLOW PAST AN AIRFOIL

Figure 1.1:

and the pressure is obtained from the equation of state

$$p = (\gamma - 1)\rho \left\{ E = \frac{1}{2}(u^2 + v^2) \right\} \tag{2.3}$$

The flux vectors for the viscous terms are

$$R = \begin{bmatrix} 0 \\ \tau_{xx} \\ \tau_{xy} \\ u\tau_{xx} + v\tau_{yy} \end{bmatrix} \quad S = \begin{bmatrix} 0 \\ \tau_{xy} \\ \tau_{yy} \\ u\tau_{xy} + v\tau_{yy} \end{bmatrix} \tag{2.4}$$

Here the viscous stresses are

$$\tau_{xx} = 2\mu u_x - \frac{2\mu}{3}(u_x + v_y), \quad \tau_{yy} = 2\mu v_y - \frac{2\mu}{3}(u_x + v_y)$$

$$\tau_{xy} = \mu(u_y + v_x)$$

where μ is the coefficient of viscosity. The computational requirements for the simulation of turbulent flow have been estimated by Chapman [6]. They are clearly beyond the reach of current computers.

The first level of approximation is to resort to time averaging of rapidly fluctuating components. This yields the Reynolds equations, which require a turbulence model for closure. Since a universally satisfactory turbulence model has yet to be found, current turbulence models have to be tailored to the particular flow. The Reynolds equations can be solved with computers of the class of the Cray 1 or Cyber 205, at least for two dimensional flows, such as flows over airfoils.

The next level of approximation is to eliminate viscosity. Equations (2.1) then reduce to the Euler equations

$$\frac{\partial w}{\partial t} + \frac{\partial f}{\partial x} + \frac{\partial g}{\partial y} = 0 \tag{2.5}$$

It is quite feasible to solve three dimensional flows with this model, as will be discussed.

If we assume the flow to be irrotational we can introduce a velocity potential ϕ, and set

$$u = \phi_x, \quad v = \phi_y$$

The Euler equations (2.5) now reduce to the potential flow equation

$$\frac{\partial}{\partial x}(\rho\phi_x) + \frac{\partial}{\partial y}(\rho\phi_x) = 0 \tag{2.6}$$

or in quasilinear form

$$(c^2 - u^2)\phi_{xx} - 2uv\phi_{xy} + (c^2 - v^2)\phi_{yy} = 0 \tag{2.7}$$

where c is the speed of sound. This is given by

$$c^2 = \frac{\gamma p}{\rho} \tag{2.8}$$

where γ is the ratio of specific heats. According to Crocco's theorem, vorticity in a steady flow is associated with entropy production through the relation

$$\mathbf{q} \times \boldsymbol{\varsigma} + \mathbf{T} \cdot \Delta S = 0$$

where $\mathbf{q}$ and $\boldsymbol{\varsigma}$ are the velocity and vorticity vectors, T is the temperature and S is the entropy. Thus the introduction of a potnetial is consistent with the assumption of isentropic flow. Then if M_∞ is the free stream Mach number

$$p = \frac{\rho^\gamma}{\gamma M_\infty^2}, \quad \rho = (M_\infty^2 c^2)^{\frac{1}{\gamma - 1}} \tag{2.9}$$

Because shock waves generate entropy, they cannot be exactly modeled by the potential flow equation. Weak solutions admitting isentropic jumps which conserve mass but not momentum are a good approximation to shock waves, however, as long as the shock waves are quite weak (with a Mach number < 1.3 for the normal velocity component upstream of the shock-wave). Stronger shock waves tend to separate the flow, with the result that the inviscid approximation is no longer adequate. Thus this model is well balanced, and it has proved extremely useful for estimating the cruising performance of transport aircraft.

If one assumes small disturbances and a Mach number close to unity, the potential equation can be reduced to the transonic small disturbance equation. A typical form is

$$(1 - M_\infty^2 - (\gamma + 1) M_\infty^2 \phi_x) \phi_{xx} + \phi_{yy} = 0 \tag{2.10}$$

Finally, if the free stream Mach number is not close to unity, the potential flow equation can be linearized as

$$(1 - M_\infty^2) \phi_{xx} + \phi_{yy} = 0 \tag{2.11}$$

Considering the limits on the available computing power, and the cost of calculations, one has to make a trade-off between the complexity of the mathematical model and the complexity of the geometric configuration which can be treated. This is illustrated in Figure 2.1. The linearized potential equation has been routinely solved for complete configurations since the early seventies. A solution of the Navier Stokes equations for a turbulent flow can be at best be attempted for something like a rectangular cavity with one moving wall. This trade-off calls for a judgement both of the suitability of the model for a particular application, and of the feasibility of the calculation. Discretization of the three dimensional nonlinear potential

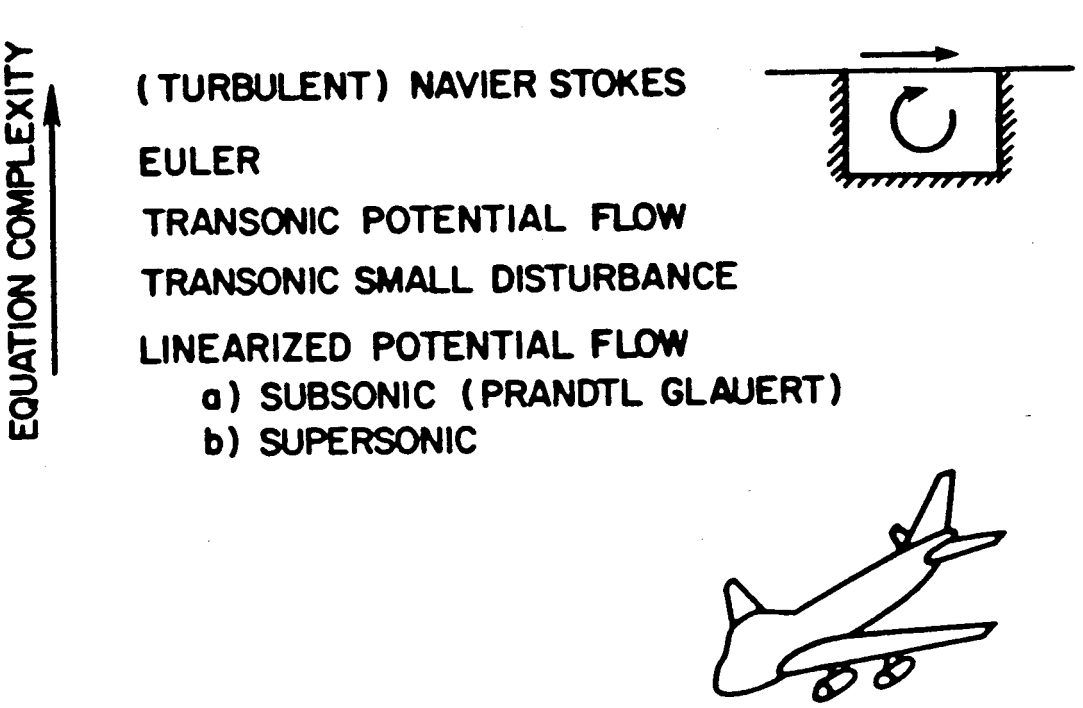

Figure 2.1: Hierarchy of Mathematical Models.

flow equation using curvilinear coordinates, for example, requires about 500 operations per mesh point. A flow over a swept wing can be quite well represented with a mesh containing 100000 points, and the resulting nonlinear equations can be solved in about 200 cycles. The Control Data 6600, which was introduced in 1964, is capable of sustaining a rate of about 1 million operations per second, and could perform such. a calculation in about 10000 seconds. The first computer program to solve the potential flow equation for a swept wing (FLO 22, written by Jameson and Caughey) did not become operational until 1976. I believe that this long delay was partly caused by a failure in the aeronautical community to recognize that such calculations were possible, with a consequent reluctance to devote the necessary effort and to make available the necessary resources.

3 Boundary Integral Methods

The first major success in computational aerydynamics was the development of boundary integral methods for the solution of the subsonic linearized potential flow equation (2.11). This can be reduced to Laplace's equation by stretching the x coordinate. Then, according to potential theory, the general solution can be represented in terms of a distribution of sources or

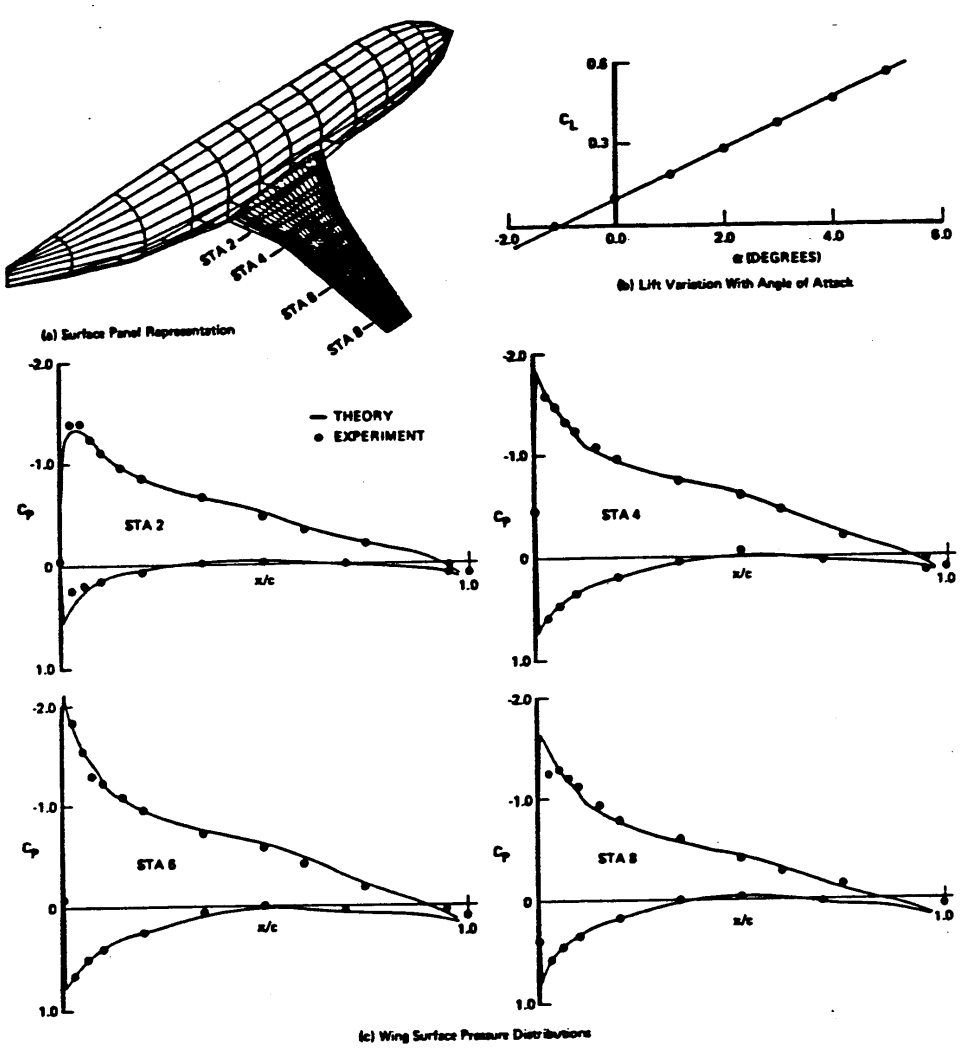

Figure 3.1: Result of a Panel Method Calculation for a Boeing 737 Wing Body Model at Low Mach Number. ∘ Test Data, -Calculated Result

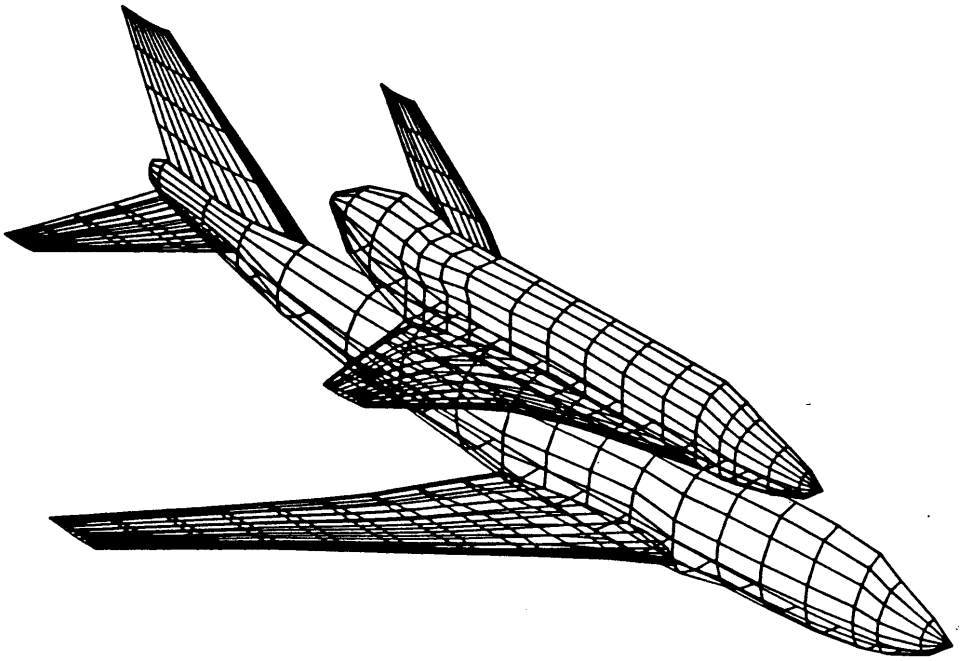

Figure 3.2: Boeing 747 with Space Shuttle

doublets, or both sources and doublets, over the boundary surface. The boundary condition is that the velocity component normal to the surface is zero. Assuming, for example, a source distribution strength $\sigma(Q)$ at the point of Q of a surface S, this leads to the integral equation

$$2\pi\sigma_P - \int\int_S \sigma(Q) n_P \cdot \Delta_P(1/r) = 0 \tag{3.1}$$

where P is the point of evaluation, and r is the distance from P to Q. A similar equation can be found for a doublet distribution, and it usually pays to use a combination. Equation (3.1) can be reduced to a set of algebraic equations by dividing the surface into quadrilateral panels, assuming a constant source strength on each panel, and satisfying the condition of zero normal velocity at the center of each panel. This leads to N equations for the source strengths on N panels. The first such method was introduced by Hess and Smith in 1962 [7]. The method was extended to lifting flows, together with the inclusion of doublet distributions, by Rubbert and Saaris [8]. Subsequently higher order panel methods (as these methods are generally called in the aircraft industry) have been introduced. A recent review has been given by Hunt [9]. An example of a calculation by a panel method is shown in Figure 3.1[1]. The results are displayed in terms of the pressure

[1]Supplied by Paul Rubbert, the Boeing Company.

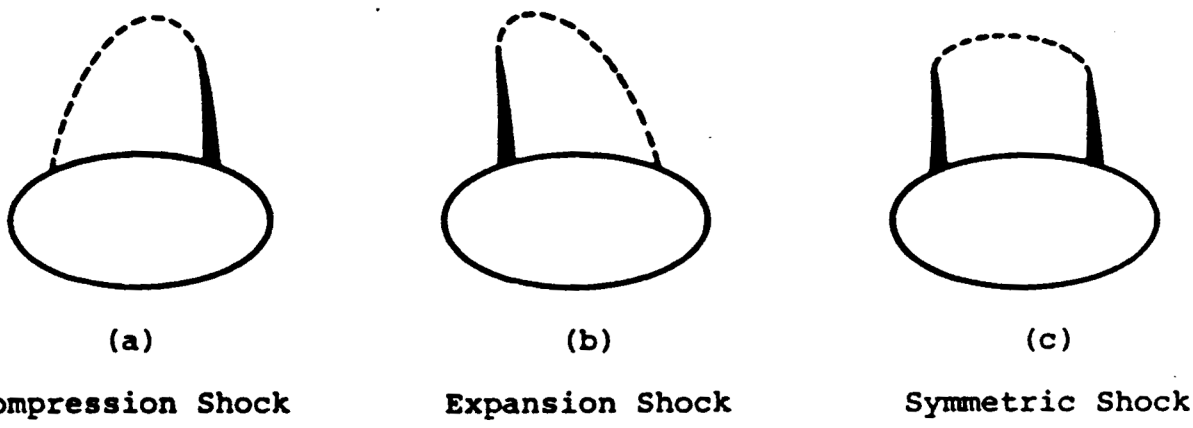

Figure 4.1: Alternative Solutions for an Ellipse

coefficient defined as

$$c_P = \frac{P - P_\infty}{\frac{1}{2} P_\infty q_\infty^2}$$

Figure 3.2 [2] illustrates the kind of geometric configuration which can be treated by panel methods.

In comparison with field methods which solve for the unknowns in the entire domain, panel methods have the advantage that the dimensionality is reduced. Consider a three dimensional flow field on an $n \times n \times n$ grid. This would be reduced to the solution of the source or doublet strengths on $N = 0(n^2)$ panels. Since, however, every panel influences every other panel, the resulting equations have a dense matrix, and $0(N^3) = 0(n^6)$ operations are required for an exact solution. If one directly discretizes the equations for the three dimensional domain the number of unknowns is n^3, but the equations are sparse, and can be solved with $0(n)$ iterations, or even with a number of Iterations independent of n if a multigrid method is used. Although the field methods appear to be potentially more efficient, the boundary integral method has the advantage that it is comparatively easy to divide a complex surface into panels, whereas the problem of dividing a three dimensional domain into hexahedral or tetrahedral cells remains a source of extreme difficulty. Panel methods thus continue to be widely used both for the solution of flows at low Mach numbers for which compressibility effects are unimportant, and also to calculate supersonic flows at high Mach numbers, for which the linearized equation (2.11) is again a good approximation.

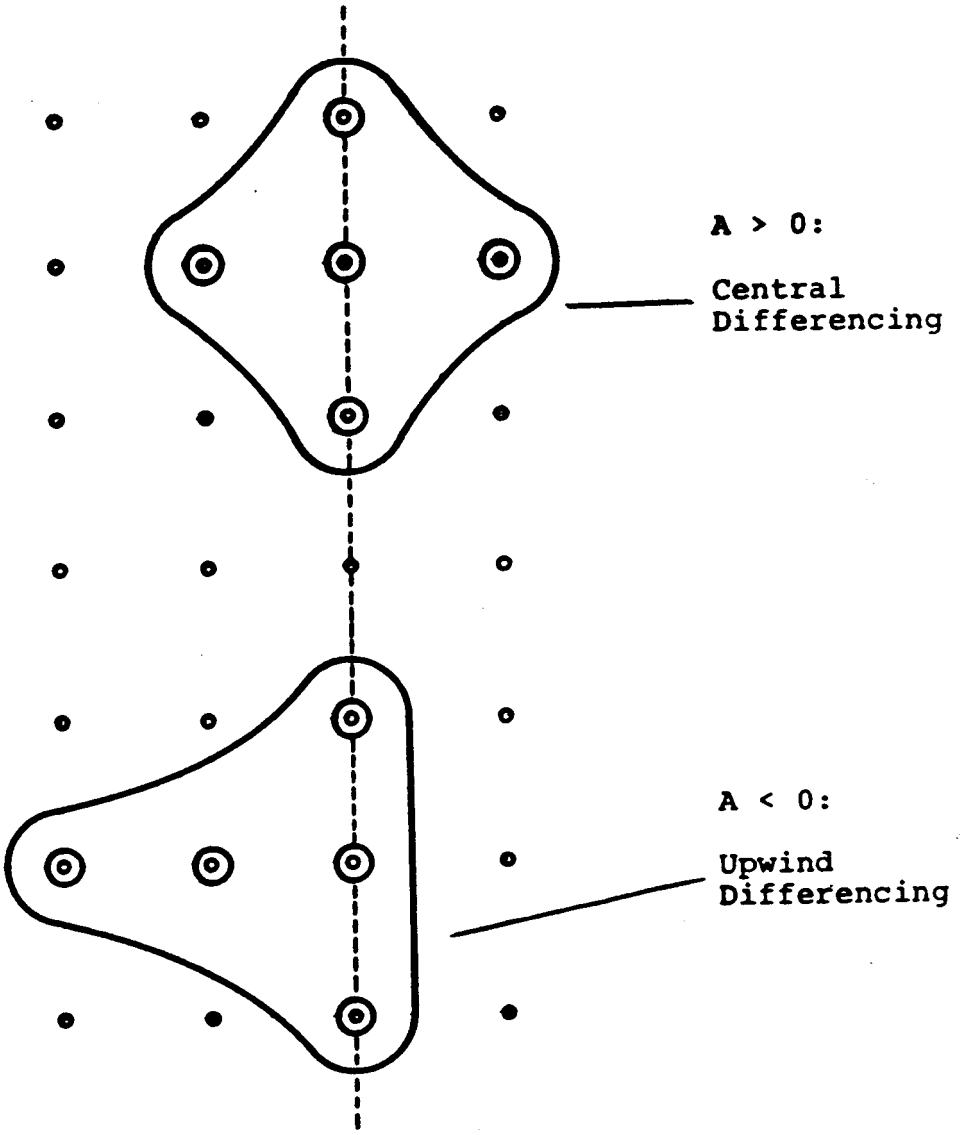

Figure 4.2: Murman-Cole Difference Scheme: $A\phi_{xx} + \phi_{yy} = 0$

4 The Transonic Potential Flow Equation

a) Upwind Differencing

When the potential flow equation (2.6) is used to predict transonic flows, the difficulty arises that the solution is invariant under a reversal of the velocity vector ($u = -\phi_x, v = -\phi_y$). Consider a transonic flow past an ellipse with a compression shock wave. Then there is a corresponding solution with an expansion shock wave (see Figures 4.1 (a,b)). In fact a central difference scheme would preserve fore and aft symmetry, leading to a solution of the type illustrated in Figure 4.1 (c). In 1970 there appeared the landmark paper of Murman and Cole [10]. This demonstrated a simple way to obtain physically relevant solutions of the transonic small disturbance equation (2.10). Writing this equation as

$$A\phi_{xx} + \phi_{yy} = 0 \tag{4.1}$$

where A is the nonlinear coefficient in (2.10), they proposed the use of central differencing if $A > 0$ (subsonic flow), but upwind differencing for ϕ_{xx} if $A < 0$ (supersonic flow), as illustrated in Figure 4.2. The equations were then solved by a line relaxation scheme, in which the unknowns were determined simultaneously on each successive vertical line, marching in the streamwise direction. The scheme amounted to a combination of a relaxation method for the subsonic zone, in which the equation is elliptic, with an implicit scheme for the wave equation in the supersonic zone. This idea can be generalized to the quasilinear potential flow equation (2.7) by writing the equations at each point in a coordinate system locally aligned with the flow. Equation (2.7) becomes

$$(c^2 - q^2)\phi_{ss} + c^2\phi_{nn} = 0$$

where

$$\phi_{ss} = \frac{u^2}{q^2}\phi_{xx} + \frac{2uv}{q^2}\phi_{xy} + \frac{v^2}{q^2}\phi_{yy}$$

and

$$\phi_{nn} = \frac{v^2}{q^2}\phi_{xx} - \frac{2uv}{q^2}\phi_{xy} + \frac{u^2}{q^2}\phi_{yy}$$

Then upwind differencing is used for all second derivatives contributing to ϕ_{ss} whenever $q > c$. This leads to Jameson's rotated difference scheme [11], (see also Albone [12]). A convergent iterative scheme can be derived by regarding the iterations as time steps in an artificial time coordinate. The principal part of the equivalent time dependent equation has the form

$$(M^2 - 1)\phi_{ss} - \phi_{nn} + 2\alpha\phi_{st} + 2\beta\phi_{nt} - 0$$

[2]Supplied by Allen Chen, the Boeing Company.

Introducing a new time coordinate

$$T = t - \frac{\alpha s}{M^2 - 1} + \beta n$$

this becomes

$$(M^2 - 1)\phi_{ss} - \phi_{nn} - \left(\frac{\alpha^2}{M^2 - 1} - \beta^2 \right) \phi_{TT} = 0$$

If the flow is locally supersonic, T is spacelike and either s or n is timelike. Since s is the timelike direction in the steady state problem, the time dependent problem is compatible with the steady state problem only if

$$\alpha^2 > \beta^2$$

This generally requires the explicit addition of a term in ϕ_{st}.

In his paper of 1973 Murman recognized that the switch in the difference scheme could violate the conservation form of the equations, leading to shock jumps which violated the conservation of mass [13]. This difficulty can be corrected by reformulating the switch to upwind differencing by the introduction of artificial viscosity. The dominant discretization error in the upwind difference formula for ϕ_{xx} is $-\Delta\phi_{xxx}$, for example, and terms of this nature can be added explicitly in conservation form, leading to special transition operators across the sonic line. Jameson showed that an appropriate form of artificial viscosity for the potential flow equation (2.6) is a difference approximation to

$$\delta x \frac{\partial}{\partial x} \mu |u| \rho_x + \Delta y \frac{\partial}{\partial y} \mu |v| \rho_y$$

where Δx and Δy are the mesh widths, and μ is a switch function

$$\mu = \max \left\{ 0, 1 - \frac{1}{M^2} \right\}$$

which cuts off the viscosity in the subsonic zone [141. It was subsequently realized by several authors that a term of this kind can be added simply by biasing the density in an upwind direction [15, 16, 17]. This has facilitated the development of discretizations on arbitrary subdivisions of the domain into hexahedra or tetrahedra.

Consistent with the assumption of isentropic flow, it is not possible to conserve both mass and momentum through a discontinuity. The conservative scheme assures a model of a shock wave in which mass, but not momentum, is conserved. There is a school of thought that it is better to use a non-conservative scheme, because a shock wave can be more closely simulated by an isentropic jump if some mass production is permitted [18], and in fact non-conservative schemes are preferred by many practicing engineers.

It also turns out that the switch in the Murman-Cole scheme is not fool proof, and can admit stationary expansion shocks in a one dimensional flow [19]. This possibility has not generally led to difficulties in practice, but it can be eliminated by modifying the transition operators [20, 21].

b) Treatment of Complex Geometric Configurations

An effective approach to the treatment of two dimensional flows over complex profiles is to map the exterior domain conformally onto the unit disk [10]. Equation (2.6) is then written in polar coordinates as

$$\frac{\partial}{\partial\theta}(\frac{\rho}{r}) + \frac{\partial}{\partial r}(r\rho\phi_r) = 0 \tag{4.2}$$

where the modulus h of the mapping function enters only in the calculation of the density from the velocity

$$\mathbf{q} = \frac{\nabla\phi}{h} \tag{4.3}$$

This procedure is very accurate. Figure 4.3 shows a numerical verification of Morawetz' theorem that a shock free transonic flow is an isolated point, and that arbitrary small changes in boundary conditions will lead to the appearance of shock waves [5]. These calculations were performed by the author's code FLO 6.

Applications to complex three dimensional configurations require a more flexible method of discretization, such as that provided by the finite element method. Jameson and Caughey proposed a scheme using isoparametric bilinear or trilinear elements [22, 23]. The discrete equations can most conveniently be derived from the Bateman variational principle. This states that the integral

$$I = \int\int p dx dy$$

is stationary in two dimensional potential flow. It follows from equations (2.9) that

$$\frac{\partial p}{\partial u} = -\rho u, \quad \frac{\partial p}{\partial v} = -\rho v$$

whence in potential flow

$$\delta I = -\int\int (\rho u \delta\phi_x + \rho v \delta\phi_y) dx dy$$

and equation (2.6) is recovered on integrating by parts and allowing arbitrary variations $\delta\phi$. In the scheme of Jameson and Caughey I is approximated as

$$I = \sum p_k V_k$$

where p_k is the pressure at the center of the k^{th} cell and V_k is its area (or volume), and the discrete equations are obtained by setting the derivative of I with respect to the nodal values of potential to zero. Artificial viscosity is added to give an upwind bias in the supersonic zone, and an interative scheme is derived by embedding the steady state equation in an artificial

time dependent equation. Several widely used codes (FLO 27, FLO 28, FLO 30) have been developed using this scheme. Figure 4.4 shows a result for a swept wing.

An alternative approach to the treatment of complex configurations has been developed by Bristeau, Pironneau, Glowinski, Periaux, Perrier, and Poirier [24, 25]. Their method uses a least square formulation of the problem, together with an iterative scheme derived with the aid of optimal control theory. The method could be used in conjunction with a subdivision into either quadrilaterals or triangles, but in practice triangulations have been used.

The simplest conceivable least squares formulation calls for the minimization of the objective function

$$I = \int_S \psi^2 dS$$

where ψ is the residual of equation (2.6), and S is the domain of the calculation. The resulting minimization problem could be solved by a steepest descent method in which the potential is repeatedly modified by a correction $\delta\phi$ proportional to $-\frac{\partial I}{\partial \phi}$. Such a method would be very slow. In fact it simulates a time dependent equation of the form

$$\phi_t = -L^* L\phi$$

where L is the differential operator in equation (2.6), and L^* is its adjoint.

Much faster convergence can be obtained by the introduction of a more sophisticated objective function

$$I = \int_S \nabla\psi^2 dS$$

where the auxiliary function ψ is calculated from

$$\nabla^2\psi = \nabla \cdot \rho\nabla\phi$$

Let g be the value of $\frac{\partial \phi}{\partial n}$ specified on the boundary C of the domain. Then this equation can be replaced by the corresponding variational form

$$\int_S \nabla\psi \cdot \nabla v dS = \int_S \rho\nabla\phi \cdot \nabla v dS - \int_C g v dS$$

which must be satisfied by ψ for all differentiable test functions v. This formulation, which is equivalent to the use of an H^{-1} norm in Sobolev space, reduces the calculation of the potential to the solution of an optimal control problem, with ϕ as the control function and ψ as the state function. It leads to an iterative scheme which calls for solutions of Poisson equations twice in each cycle. A further improvement can be realized by the use of a conjugate gradient method instead of a simple steepest descent method.

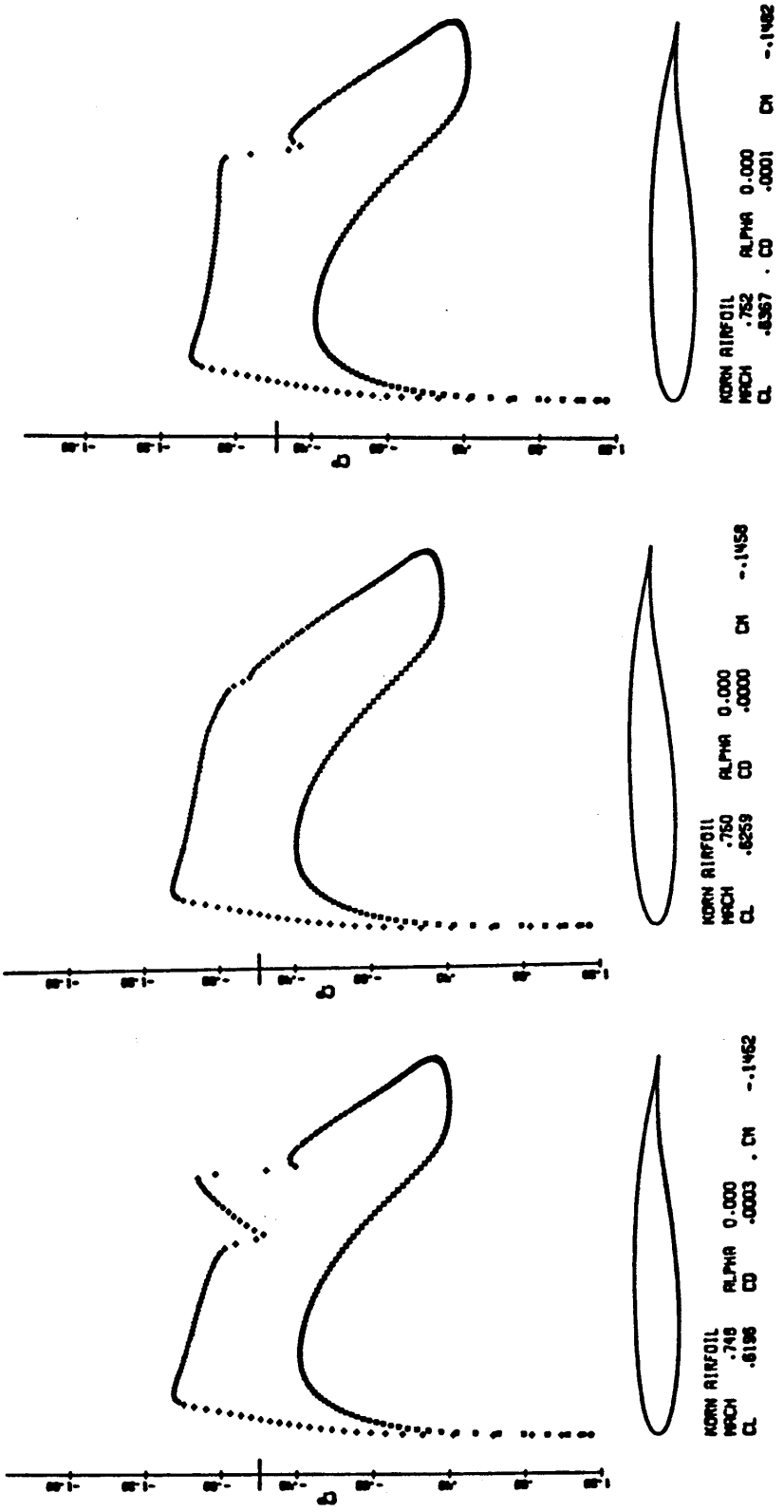

-1in-1i

Figure 4.3: Sensitivity of shock-free transonic flow: verification of the Morawetz theorem.

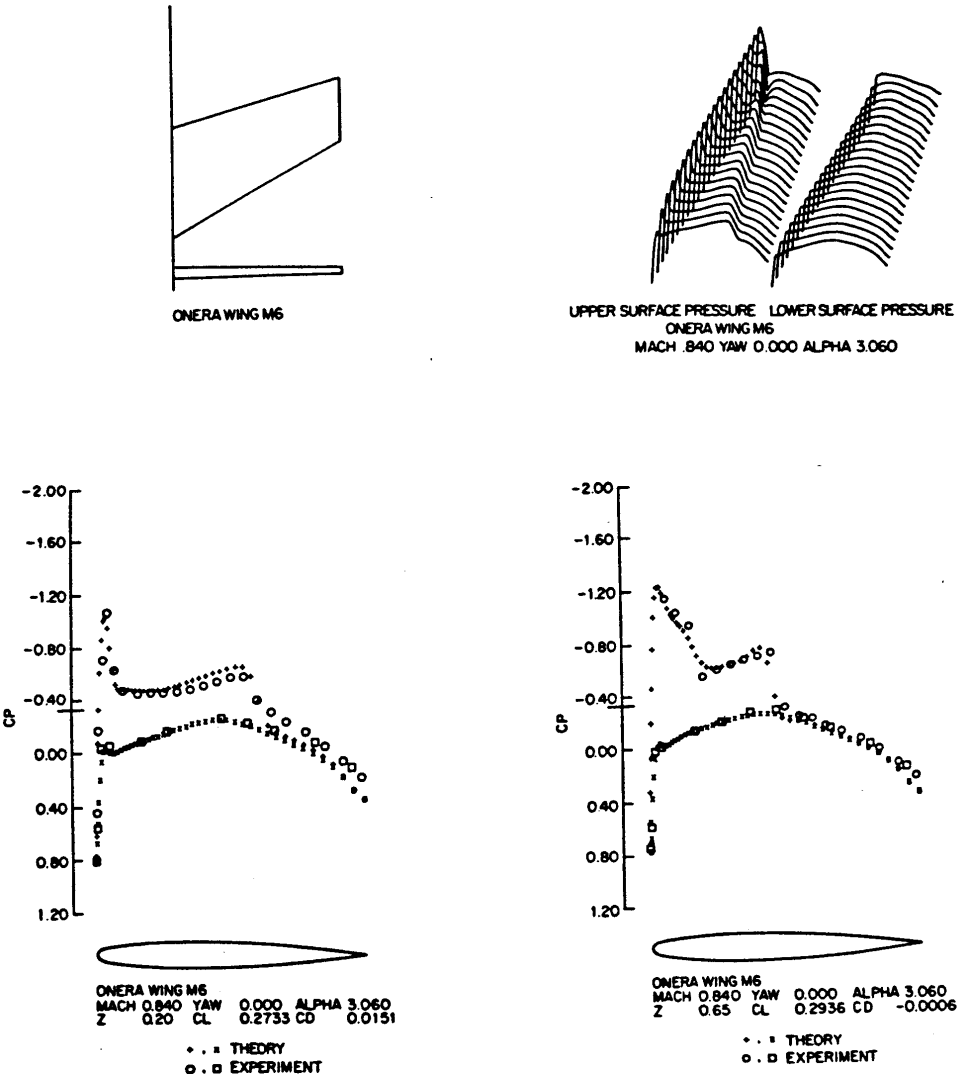
ONERA WING M6
UPPER SURFACE PRESSURE LOWER SURFACE PRESSURE
ONERA WING M6
MACH .840 YAW 0.000 ALPHA 3.060
-2.00
-1.60
-1.20
-0.80
-0.40
0.00
0.40
0.80
1.20
CP
ONERA WING M6
MACH 0.840 YAW 0.000 ALPHA 3.060
Z 0.20 CL 0.2733 CD 0.0151
THEORY
EXPERIMENT
ONERA WING M6
MACH 0.840 YAW 0.000 ALPHA 3.060
Z 0.65 CL 0.2936 CD -0.0006
THEORY
EXPERIMENT

Figure 4.4:

The least squares method in its basic form allows expansion shocks. In early formulations these were eliminated by penalty functions. Subsequently it was found best to use upwind biasing of the density. The method has been extended at Avions Marcel Dassault to the treatment of extremely complex three dimensional configurations, using a subdivision of the domain into tetrahedra.

c) Convergence Acceleration

Transonic flow calculations by relaxation methods generally require a very large number of iterations to converge (of the order of 500 - 2000). This has inhibited the more widespread use of these methods, particularly for three dimensional calculations, and stimulated numerous efforts to find more rapidly convergent methods. The two most effective approaches have been approximate factorization of the difference operator, and acceleration by the use of multiple grids.

Let the difference equations be written as

$$L\phi = 0$$

where L is a nonlinear difference operator and ϕ is the solution vector. Then a typical iterative scheme can be written as

$$N\delta\phi + L\phi^n = 0$$

where $\delta\phi$ is the correction, and N is a linear operator which can be inverted relatively cheaply, and should approximate L (In the linear case the error is reduced at each cycle by $I - N^{-1}L$). In an approximate factorization method N is formed as a product

$$N = N_1 N_2 \ldots N_q$$

of easily invertible operators. Ballhaus, Jameson and Albert found [26] that a good choice for the small disturbance equation (4.1) is

$$(\alpha - AD_x^{\sim})(\alpha D_x^- - D_y^+)\delta\phi + \alpha L\phi^-$$

where D_x^+ and D_x^- are forward and backward difference operators, and

$$D_x^{\sim} = \begin{cases} D_x^+ \text{ if } A > 0 \\ D_x^- \text{ if } A < 0 \end{cases}$$

Very efficient schemes of this type have been developed for the transonic potential flow equation by Holst [17, 27] and Baker [28].

The multigrid method was first proposed by Fedorenko [29], and some promising results for the small disturbance equation were obtained by Brandt

and South [30]. The idea is to use corrections calculated on a sequence of successively coarser grids to improve the solution on a fine grid. Consider a linear problem and let

$$L_h \phi_h = 0 \tag{4.4}$$

be the discrete equations for a mesh with a spacing proportional to h. Let u_h be an estimate of ϕ_h, and let v_h be a correction which should reduce $L_h(u_h + v_h)$ to zero. Then instead one can write an equation for v on a mesh with twice as large a spacing:

$$L_{2h} v_{2h} + Q_{2h}^h L_h u_h = 0 \tag{4.5}$$

where Q_{2h} is a collection operator which forms a weighted average of the residuals on the fine grid in the neighborhood of each mesh point of the coarse grid. The correction is finally interpolated back to the fine grid:

$$u_h^{\text{new}} = u_h + P_h^{2h} v_{2h} \tag{4.6}$$

whereP_h^{2h} is an interpolation operator. Corrections to the solution of equation (4.5) can in turn be calculated on a still coarser grid, and so on. The same basic iterative scheme can be used on all the grids in the sequence. It has been proved that solutions to elliptic problems with N unknowns can be obtained in $O(N)$ operations by the use of multiple grids [31]. A condition for the successful use of multiple grids is that before passing to a coarser grid, the high frequency error modes should be reduced to the point that the remaining error can be properly resolved on the coarser grid.

The method can be reformulated for a nonlinear problem by explicitly introducing the solution vector ugh on the coarse grid. An updated solution vector ugh is then calculated from the equation

$$L_{2h} u\bar{}_{2h} + Q_{2h}^h L_h u_h - L_{2h} u_h = 0$$

Here the difference between the collected residuals from neighboring points on the fine grid and the residual calculated on the coarse grid appears as a forcing function. The correction $u\bar{}_{2h} - u_{2h}$ is then interpolated back to the fine grid.

Early attempts to solve transonic flow problems by multigrid methods produced schemes which were not at all reliable. Sometimes they would converge rapidly, and at other times they would enter into limit cycles or even diverge. The multigrid alternating direction scheme introduced by Jameson [32] has proved robust. This scheme uses a generalized alternating direction method to drive the multigrid iteration. The ADI scheme differs from the standard ADI scheme in replacing the scalar parameter by a difference operator (which also operates on the residuals). The purpose of this is to retain a well posed problem in the supersonic zone. The most efficient strategy seems to be a simple V cycle in which 1 ADI iteration is performed on each

grid until the coarsest grid is reached, and then 1 ADI iteration on each grid on the way back up to the fine grid. Figure 4.5 shows the result of a transonic flow calculation by this method. A solution on a 192×32 grid accurate to 4 figures was obtained by 3 V cycles on a 48×8 grid, followed by 3 V cycles on a 96×16 grid and 3 V cycles on the 192×32 grid. The total calculation is equivalent to 4 V cycles on the 192×32 grid. It seems likely that this must be close to the lower bound for the number of operations required to solve 6144 similtaneous non-linear equations.

Caughey has succeeded in developing a multigrid method for three dimensional transonic flow calculations, using the finite volume method for space discretization [33]. In his scheme, line relaxation in alternate chordwise and normal directions is used to drive the multigrid iteration.

5 Solution of the Euler Equations

a) Formulation

The results of potential flow calculations have proved accurate enough to be used as the basis of the wing design of the latest generation of transport aircraft, such as the Boeing 767 and Airbus A 310. Nevertheless, the assumption of potential flow is not strictly correct when shock waves are present, and this inconsistency must set a limit to the accuracy that could be obtained even if the discretion errors were entirely eliminated. To provide a correct description of inviscid transonic flow we must solve the Euler equations. The widespread use of Euler codes has so far been impeded by large numerical errors (leading, for example, to generation of ‚spurious vorticity), and excessively slow convergence (often no convergence). Recent developments promise to correct this situation.

The emphasis here will be on the calculation of steady state solutions. While other iterative methods can be conceived, most of the methods so far developed are based on the concept of integrating the equations in time until they reach a steady state. An exterior problem can reach a steady state as a result of the propagation of disturbances away to infinity. This mechanism of convergence by expulsion of errors is effective as long as outgoing disturbances are not too strongly reflected back into the interior, and boundary conditions must therefore be treated with care. Since the time dependent terms are used merely as a device for generating an iterative scheme, they may be modified to increase the rate of convergence. The time dependent formulation is similar in principle to the Jacobi method. When applied to Laplace's equation, for example, the Jacobi method is equivalent to integrating the heat equation

$$\phi_t = \phi_{xx} + \phi_{yy}$$

until it reaches a steady state.

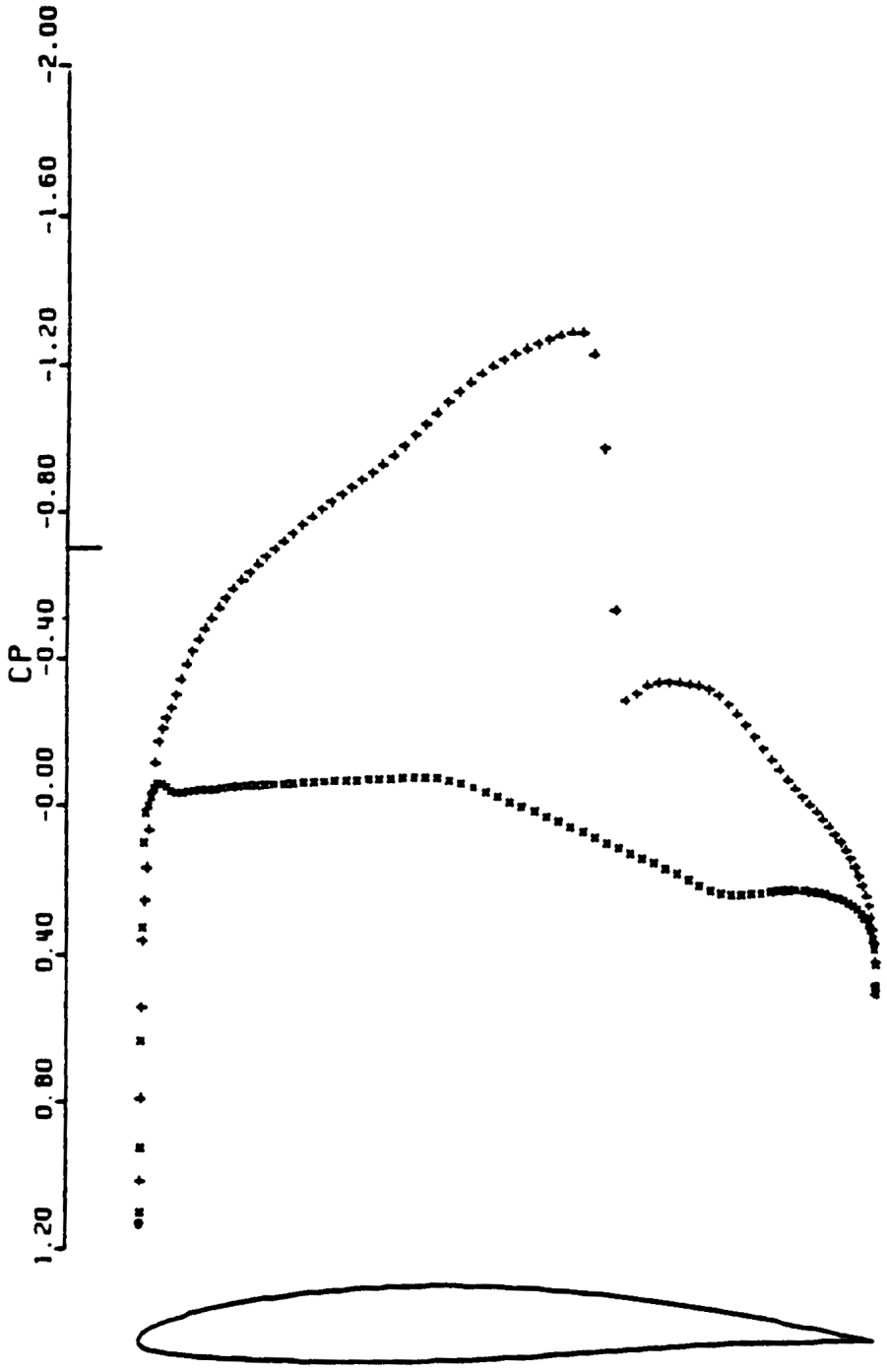

Figure 4.5: Transonic flow solution obtained with 3 multigrid cycles NACA 640410, Mach .720, $\alpha = 0°$, CL=.6640, CD=.0031, 192×32 grid Residual $.58010^{-6}$

An advantage of the time dependent formulation is that it brings the problem within the frame work of the mathematicl theory of difference methods for hyperbolic equations. Stemming from the early work of Courant, Von Neumann, and Lax, this theory is by now highly developed [34, 35, 36, 37, 38]. A stability theory for the initial boundary value problem has been formulated and refined by Kreiss, Gustaffson and Sundstrom [39, 40, 41], and the application of this theory has been worked out for a variety of discretization schemes [42]. Procedures have also been developed for the construction of boundary conditions designed to allow outgoing waves to pass through the outer boundary [43, 44]. The availability of this body of theory provides a solid foundation for the development of codes to treat practical aerodynamic problems.

A special case occurs when the flow is everywhere supersonic. The steady state equations then constitute a hyperbolic system in which the streamwise coordinate plays the role of the timelike variable, and the entire flow field can be calculated in a single sweep, marching downstream [45, 46].

b) Modification of the Equations for Faster Convergence to a Steady State

Aside from trying to construct the most efficient possible numerical method, it is natural to consider the possibility of modifying the Euler equations to improve the rate of convergence to a steady state. Three approaches are suggested in the following paragraphs.

The first is to use locally varying time steps such that the difference scheme operates everywhere in the flow field close to its stability limit. This is equivalent to solving

$$\frac{\partial w}{\partial t} + \alpha \left\{ \frac{\partial}{\partial x} f(w) + \frac{\partial}{\partial y} g(w) \right\} = 0$$

where α is a variable scaling factor. This method ensures that disturbances will be propagated to the outer boundary in a fixed number of steps, proportional to the number of mesh intervals between the body and the outer boundary.

The second approach is based on the observation that if the enthalpy has a constant value H_∞ in the far field, it is constant everywhere in a steady flow, as can be seen by comparing the equations for conservation of mass and energy. If we set $H = H_\infty$. everywhere in the flow field throughout the evolution, then the, pressure can be calculated from the equation

$$p = \frac{\gamma - 1}{\gamma} \rho \left(H_\infty - \frac{u^2 + v^2}{2} \right)$$

This eliminates the need to integrate the energy equation. The resulting three equation model still constitutes a hyperbolic system, which approaches

the same steady state as the original system. The use of this model has been advocated by Veuillot and Viviand [47].

The third approach is to retain the energy equation, and to add forcing terms proportional to the difference between H and H_∞ [48]. In a subsonic irrotational flow one can introduce a velocity potential ϕ and set

$$u = \phi_x, \quad v = \phi_y$$

The Euler equations then reduce to the unsteady potential flow equation

$$\begin{gathered}\phi_{tt} + 2u\phi_{xt} + 2v\phi_{yt} \\ = (c^2 - u^2)\phi_{xx} - 2uv\phi_{xy} + (c^2 - v^2)\phi_{yy}\end{gathered}$$

This is simply the equation for undamped wave motion in a moving coordinate frame. Damping could be introduced by adding a term $\alpha\phi_t$ to this equation. Such a term cannot directly be added to the Euler equations. However, the Bernoulli equation for unsteady potential flow is

$$\phi_t + H = H_\infty$$

Thus one can simulate the addition of a term aft to the potential flow equation by adding terms proportional to $H - H_\infty$ to the Euler equations. Provided that the space discretization scheme is constructed in such a way that $H = H_\infty$, is consistent with the steady state solution of the difference equations, these terms do not alter the final steady state. Numerical experiments have confirmed that they do assist convergence. The terms added to the mass and momentum equations are $\alpha\rho(H - H_\infty), \alpha\rho u(H - H_\infty)$ and $\alpha\rho v(H - H_\infty)$, while that added to the energy equation is $\alpha\rho(H - H_\infty)$. In calculations using multiple grids an effective strategy is to include these terms only on the fine grid, and to increase the parameter α.

c) The MacCormack Scheme

The scheme which has so far been most widely used in aerodynamic computations is the famous two stage scheme of MacCormack [49]. To solve the one dimensional system

$$\frac{\partial w}{\partial f} + \frac{\partial}{\partial x} f(w) = 0 \tag{5.1}$$

the scheme advances from time level n to time level $n + 1$ by setting

$$\tilde{w} = w^n - \Delta t D_x^+ f(w^n)$$

and

$$w^{n+1} = w^n - \frac{\Delta t}{2} D_x^+ [f(w^n) + D_x^- f(\tilde{w})] \tag{5.2}$$

Here the superscripts denote the time level, and D_x^+ and D_x^- are forward backward difference operators approximating $\frac{\partial}{\partial x}$:

$$D_x^+ f_i = \frac{f_{i+1} - f_i}{\Delta x}, \quad D_x^- f_i = \frac{f_i - f_{i-1}}{\Delta y}$$

The value at the end of the time step is first predicted using forward differences, and then the predicted value is used in the calculation of the final corrected value w^{n+1} by a formula which is centered about the middle of the time step. This is the simplest known two-level difference scheme which is both stable and second order accurate. MacCormack and Paullay also introduced the idea of deriving approximations to the Euler equations (2.5) from the integral form

$$\frac{\partial}{\partial t} \int_S w dS + \int_{\partial S} [f(w)dy - g(w)dx] = 0 \tag{5.3}$$

for a domain S with boundary ∂S [50, 51].

Many codes were written using these ideas, for example, the code of Rizzi and, Schmidt [52]. These codes were useful, but generally not very robust. The tendency to produce oscillations in the neighborhood of shockwaves cannot easily be controlled, and requires the-introduction of additional dissipative terms. Another difficulty is entropy production in regions where there should be none, such as the neighborhood of the stagnation point at the leading edge. Codes using the MacCormack scheme also generally require a very large number of time steps to reach a steady state, typically of the order of 5000, and sometimes oscillations with a small amplitude persist indefinitely. The final steady state, if it is obtained, depends on the time step.

Lerat has considered the general class of two level explicit difference schemes with 9 point support [53]. He has shown that spurious entropy production and preshock oscillations can be reduced by controlling the higher order terms in the discretization error.

d) Semi-Discrete Finite Volume Schemes

A convenient way to assure a steady state solution independent of the time step is to separate completely the space and time discretization procedures. In the scheme proposed by Jameson, Schmidt and Turkel [54] one begins by applying a semi-discretization in which only the spatial derivatives are approximated. The resulting ordinary differential equations are then solved by a multi-stage time stepping procedure.

The space discretization scheme can be developed by writing the Euler equations in the integral form (5.3). The computational domain is divided into quadrilateral cells denoted by the subscripts i, j as, sketched in Figure 5.1. Assuming that the dependent variables are known at the center of

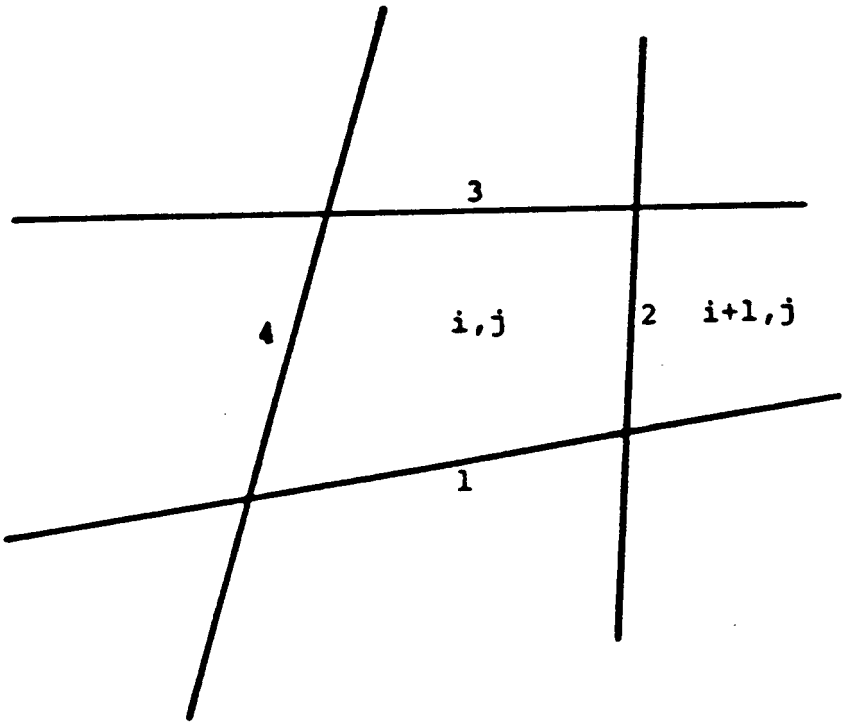

Figure 5.1: Finite Volume Scheme

each cell, a system of ordinary differential equations is obtained by applying equation (5.3) separately to each cell. These have the form

$$\frac{d}{dt}(S_{i,j}w_{i,j}) + Q_{i,j} = 0 \tag{5.4}$$

where $S_{i,j}$ is the cell area, and $Q_{i,j}$ is the net flux out of the cell. This can be evaluated as

$$\sum_{k=1}^{4}(\Delta y_k f_k - \Delta x_k g_k) \tag{5.5}$$

where f_k and g_k denote values of the flux vectors f and g on the kth edge, Δx_k and Δy_k are the increments of x and y along the edge with appropriate signs, and the sum is over the four sides of the cell. The flux vectors are evaluated by taking the average of the values in the cells on either side of each edge. For example

$$f_2 = \frac{1}{2}(f_{i+1,j} + f_{i,j})$$

where $f_{i,j}$ denotes $f(w_{i,j})$. Alternatively one may evaluate first the flux velocity

$$Q_k = \frac{\Delta y_k(\rho u)_k - \Delta x_k(\rho v)_k}{\rho_k} \tag{5.6}$$

on each edge. Then the flux for the x momentum component, for example, is

$$\sum_{k=1}^{4}[Q_k(\rho u)_k + \Delta y_k p_k] \tag{5.7}$$

Schemes constructed in this manner reduce to central difference schemes on Cartesian meshes, and are second order accurate if the mesh is sufficiently smooth. They also have the property that uniform flow is an exact solution of the difference equations. Provided that they are augmented by appropriate dissipative terms, they have been found to give quite accurate results, and they can easily be extended to three dimensional flows [48, 55, 56].

e) Adaptive Dissipation

The finite volume scheme defined by equations (5.4-5.5) is not dissipative, allowing undamped oscillations with alternate sign at odd and even mesh points. In order to eliminate spurious oscillations, which will be triggered by discontinuities in the solution, one can follow either of two strategies. The first is to begin with a non-dissipative scheme, and to attempt to add just enough dissipation where it is needed to control the tendency to produce spurious oscillations. The second approach is to try to construct a scheme which is guaranteed to prevent oscillations by preserving the monotonicity of an initially monotone profile, typically through the use of one-sided upwind differencing. A fairly extensive theory has been developed for the case of a scalar conservation law. Schemes based on this theory are reviewed in the next section.

In this section I describe an adaptive scheme for adding dissipation which has proved effective in practice. The idea of the adaptive scheme is to add third order dissipative terms throughout the domain to provide a base level of dissipation sufficient to prevent nonlinear instability, but not sufficient to prevent oscillations in the neighborhood of shock waves. In order to capture shock waves additional first order dissipative terms are added locally by a sensor designed to detect discontinuities.

With the addition of dissipative terms D_{ij}, the semi-discrete equations (5.4) take the form

$$\frac{d}{dt}(S_{i,j}w_{i,j}) + Q_{i,j} - D_{i,j} = 0 \tag{5.8}$$

To preserve conservation form the dissipative terms are generated by dissipative fluxes. The dissipation for the density equation, for example, is

$$D_{i,j}(\rho) = d_{i+1/2,j} - d_{i-1/2,j} + d_{i,j+1/2} - d_{i,j-1/2} \tag{5.9}$$

where the dissipative flux $d_{i+1/2,j}$ is defined by

$$\begin{aligned} d_{i+1/2,j} \quad = \quad & \epsilon^{(2)}_{i+1/2,j} R_{i+1/2,j}(\rho_{i,j} - \rho_{i-1,j}) \\ & -\epsilon^{(4)}_{i+1/2,j} R_{i+1/2,j}(\rho_{i+2,j} - 3\rho_{i+1,j} + 3\rho_{i,j} - \rho_{i-1,j}) \end{aligned} \tag{5.10}$$

Here $\epsilon^{(2)}_{i+1/2,j}$ and $\epsilon^{(4)}_{i+1/2,j}$ are adaptive coefficients, and $R_{i+1/2,j}$ is a coefficient chosen to give the dissipative terms the proper scale. An appropriate scaling factor is

$$R_{i+1/2,j} = \lambda_{i+1/2,j} \tag{5.11}$$

where λ is the spectral radius of the Jacobian matrix

$$\Delta y \frac{\partial f}{\partial w} - \Delta x \frac{\partial g}{\partial w}$$

for the flux across the cell face. This can be estimated as

$$\lambda = |\Delta y u - \Delta x v| + c\sqrt{\Delta x^2 + \Delta y^2} \tag{5.12}$$

where c is the speed of sound, and Δx and Δy are the displacements of the face in the x and y directions.

If one is using an explicit time stepping scheme one needs an estimate of the time step limit. A conservative estimate for a nominal Courant number of unity is

$$\Delta t^*_{i,j} = \frac{S_{i,j}}{\lambda_{i,j} + \mu_{i,j}}$$

where $\lambda_{i,j}$ and $\mu_{i,j}$ are the average spectral radii of the Jacobian matrices in the i and j directions. It is then convenient to avoid duplicate calculations by taking

$$R_{i+1/2,j} = \frac{i}{2}\left(\frac{S_{i+1,j}}{\Delta t^*_{i+1,j}} + \frac{S_{i,j}}{\Delta t^*_{i,j}}\right)$$

An effective sensor of the presence of a shock wave can be constructed by taking the second difference of the pressure. Define

$$\nu_{i,j} = \left|\frac{p_{i+1,j} - 2p_{i,j} + p_{i-1,j}}{p_{i+1,j} + 2p_{i,j} + p_{i-1,j}}\right| \tag{5.13}$$

Set

$$\nu_{i+\bar{1}/2,j} = \max(\nu_{i+2,j}, \nu_{i+1,j}, \nu_{i,j}, \nu_{i-1,j})$$

Then we take

$$\epsilon^{(2)}_{i+1/2,j} = \min(\frac{1}{2}, k^{(2)}\nu_{i+\bar{1}/2,j})$$

and

$$\epsilon^{(4)}_{i+1/2,j} = \max(0, k^{(4)} - \alpha\nu_{i+\bar{1}/2,j}) \tag{5.14}$$

where $k^{(2)}, k^{(4)}$ and α are constants. Typically,

$$k^{(2)} = 1, k^{(4)} = \frac{1}{32}, \alpha = 2$$

In a smooth region of the flow vij is proportional to the square of the mesh width, with the result that $\epsilon^{(2)}_{i+1/2,j}$ is also proportional to the square of the

mesh width, while $\epsilon^{(4)}_{i+1/2,j}$ is of order one, and the dissipative fluxes are of third order in comparison with the convective fluxes. In the neighborhood of a shock wave $\nu_{i,j}$ is of order 1, so that the scheme behaves locally like a first order scheme. The term $\alpha v \nu_{i+1/2,j}$ is subtracted from $k^{(4)}$ to cut off the fourth differences which would otherwise cause an oscillation in the neighborhood of the shock wave.

The dissipative terms for the momentum and energy equations are constructed in the same way as those for the mass equation, substituting $\rho u, \rho v$ or ρH for ρ in equation (5.10). The purpose of using differences of ρH rather than ρE in the dissipative terms for the energy equation is to produce difference equations which admit the solution $H = H_\infty$, in the steady state. With this choice the energy equation reduces to the mass equation multiplied by H. when the time derivatives vanish.

f) Upwind Differencing, Total Variation Diminishing Schemes, and Flux Vector Splitting

It is not easy to simulate a propagating discontinuity by a numerical method. The simplest model of convection is provided by the one dimensional wave equation

$$u_t + u_x = 0$$

This equation can be approximated by the one sided scheme

$$u_i^{n+1} = u_i^n - \lambda(u_i^n - u_{i-1}^n)$$

where λ is the Courant number $\Delta t/\Delta x$. This scheme is stable for $0 < \lambda < 1$ and it is appealing for two reasons:

1. It simulates the physical process of wave propagation by looking backwards along the direction of propagation: if $\lambda = 1$, it exactly represents propagation along characteristics.

2. It has the property of preserving the monoticity of an Initially monotone profile: this excludes the possibility of generating an overshoot behind a shock wave.

These observations have motivated numerous studies of one sided schemes, dating back to the early work of Courant, Isaacson and Rees [57]. There has recently been a revival of interest in the use of one sided differencing for compressible flow calculations, beginning with the nonconservative λ scheme of Moretti [45], and the conservative scheme of Steger and Warming [58].

There is by now a rather extensive theory of difference schemes for the treatment of a scalar conservation law

$$\frac{\partial u}{\partial f} + \frac{\partial}{\partial x} f(u) = 0 \tag{5.15}$$

This theory stems from the mathematical theory of shock waves, as it has been formulated by Lax [59]. It is known that the total variation

$$TV = \int_{-\infty}^{\infty} \left| \frac{\partial u}{\partial x} \right| dx$$

of a solution of (5.15) can never increase. Correspondingly it seems desirable that the discrete total variation

$$TV = \sum_{i=-\infty}^{\infty} |u_{i+1} - u_i|$$

of a solution of a difference approximation to (5.15) should not increase. A semi-discretization will have this property (now generally called total variation diminishing or TVD) if it can be cast in the form

$$\frac{du_i}{dt} = c^+_{i+1/2}(u_{i+1} - u_i) - c^-_{i-1/2}(u_i - u_{i-1}) \tag{5.16}$$

where the coefficients $c^+_{i+1/2}$ and $c^-_{i-1/2}$ are non-negative [60, 61].

This can be proved as follows. The total variation can be expressed as

$$TV = \sum_{i=-\infty}^{\infty} s_{i+1/2}(u_{i+1} - u_i)$$

where

$$s_{i+1/2} = \begin{cases} \quad 1 \text{ if } u_{i+1} - u_i \geq 0 \\ - \quad 1 \text{ if } u_{i+1} - u_i < 0 \end{cases}$$

Thus

$$\begin{aligned} \tfrac{d}{dt}TV &= \sum_{i=-\infty}^{\infty} s_{i+1/2} \frac{d}{dt}(u_{i+1} - u_i) \\ &= \sum_{i=-\infty}^{\infty} s_{i+1/2} \Big\{ c^+_{i+3/2}(u_{i+2} - u_{i+1}) \\ &\qquad -(c^+_{i+1/2} + c^-_{i+1/2})(u_{i+1} - u_i) \\ &\qquad +c^-_{i-1/2}(u_i - u_{i-1}) \Big\} \\ &= -\sum_{i=-\infty}^{\infty} v_{i+1/2}(u_{i+1} - u_i) \end{aligned}$$

where

$$\begin{aligned} v_{i+1/2} &= (c^+_{i+1/2} + c^-_{i+1/2}) s_{i+1/2} \\ &\qquad -c^+_{i+1/2} s_{i-1/2} - c^-_{i+1/2} s_{i+3/2} \end{aligned}$$

If $c^+_{i+1/2}$ and $c^-_{i+1/2}$ are non-negative it follows that $v_{i+1/2}$ is either zero, or else it has the same sign as $u_{i+1} + u_i$ Hence

$$\frac{d}{dt}TV \leq 0$$

This is a special case of a more general result for multipoin.t schemes [60].

Since the total variation will increase if an initially monotone profile ceases to be monotone, TVD schemes preserve monotonicity. The TVD property does not, however, guarantee the entropy condition that the only admissable discontinuous solutions are those for which the characteristics of (5.15) converge on the discontinuities from both sides [59]. Some TVD schemes admit stationary expansion shock waves, for example. Monotone time stepping schemes of the form

$$u_i^{n+1} = H(u_{i-l}^n, u_{i-l+1}^n, \ldots, u_{i+l}^n)$$

where

$$\frac{\partial H}{\partial u_\alpha} \leq 0 \text{ for all } \alpha$$

are known to exclude entropy violating solutions [61, 62]. Recently Osher has shown that semi-discrete approximations to (5.15) of the form

$$\frac{du_i}{dt} + \frac{1}{\Delta}(h_{i+1/2} - h_{i-1/2}) = 0 \tag{5.17}$$

exclude entropy violating solutions if the numerical flux $h_{i+1/2}$ satisfies the condition

$$\text{sgn}(u_{i+1} - u_i)(h_{i+1/2} - f(u)) \leq 0$$

for all u between u_i and u_{i+l}. Osher calls schemes which satisfy this condition E schemes [61].

It can be shown that monotone and E schemes are at best first order accurate [61, 62]. Harten devised a method of constructing TVD schemes which are second order accurate almost everywhere [63]. His construction can be adapted to a semi-discrete scheme as follows. Denoting $f(u_i)$ by f_i, define the numerical flux in equation (5.17) as

$$h_{i+1/2} = \frac{1}{2}(f_{i+1} + f_i) - \alpha_{i+1/2}(u_{i+1} - u_i). \tag{5.18}$$

Now suppose that

$$\alpha_{i+1/2} = \frac{1}{2}k|a_{i+1/2}| \tag{5.19}$$

where

$$a_{i+1/2} = \begin{cases} \frac{f_{i+1}-f_i}{u_{i+1}-u_i} \text{ if } u_{i+1} \neq u_i \\ \frac{\partial f}{\partial u}|_{u=u_i} \text{ if } u_{i+1} = u_i \end{cases} \tag{5.20}$$

Then it follows that

$$h_{i+1/2} = f_i - \frac{1}{2}(k|a_{i+1/2}| - a_{i+1/2})(u_{i+1} - u_i)$$

and

$$h_{i-1/2} = f_i - \frac{1}{2}(k|a_{i-1/2}| + a_{i-1/2})(u_i - u_{i-1})$$

This gives (5.6) with

$$c^+_{i+1/2} = \frac{1}{2}(k|a_{i+1/2}| - a_{i+1/2})$$

and

$$c^-_{i-1/2} = \frac{1}{2}(k|a_{i-1/2}| + a_{i-1/2})$$

Then $c^+_{i+1/2} \geq 0, c^-_{i-1/2} \geq 0$, provided that $k > 1$. In order to achieve a 2nd order accurate scheme which satisfies the TVD condition, one need only apply the same sequence of operations defined by equations (5.17-5.20) to

$$F_i = f_i + g_i$$

in which g_i is an anti-diffusive flux which approximates

$$\Delta x \alpha \frac{\partial u}{\partial x}$$

and thus cancels the first order error. It is necessary to limit the anti diffusive flux, however, to prevent the possibility of $(g_{i+1} - g_i)/(u_{i+l} - u_i)$ becoming unbounded. For this purpose define

$$\tilde{g}_{i+1/2} = \alpha_{i+1/2}(u_{i+1} - u_i) \tag{5.21}$$

and

$$g_i = B(\tilde{g}_{i+1/2}, \tilde{g}_{i-1/2}) \tag{5.22}$$

where B is an averaging function which limits the magnitude attainable by $(g_{i+1} - g_i)/(u_{i+l} - u_i)$ and satisfies the condition

$$B(r, r) = r$$

A simple choice is the min-mod function

$$B(r,s) = \begin{cases} 0 \text{ if } r \text{ and } s \text{ have opposite signs} \\ r \text{ if } |r| \leq |s| \text{ and have } r \text{ and } s \text{ have the same sign} \\ s \text{ if } |s| \leq |r| \text{ and } r \text{ and } s \text{ have the same sign} \end{cases} \tag{5.23}$$

The numerical flux is now

$$\begin{aligned} h_{i+1/2} &= \tfrac{1}{2}(f_{i+1} + f_i) + \tfrac{1}{2}(g_{i+1} + g_i) \\ &\quad -\alpha_{i+1/2}(u_{i+1}u_i) - \tfrac{1}{2}k|g_{i+1} - g_i|\text{sign}(u_{i+1} - u_i) \end{aligned} \tag{5.24}$$

In most of the domain the second term cancels the third term to order Δx^2, and the last term is of order Δx^2, yielding the desired second order accuracy.

Alternative flux limiting functions have been studied by Roe [64], and Sweby [65]. Let r_i be the ratio of consecutive gradients

$$r_i = \frac{\tilde{g}_{i-1/2}}{\tilde{g}_{i+1/2}}$$

One can set

$$B\tilde{g}_{i+1/2}, \tilde{g}_{i-1/2} = \phi(r_i)\tilde{g}_{i+1/2}$$

where the function ϕ satisfies the symmetry condition

$$\phi(r) = r\phi(1/r)$$

and

$$\phi(1) = 1$$

Then denoting $\phi(r_i)$ by ϕ_i,

$$\frac{g_{i+1} - g_i}{u_{i+1} - u_i} = (\frac{\phi_{i+1}}{r_{i+1}} - \phi_i)\alpha_{i+1/2}$$

which is bounded if $\phi(r)/r$ and $\phi(r)$ are bounded for all r. The resulting flux is

$$\begin{aligned} h_{i+1/2} &= f_i + g_i - (\alpha_{i+1/2} - \tfrac{1}{2}a_{i+1/2})(u_{i+1} - u_i) \\ & \quad \tfrac{1}{2}\left\{k\left|\tfrac{\phi_{i+1}}{r_{i+1}} - \phi_i\right| - \left(\tfrac{\phi_{i+1}}{r_{i+1}} - \phi_i\right)\right\}(u_{i+1} - u_i) \end{aligned}$$

and it can be seen that the TVD condition (5.16) is satisfied.

The min-mod function (5.23) is obtained by setting

$$\phi(r) = \begin{cases} 0, r \leq 0 \\ r, 0 \leq r \leq 1 \\ 1, r \leq 1 \end{cases}$$

A less stringent limiter which may be expected to improve the accuracy is

$$\phi(r) = \frac{|r| + r}{1 + r}$$

Roe [64], Sweby [65], and Osher and Chakravarthy [66] have constructed TVD schemes which omit the last term of equation (5.24) by suitably restricting $\phi(r)$.

The concept of converting a first order monotone scheme to a second order scheme by adding an anti-diffusive flux which is limited to prevent spurious oscillations may already be found in the work of Boris, Book and Zalesak [67, 68]. Harten's advance was to develop a mathematical formulation of the idea which allowed the TVD property to be proved for a second order scheme. The concept of flux limiting was independently introduced by van Leer [69].

There are difficulties in extending these ideas to systems of equations, and also to equations in more than one space dimension. Firstly the total variation of the solution of a system of hyperbolic equations may increase. Secondly it has been shown by Goodman and Leveque that a TVD scheme in two space dimensions is no better than first order accurate [70]. One might

add dissipative terms by applying the same construction to the complete system of equations, using for $\alpha_{i+1/2}$ the spectral radius of the Jacobian matrix $\partial f/\partial u$, evaluated for an average value $u_{i+1/2}$. My own numerical experiments indicate that this leads to an excessively dissipative scheme. It can be seen however, that with the scaling (5.11), the adaptive dissipation proposed in the previous section leads to a scheme which will behave locally like a TVD scheme if the constants are chosen to make sure that the coefficient $\epsilon^{(2)}_{i+1/2,j} = 1/2$ in the neighborhood of a shock wave. This will be illustrated in Section 5k for the case of Burger's equation.

If one wishes to use one sided differencing one must allow for the fact that the general one-dimensional system defined by equation (5.1) produces signals travelling in both directions. one way of generalizing one sided differencing to a system of equations is the flux vector splitting method proposed by Steger and Warming [58]. Considering the system (5.1), let the flux f be divided in two parts f^+ and f^- , such that all the eigenvalues of $\frac{\partial f^+}{\partial w}$ are non-negative, and the eigenvalues of f are non-positive. Then equation (5.1) is replaced by

$$w^{n+1} = w^n - \Delta t[D_x^- f^+(w) + D_x^+ f^-(w)] \tag{5.25}$$

where D_x^+ and D_x^- are forward and backward difference operators approximating $\frac{\partial}{\partial x}$.

The splitting is not unique. The flux vector f(w) of the Euler equations has the property that

$$f(w) = Aw$$

where $A = \frac{\partial f}{\partial w}$. A can be represented as $T\lambda T^{-1}$, where the columns of T are the eigenvectors of A, and A is a diagonal matrix containing its eigenvalues. Steger and Warming proposed the splitting

$$f^+(w) = A^+ w, \quad f^-(w) = A^- w$$

where

$$A^+ = T\lambda^+ T^{-1}, \quad A^- = T\lambda^- T^{-1}$$

and A^+ and A^- contain the positive and negatives eigenvalues of A. This splitting is discontinuous across the sonic line. Van Leer has proposed a splitting which preserves smoothness [71].

An alternative formulation was proposed by Godunov [721. Suppose that (5.1) is approximated by

$$w_i^{n+1} = w_i^n - \frac{\Delta t}{\Delta x}(F_{i+1/2} - F_{i-1/2}) \tag{5.26}$$

where the numerical flux function $F_{i+1/2} = F(w_i, w_{i+1})$ is an approximation to the flux across the cell boundary $x_{1+1/2}$. This function must satisfy the consistency condition $F(w, w) = F(w)$. In the Godunov scheme $F_{i+1/2}$ is

taken to be the flux value arising at $x_{i+1/2}$ In the exact solution of the initial value problem defined by piecewise constant data between each cell boundary. This simulates the motion of both shocks and expansion fans, but it is expensive.

Various simpler schemes designed to distinguish between the Influence of forward and backward moving waves have recently been developed, based on the concept of flux difference splitting introduced by Roe [73]. Roe's idea was to split the flux difference $F_{i+1/2} - F_{i_1/2}$ into characteristic fields through the introduction of a matrix $A(w_{i+1/2}, w_{i-1/2})$ with the property that

$$A(w_{i+1/2}, w_{i-1/2})(w_{i+1/2} - w_{i-1/2}) = F_{i+1/2} - F_{i-1/2} \tag{5.27}$$

Roe has also given a method of constructing such a matrix [74]. After $F_{i+1/2} - F_{i-1/2}$ has been decomposed into components in the basis defined by the eigenvectors of $A(w_{i+1/2}, w_{i-1/2})$, dissipative terms are separately defined for each field to produce a scheme with the TVD property by taking for $a_{i+1/2}$ the eigenvalues of $A(w_{i+1/2}, w_{i-1/2})$. These correspond to the characteristic speeds $q, q, q + c$ and $q - c$. The dissipative terms are finally recombined to form dissipative fluxes corresponding to the original variables. One consequence of the property (5.27) is that it allows the construction of schemes which resolve a stationary shockwave with a single interior point. This is achieved by using the minimum value of the dissipative coefficient consistent with the TVD property, $\alpha_{i+1/2} = 1/2a_{i+1/2}$, corresponding to an upwind scheme. Otherwise a non oscillatory scheme will produce a smeared out shock wave with an extended tail.

These properties are not obtained without a cost. Firstly there is a large increase in the number of arithmetic operations required in the realization of the scheme. Secondly it is no longer possible to satisfy exactly the condition that the total enthalpy of the steady state solution should be constant. Because the dissipative terms entering the mass and energy equations are independently constructed, these two equations are not consistent with each other in the steady state when the total enthalpy is constant.

There remains the pitfall of perhaps generating an unphysical solution which violates the entropy condition. The scheme defined by equations (5.17)-(5.20) allows a stationary discontinuous expansion. The flux is conserved across a stationary discontinuity of a solution of (5.15). Thus if u_{i+l} and u_i lie on either side of a stationary discontinuity, $f_{i+l} = f_i$, and according to equation (5.20) $a_{i+1/2} = 0$, with the result that the dissipative coefficient $\alpha_{i+1/2}$ defined by equation (5.19) also vanishes, and the difference equations are satisfied whether or not the discontinuity is an expansion or a compression. This difficulty can be corrected by modifying the definition of $\alpha_{i+1/2}$ to make sure that it cannot vanish in this situation.

g) Boundary Conditions

At a solid boundary the only contribution to the flux balance (5.5) comes from the pressure. The normal pressure gradient $\frac{\partial p}{\partial n}$ at the wall can be estimated from the condition that at $\frac{\partial}{\partial t}(\rho q_n) = 0$, where q_n is the normal velocity component. The pressure at the wall is then estimated by extrapolation from the pressure at the adjacent cell centers, using the known value of $\frac{\partial p}{\partial n}$.

The rate of convergence to a steady state will be impaired if outgoing waves are reflected back into the flow from the outer boundaries. The treatment of the far field boundary condition is based on the introduction of Riemann invariants for a one dimensional flow normal to the boundary. Let subscripts and e denote free stream values and values extrapolated from the interior cells adjacent to the boundary, and let q_n and c be the velocity component normal to the boundary and the speed of sound. Assuming that the flow is subsonic at infinity, we introduce fixed and extrapolated Riemann invariants

$$R_\infty = q_{n_\infty} - \frac{2c_\infty}{\gamma - 1}$$

and

$$R_e = q_{n_e} + \frac{2c_e}{\gamma - 1}$$

corresponding to incoming and outgoing waves. These may be added and subtracted to give

$$q_n = \frac{1}{2}(R_e + R_\infty)$$

and

$$c = \frac{\gamma - 1}{4}(R_e - R_\infty)$$

where q_n and c are the actual normal velocity component and speed of sound to be specified in the far field. At an outflow boundary, the tangential velocity component and entropy are extrapolated from the interior, while at an inflow boundary they are specified as having free stream values. These four quantities provide a complete definition of the flow in the far field. If the flow is supersonic in the far field, all the flow quantities are specified at an inflow boundary, and they are all extrapolated from the interior at an outflow boundary.

h) Explicit Time Stepping Schemes

Multi-stage schemes for the numerical solution of ordinary differential equations are usually designed to give a high order of accuracy. Since the present objective is simply to obtain a steady state as rapidly as possible, the order of accuracy is not important. This allows the use of schemes selected purely for their properties of stability and damping. For this purpose it pays to

distinguish the hyperbolic and parabolic parts stemming respectively from the convective and dissipative terms, and to treat them differently. This leads to a new class of hybrid multi-stage schemes.

Since the cell area S_{ij} is independent of time, equation (5.8) can be written as

$$\frac{dw}{dt} + R(w) = 0 \tag{5.28}$$

where $R(w)$ is the residual

$$R_{i,j} = \frac{1}{S_{i,j}}(Q_{i,j} - D_{i,j}) \tag{5.29}$$

Let w^n be the value of w after n time steps. Dropping the subscripts i, j the general $m/$ stage hybrid scheme to advance a time step Δt can be written as

$$\begin{array}{lcl} w^{(0)} & = & w^n \\ w^{(1)} & = & w^{(0)} - \alpha_1 \Delta t R^{(0)} \\ \cdots & & \\ w^{m-1} & = & w^{(0)} - \alpha_{m-1} \Delta t R^{(m-2)} \\ w^{(m)} & = & w^{(0)} - \Delta t R^{(m-1)} \\ w^{n+1} & = & w^{(m)} \end{array} \tag{5.30}$$

where the residual in the $q + 1^{st}$ stage is evaluated as

$$R^{(q)} = \frac{1}{S} \sum_{r=0}^{q} \left\{ \beta_{rq} Q(w^{(r)}) - \gamma_{qr} D(w^{(r)}) \right\} \tag{5.31}$$

subject to the consistency constraint that

$$\sum_{r=0}^{q} \beta_{qr} = \sum_{r=0}^{q} \gamma_q r = 1 \tag{5.32}$$

In order to assess the properties of these schemes it is useful to consider the model problem

$$u_t + u_x + \mu \Delta x^3 u_{xxxx} = 0 \tag{5.33}$$

In the absence of the third order dissipative term this equation describes the propagation of a disturbance without distortion at unit speed. With centered differences the residual has the form

$$\begin{array}{lcl} \Delta t R_i & = & \frac{\lambda}{2}(u_{i+1} - u_{i-1}) \\ & & +\lambda\mu(u_{i+2} - 4u_{i+1} + 6u_i - 4u_{i-1} + u_{i-2}) \end{array}$$

where $\lambda = \Delta t / \Delta x$ is the Courant number. If we consider a Fourier mode $\hat{u} = e^{ipx}$ the discretization in space yields

$$\Delta t \frac{d\hat{u}}{dt} = z\hat{u}$$

where z is the Fourier symbol of the residual. Setting $\xi = p\Delta x$, this is

$$z = -\lambda i \sin\xi - 4\lambda\mu(1-\cos\xi)^2 \tag{5.34}$$

A single step of the multistage scheme yields

$$\hat{u}^{n+1} = g(z)\hat{u}^n$$

where $g(z)$ is the amplification factor. The stability region of the scheme is given by those values of z for which $g(z) \leq 1$.

A simple procedure is to recalculate the residual at each stage using the most recently updated value of w. Then (5.31) becomes

$$R^{(q)} = \frac{1}{S}\left\{Q(w^{(q)}) - D(W^{(q)})\right\} \tag{5.35}$$

Schemes of this subclass have been analyzed in a book by van der Houwen [75], and more recently in papers by Sonneveld and van Leer [76], and Roe and Pike [77]. They are second order accurate in time for both linear and nonlinear problems if $\alpha_{m-1} = 1/2$. An efficient 4 stage scheme, which is also fourth order accurate for linear problems, has the coefficients

$$\alpha_1 = 1/4, \quad \alpha_2 = 1/3, \quad \alpha_3 = 1/2 \tag{5.36}$$

The amplification factor of this scheme is given by the polynomial

$$g(z) = 1 + z + \frac{z^2}{2} + \frac{z^3}{6} + \frac{z^4}{24}$$

The stability region of this scheme is shown in Figure 5.2(a), which displays contour lines for $|g| = 1, .9, .8, \ldots$The figure also shows the locus of z as the wave number is varied between 0 and 2π for a Courant number $\lambda = 2.8$, and a dissipation coefficient $\mu = 1/32$. The corresponding variation of $|g|$ with ξ is shown in Figure 5.2(b). The intercept of the stability region with the imaginary axis is $2\sqrt{2}$; the corresponding bound on the time step is $\Delta t < 2\sqrt{2}\Delta x$.

The maximum stability interval along the imaginary axis attainable by an m stage scheme is $m-1$. This has been proved for the case when m is odd by van der Houwen, who also gave formulas for the coefficients α_q [75]. The case of m even has recently been solved by Sonneveld and van Leer [76]. For example, the 4 stage scheme with coefficients

$$\alpha_1 = 1/3, \quad \alpha_2 = 4/15, \quad \alpha_3 = 5/9$$

has a stability region extending to 3 along the imaginary axis, at the expense of a slight reduction along the real axis.

A substantial saving in computational effort can be realized by evaluating the dissipative part only once. This leads to a class of schemes in which (5.31) becomes

$$R^{(q)} = \frac{1}{S}\left\{Q(w^{(q)}) - D(w^{(0)})\right\} \tag{5.37}$$

The amplification factor can no longer be represented as a polynomial, but it can easily be calculated recursively. The stability region for a 4 stage scheme of this class with the coefficients (5.36) is shown in Figure 5.3. This also shows that this scheme is stable for the model problem (5.33) with a Courant number $\lambda = 2.6$, and dissipation coefficient $\mu = 1/32$. Schemes in the subclass defined by (5.37) are clearly more efficient than the more conventional schemes defined by (5.35), in which the dissipative terms are repeatedly evaluated.

i) Implicit Schemes

An obvious way to accelerate convergence to a steady state is to increase the time step. The time step of an explicit scheme is limited by the Courant Friedrichs Lewy condition, which requires that the region of dependence of the difference scheme must at least contain the region of dependence of the differential equation. This motivates the introduction of implicit schemes.

The celebrated paper of Beam and Warming give an elegant formulation of implicit schemes for nonlinear hyperbolic equations [78]. A prototype implicit scheme for a system of equations such as the Euler equations (2.5), can be formulated as

$$\begin{aligned} w^{n+1} \quad = \quad & w^n - \beta\Delta t[D_x f(w^n) + D_y g(w^n)] \\ & (1-\beta)\Delta t[D_x f(w^{n+1} + D_y g(w^{n+1}))] \end{aligned} \tag{5.38}$$

where D_x and D_y are difference operators approximating $\frac{\partial}{\partial x}$ and $\frac{\partial}{\partial y}$. The scheme is second order accurate in time if $\beta = 1/2$, and in the linear scalar case it will be unconditionally stable for all $\Delta t > 0$ if $\beta > 1/2$. In this form the scheme is too expensive, since it calls for the solution of coupled nonlinear equations at each time step. Let the Jacobian matrices be

$$A = \frac{\partial f}{\partial w}, \quad B = \frac{\partial g}{\partial w} \tag{5.39}$$

and let the correction be

$$\delta w = w^{n+1} - w^n$$

The scheme can be linearized by setting

$$\begin{aligned} f(w^{n+1}) &= f(w^n) + A\delta w + O(||\delta w||^2) \\ g(w^{n+1}) &= g(w^n) + B\delta w + O(||\delta w||^2) \end{aligned}$$

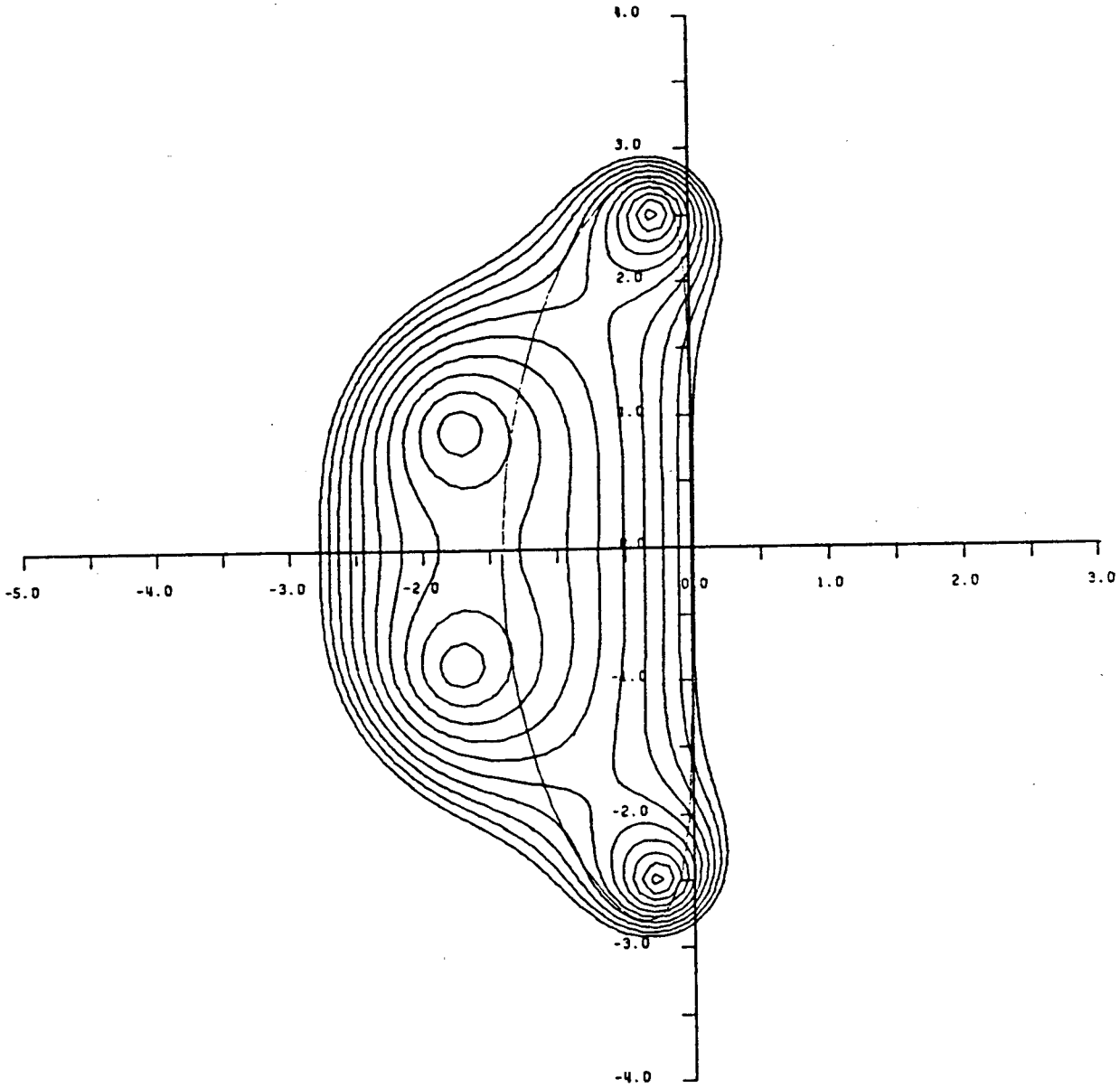

(a) Stability region of standard 4 stage scheme Contour lines $|g| = 1., .9, .8, \ldots$ and locus of $z(\xi)$ for $\lambda = 2.8, \mu = 1/32$ Coefficients $\alpha_1 = 1/4, \alpha_2 = 1/2, \alpha_3 = 1/2$

Figure 5.2:

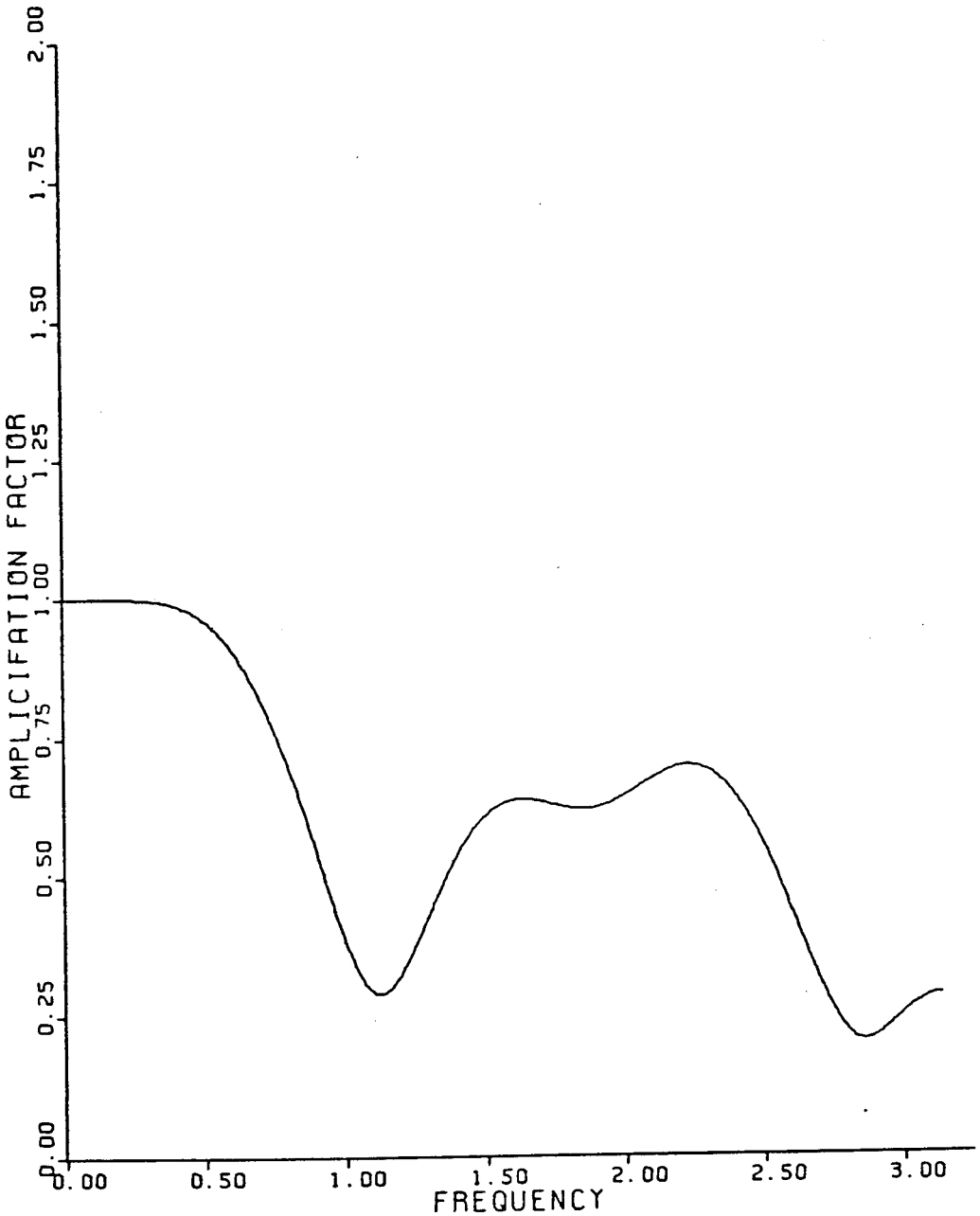

(b) Amplification factor $|g|$ of standard 4 stage scheme for $\lambda = 2.8, \mu = 1/32$ Coefficients $\alpha_1 = 1/4, \alpha_2 = 1/2, \alpha_3 = 1/2$

Figure 5.2:

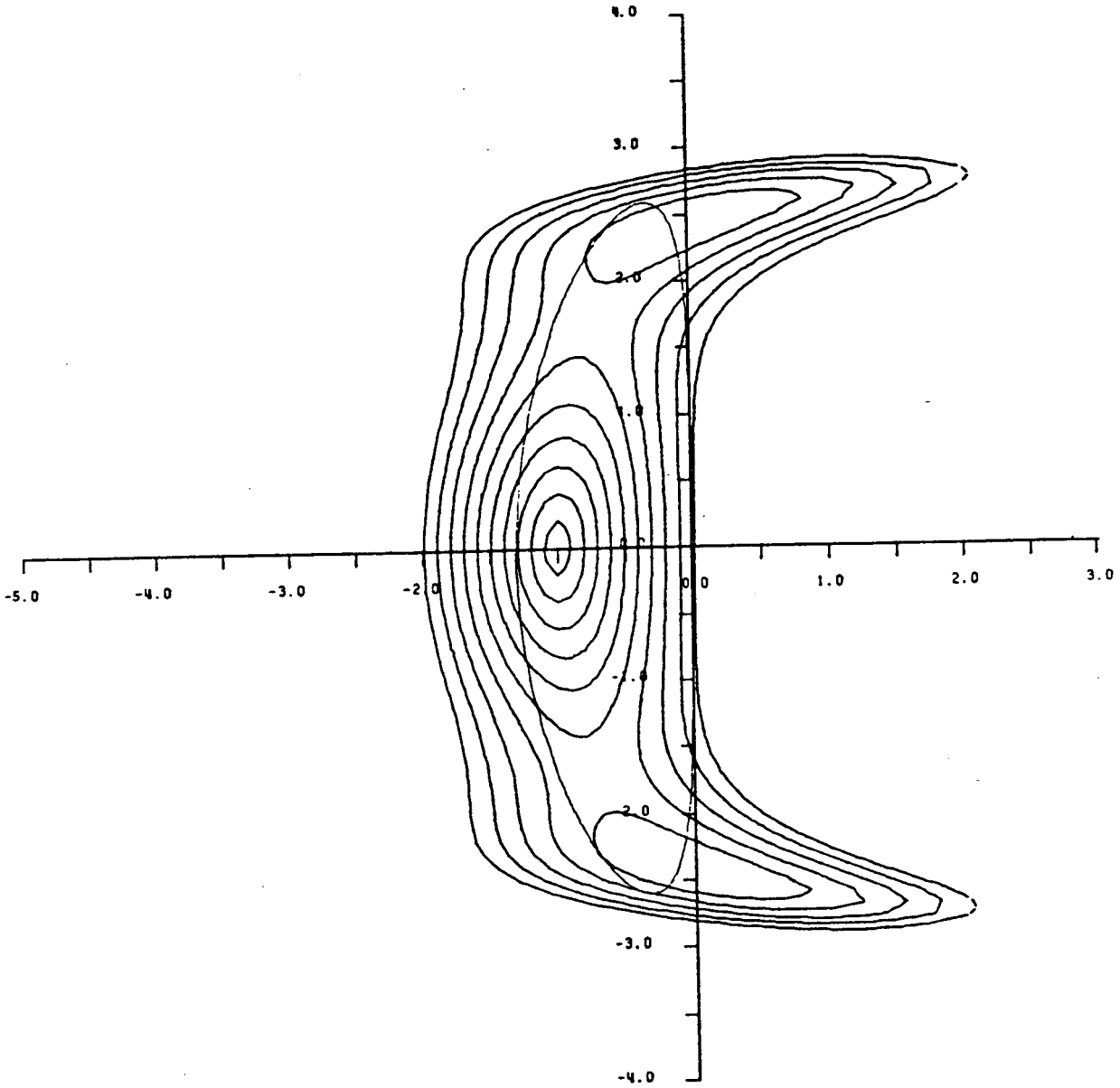

(a) Stability region of standard 4 stage scheme Contour lines $|g| = 1., .9, .8, \ldots$ and locus of $z(\xi)$ for $\lambda = 2.6, \mu = 1/32$ Coefficients $\alpha_1 = 1/4, \alpha_2 = 1/2, \alpha_3 = 1/2$

Figure 5.3:

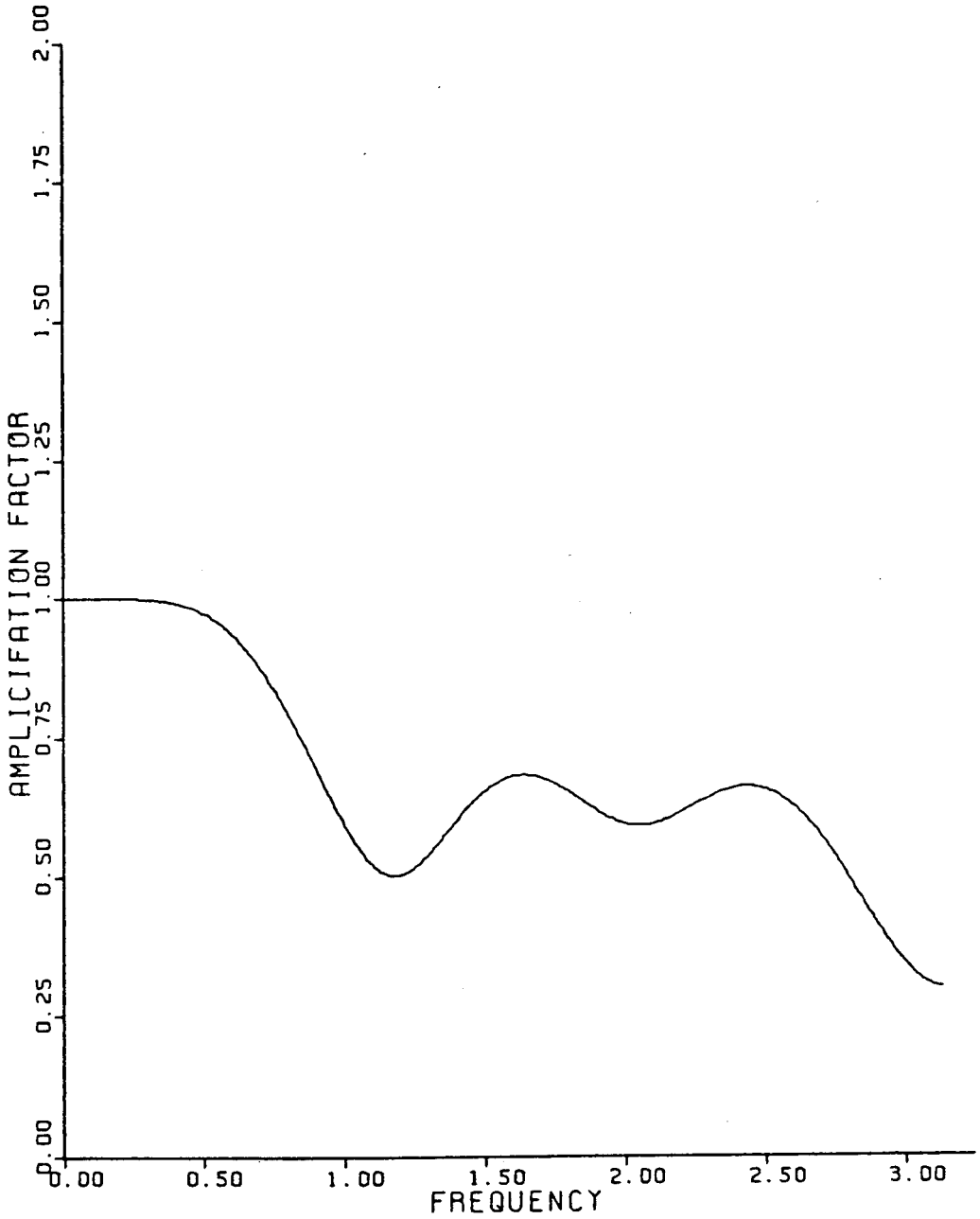

(b) Amplification factor $|g|$ of standard 4 stage scheme for $\lambda = 2.6, \mu = 1/32$ Coefficients $\alpha_1 = 1/4, \alpha_2 = 1/2, \alpha_3 = 1/2$

Figure 5.3:

and dropping the terms of second and higher order. This yields

$$[I + \beta\Delta t(D_x A + D_y B)]\delta w + \Delta t R = 0 \tag{5.40}$$

where R is the residual

$$R = D_x f(w^n) + D_y g(w^n)$$

If $\beta = 1/2$ the scheme remains second order accurate because $||\delta w|| = O(\Delta t)$, with the consequence that the neglected terms are $0(\Delta t^2)$. Note also that if $\beta = 1$ the scheme reduces to a Newton iteration in the limit $\Delta t \to \infty$ The Newton iteration has been the subject of experimentation [79]. Written for an $n \times n$ mesh, equation (5.40) has a block tridiagonal form, requiring $O(n^4)$ operations for inversion. Because of this rapid growth of the operation count with n, the Newton method appears to be uncompetitive except on very coarse meshes.

Beam and Warming derive a relatively inexpensive scheme by replacing the operator on the left side of equation (5.40) by a product of two one dimensional operators:

$$(I + \beta\Delta t D_x A)(I + \beta\Delta t D_y B)\delta w + \Delta t R = 0 \tag{5.41}$$

Equation (5.41) can be inverted in two setps

$$\begin{aligned}(I + \beta\Delta t D_x A)\delta w^* + \Delta t R = 0\\ (I + \beta\Delta t D_y B)\delta w = \delta w^*\end{aligned}$$

and the operation count is now $O(n^2)$. Equation (5.41) remains second order accurate if $\beta = 1/2$, and unconditionally stable for the linear scalar case if $\beta > 1/2$. It also has the desirable feature for steady state calculations that the steady state is independent of Δt. The corresponding scheme in three dimensions is unstable.

This reduction of an implicit scheme to an alternating direction scheme was originally introduced by Mitchell and Gourlay [80]. Briley and MacDonald have also developed an equivalent alternating direction procedure for solving nonlinear hyerbolic equations [81]. The alternating direction method has been used for transonic flow calculations by Steger and Pulliam [82].

An alternative reduction is to replace the operator on the left hand side of equation (5.40) by a product of factors with upwind and downwind differencing, leading to an LU implicit scheme [83]. Care must then be taken to ensure that the operators in the two factors have respectively positive and negative eigenvalues. This scheme has been used to calculate transonic flows through cascades by Buratynski and Caughey [84].

Another approach to Increasing the time step is to replace the residual at each point by a weighted average of residuals at neighboring points. Consider

the multi-stage scheme described by equation (5.30). In the one dimensional case one might replace the residual R_i by the average

$$\bar{R}_i = \epsilon R_{i-1} + (1-2\epsilon)R_i + \epsilon R_{i+1}$$

at each stage of the scheme. This smooths the residuals and also increases the support of the scheme, thus relaxing the restriction on the time step imposed by the Courant Friedrichs Lewy condition. If $\epsilon > 1/4$, however, there are Fourier modes such that $\bar{R}_i = 0$ when $R_i \neq 0$. To avoid this restriction it is better to perform the averaging implicitly by setting

$$-\epsilon\bar{R}_{i-1} + (1-2\epsilon)\bar{R}_i - \epsilon\bar{R}_{i+1} = R_i \tag{5.42}$$

For an infinite interval this equation has the explicit solution

$$R_i = \frac{1-r}{1+r}\sum_{q=-\infty}^{\infty} r^q R_{i+q} \tag{5.43}$$

where

$$\epsilon = \frac{r}{(1-r)^2}, \quad r < 1 \tag{5.44}$$

Thus the effect of the implicit smoothing is to collect information from residuals at all points in the field, with an influence coefficient which decays by factor r at each additional mesh interval from the point of interest.

Consider the model problem (5.33). According to equation (5.43) the Fourier symbol (5.34) will be replaced by

$$z = -\lambda\frac{i\sin\xi + 4\mu(1-\cos\xi)^2}{1+2\epsilon(1-\cos\xi)}$$

In the absence of dissipation one now finds that stability can be maintained for any Courant number λ, provided that the smoothing parameter satisfies

$$\epsilon > \frac{1}{4}\left\{\frac{\lambda^2}{\lambda^{*2}} - 1\right\}$$

where λ^* is the stability limit of the unsmoothed scheme. In terms of the decay parameter r the stability condition becomes

$$\frac{1+r}{1-r} > \frac{\lambda}{\lambda^*}$$

Suppose that the time step is increased to the limiting value permitted by a given value of r. Then according to equation (5.43) the Fourier symbol in the absence of dissipation is

$$\begin{aligned} z &= -\lambda^*\left\{1 + 2\textstyle\sum_{q=-\infty}^{\infty} r^q\cos q\xi\right\} i\sin\xi \\ &= -\lambda^*\frac{1-r^2}{1-2r\cos\xi+r^2}i\sin\xi \end{aligned}$$

and it may be verified that $|z| \leq \lambda^*$

In the case of a finite interval with periodic conditions equation (5.43) still holds, provided that the values R_{i+q} outside the interval are defined by periodicity. In the absence of periodicity one can also choose boundary conditions such that (5.43) Is a solution of (5.42), with $R_{i+q} = 0$ if $i + q$ lies outside the interval. This solution can be realized by setting

$$\begin{aligned} \tilde{R}_1 &= R_1 \\ \tilde{R}_i &= R_i - r(R_i - \tilde{R}_{i-1}) \text{ for } 2 \leq i \leq n \end{aligned}$$

and then

$$\bar{R}_n = \frac{1}{1+r}\tilde{R}_n$$

$$\bar{R}_i = \tilde{R}_i - r(\tilde{R}_i - \bar{R}_{i+1}) \text{ for } 1 \leq i \leq n-1$$

It turns out that it is sufficient to apply the smoothing only at alternate stages, provided that the smoothing parameter ϵ is sufficiently increased. If the total number of stages is even, smoothing should be applied at stages $2, 4, 6 \ldots$, and if it is odd it should be applied at stages $1, 3, 5 \ldots$.In the two dimensional case smoothing is applied in product form:

$$(1 - \epsilon_x \delta_x^2)(1 - \epsilon_y \delta_y^2)\bar{R} = R$$

where δ_x^2 and δ_y^2 are second difference operators in the x and y directions, and ϵ_x and ϵ_y are the corresponding smoothing parameters. The smoothed multi-stage scheme is in use in a code currently being developed by Baker and Jameson to calculate the flow past a wing-body-fin-tail combination [56]. The best rate of convergence is obtained with a Courant number of about 9.

Two other interesting formulations of implicit schemes have been proposed by MacCormack [85], and Lerat and Sides [86]. MacCormack adds implicit stages requiring bidiagonal inversions to his explicit scheme. If the stages are reordered and the two implicit stages combined, it is equivalent in the scalar case to residual averaging. Lerat and Sides consider a general class of implicit schemes using 9 point support in 2 dimensions. Their choice of parameters again leads to a form of residual averaging.

j) Multigrid Scheme

While the available theorems in the theory of multigrid methods generally assume ellipticity, it seems that it ought to be possible to accelerate the evolution of a hyperbolic system to a steady state by using large time steps on coarse grids, so that disturbances will be more rapidly expelled through the outer boundary. The interpolation of corrections back to the fine grid will introduce errors, however, which cannot be rapidly expelled from the

fine grid, and ought to be locally damped, if a fast rate of convergence is to be attained. Thus it remains important that the driving scheme should have the property of rapidly damping out high frequency modes.

In a novel multigrid scheme proposed by Ni [87], the flow variables are stored at mesh nodes, and the rates of change of mass, momentum and energy in each mesh cell are estimated from the flux integral appearing in equation (3.1). The corresponding change 6wo associated with the cell is then distributed unequally between the nodes at its four corners by the rule

$$\delta w_c = \frac{1}{4}(\delta w_o \pm A\delta w_o \pm B\delta w_o)$$

where δw_o is the correction at a corner, and A and B are the Jacobian matrices (5.39). The signs are varied in such a way that the accumulated corrections at each node correspond to the first two terms of a Taylor series in time, like a Lax Wendroff scheme. As it stands, this scheme does not damp oscillations between odd and even points. Ni introduces artificial viscosity by adding a further correction proportional to the difference between the value at each corner and the average of the values at the four corners of the cell. Residuals on the coarse grid are formed by taking weighted averages of the corrections at neighboring nodes of the fine grid, and corrections are then assigned to the corners of coarse grid cells by the same distribution rule. When several grid levels are used, the distribution rule is applied once on each grid down to the coarsest grid, and the corrections are then interpolated back to the fine grid. Using 3 or 4 grid levels, Ni obtained a mean rate of convergence of about .95, measured by the average reduction of the residuals in a multigrid cycle. The performance of the scheme seems to depend critically on the presence of the added dissipative terms to provide the necessary damping of high frequency modes. In Ni's published version of the scheme these introduce an error of first order.

The flexibility in the formulation of the hybrid multi-stage schemes allows them to be designed to provide effective damping of high frequency modes with higher order dissipative terms. This makes it possible to devise rapidly convergent multigrid schemes without any need to compromise the accuracy through the introduction of excessive levels of dissipation [88].

In order to adapt the multi-stage scheme for a multigrid algorithm , auxiliary meshes are introduced by doubling the mesh spacing. Values of the flow variables are transferred to a coarser grid by the rule

$$w_{2h}^{(0)} = \left(\sum S_h w_h\right)/S_{2h}$$

where the subscripts denote values of the mesh spacing parameter, S is the cell area, and the sum is over the 4 cells on the fine grid composing each cell on the coarse grid. This rule conserves mass, momentum and energy. A forcing function is then defined as

$$P_{2h} = \sum R_h(w_h) - R_{2h}(w_{2h}^{(0)}) \tag{5.45}$$

where R is the residual of the difference scheme. In order to update the solution on a coarse grid, the multistage scheme (5.30) is reformulated as

$$\begin{aligned} w^{(1)} &= w_{2h}^{(0)} - \alpha_1 \Delta t (R_{2h}^{(0)} + P_{2h}) \\ \dots & \\ w_{2h}^{q+1} &= w_{2h}^{(0)} - \alpha_q \Delta t (R_{2h}^{(q)} + P_{2h}) \end{aligned} \tag{5.46}$$

where $R(q)$ is the residual at the $(q+1)^{st}$ stage. In the first stage of the scheme, the addition of P_{2h} cancels $R_{2h}(w_{2h}^{(0)})$ and replaces it by $\sum R_h(w_h)$, with the result that the evolution on the coarse grid is driven by the residuals on the fine grid. This process is repeated on successively coarser grids. Finally the correction calculated on each grid is passed back to the next finer grid by bilinear interpolation.

Since the evolution on a coarse grid is driven by residuals collected from the next finer grid, the final solution on the fine grid is independent of the choice of boundary conditions on the coarse grids. The surface boundary condition is treated in the same way on every grid, by using the normal pressure gradient to extrapolate the surface pressure from the pressure-in the cells adjacent to the wall. The far field conditions can either be transferred from the fine grid, or recalculated by the procedure described in Section 5g. It is also possible to use different dissipative terms on the coarse grids. In practice the best convergence rates have been obtained by using second differences.

It turns out than an effective multigrid strategy is to use a simple saw tooth cycle (as illustrated in Figure 5.4), in which a transfer is made from each grid to the next coarser grid after a single time step. After reaching the coarsest grid the corrections are then, successively interpolated back from each grid to the next finer grid without any intermediate Euler calculations. On each grid the time step is varied locally to yield a fixed Courant number, and the same Courant number is generally used on all grids, so that progressively larger time steps are used after each transfer to a coarser grid. In comparison with a single time step of the Euler scheme on the fine grid, the total computational effort in one multigrid cycle is

$$1 + \frac{1}{4} + \frac{1}{16} + \dots \leq \frac{4}{3}$$

plus the additional work of calculating the forcing functions P, and interpolating the corrections.

It is important that the time stepping scheme should be effective at damping the high frequency modes. One can fairly easily devise 3 and 4 stage schemes in the class defined by (5.37) which meet this requirement. An effective 3 stage scheme is given by the coefficients

$$\alpha_1 = .6, \quad \alpha_2 = .6 \tag{5.47}$$

Its stability region is shown in Figure 5.5.

Additional flexibility is provided by a class of schemes in which the dissipative terms are evaluated twice. This may be used to make a further improvement in the high frequency damping properties, or else to extend the stability region along the real axis to allow more margin for the dissipation Introduced by an upwind or TVD scheme of the type described in Section 5f. In this class of schemes

$$\begin{aligned} R^{(0)} &= \tfrac{1}{S}\left\{Q(w^{(0)}) - D(w^{(0)})\right\} \\ r^{(q)} &= \tfrac{1}{S}\left\{Q(w^{(q)}) - \beta D(w^{(1)} - (1-\beta)D(w^{(0)}))\right\}, \qquad q \geq 1 \end{aligned} \tag{5.48}$$

In the case of pure dissipation ($Qw = 0$), the amplification factor reduces to

$$g = 1 + x + \alpha_1 \beta z^2$$

Thus if β is chosen such that $\alpha_1 \beta = 1/4$, the stability region will contain a double zero at $z = -2$ on the real axis. A maximum stability interval of β can be attained along the real axis by choosing β such that $\alpha_1 \beta = 1/8$. Figures 5.6 and 5.7 show stability regions of 4 and 5 stage schemes in this class with the coefficients

$$\alpha = 1/4, \quad \alpha_2 = 1/3, \quad \alpha_3 = 1/2, \qquad \beta = 1 \tag{5.49}$$

and

$$\alpha_1 = 1/4, \quad \alpha_2 = 1/6, \quad \alpha_3 = 3/8, \quad \alpha_4 = 1/2, \qquad \beta = 1 \tag{5.50}$$

The improvement of Figure 5.6 over Figure 5.2 is clear. The 5 stage scheme combines van der Houwen's optimal coefficients with two evaluations of the dissipative terms to attain a stability interval of 4 along both the imaginary and the real axes.

k) Trials with Burger's Equation

The simplest nonlinear conservation law is Burger's equation without viscosity:

$$\frac{\partial u}{\partial t} + \frac{\partial}{\partial x}\left(\frac{u^2}{2}\right) = 0 \tag{5.51}$$

This provides a useful test of the properties of numerical schemes which avoids other complicating factors such as boundary conditions and complex geometry. If the boundary conditions are given as

$$u(0) = v, \quad u(1) = -v, \quad v \geq 0 \tag{5.52}$$

equation (5.51) admits a steady entropy satisfying solution with a shock wave at a location which depends on the initial state. This section presents

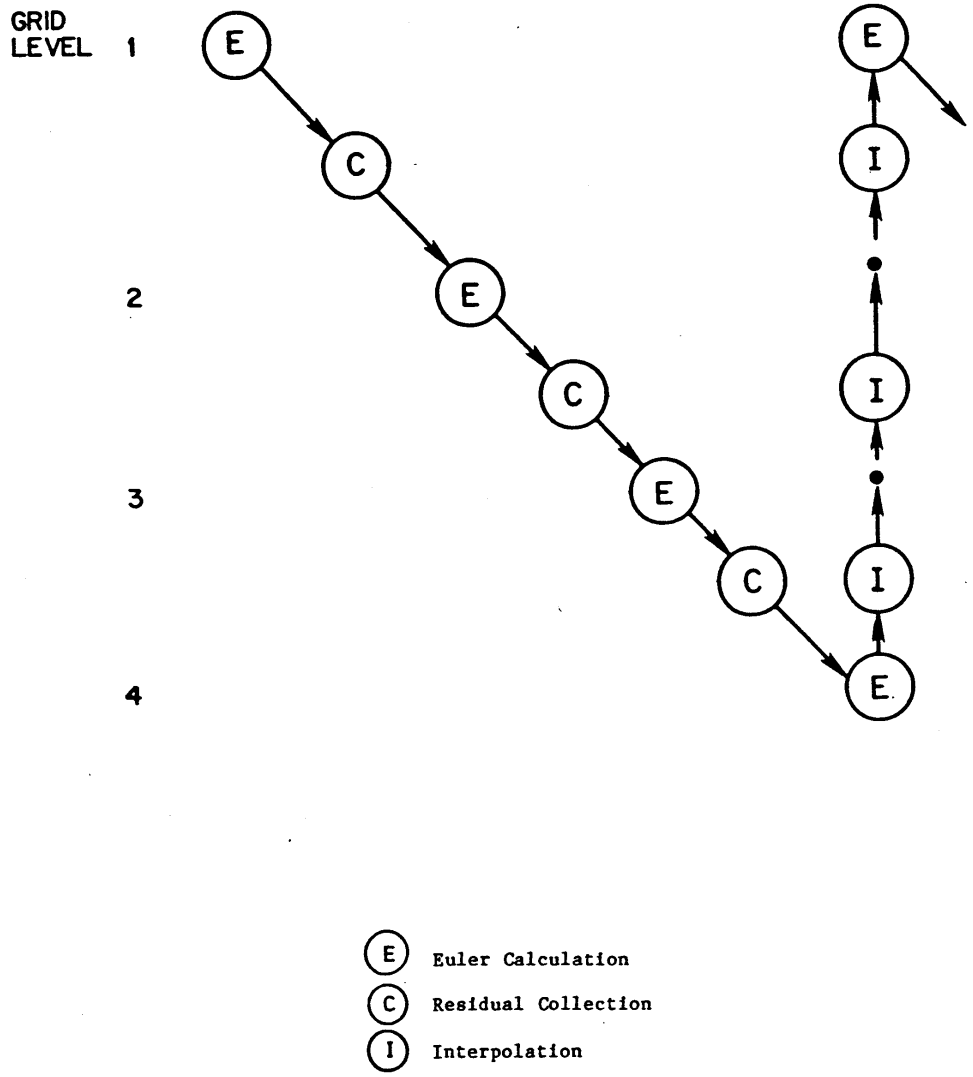

Figure 5.4: Saw Tooth Multigrid Cycle

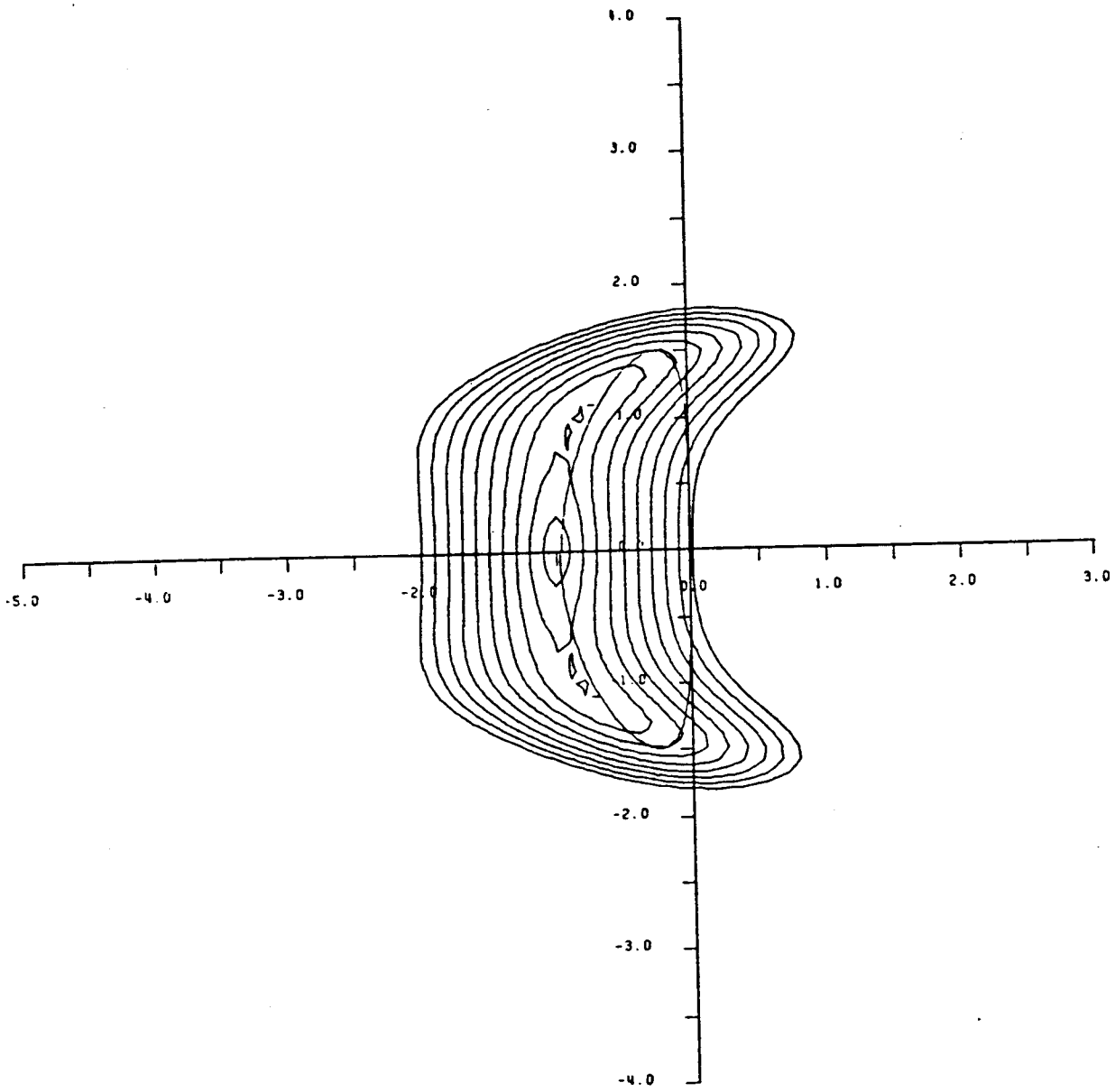

(a) Stability region of 3 stage scheme with single evaluation of dissipation Contour lines $|g| = 1., .9, .8, \ldots$ and locus of $z(\xi)$ for $\lambda = 1.5, \mu = 0.04$ Coefficients $\alpha_1 = .6, \alpha_2 = .6$

Figure 5.5:

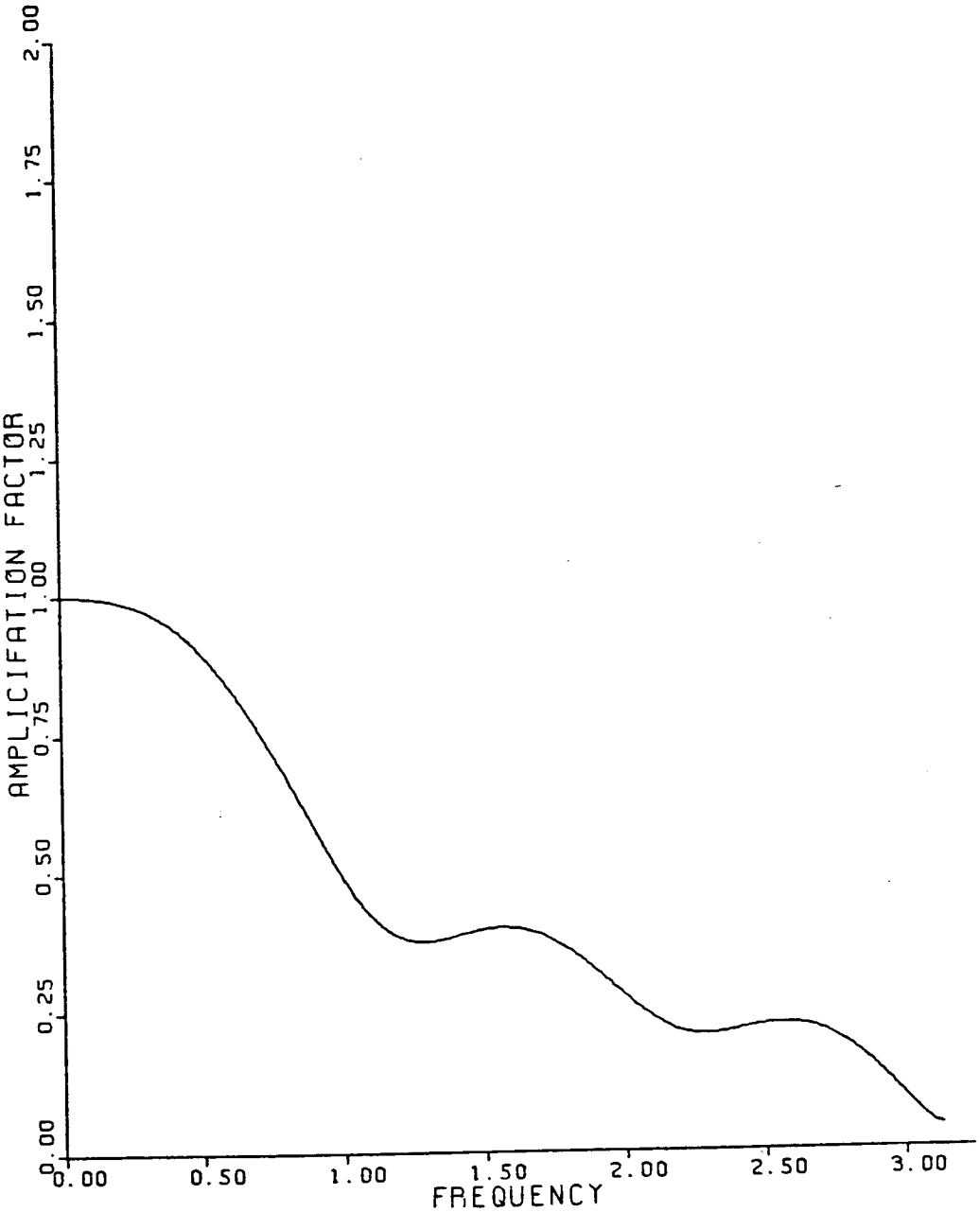

(b) Amplification factor $|g|$ of 3 stage scheme with single evaluation of dissipation for $\lambda = 1.5, \mu = 1/32$ Coefficients $\alpha_1 = 1/4, \alpha_2 = 1/2, \alpha_3 = 1/2$

Figure 5.5:

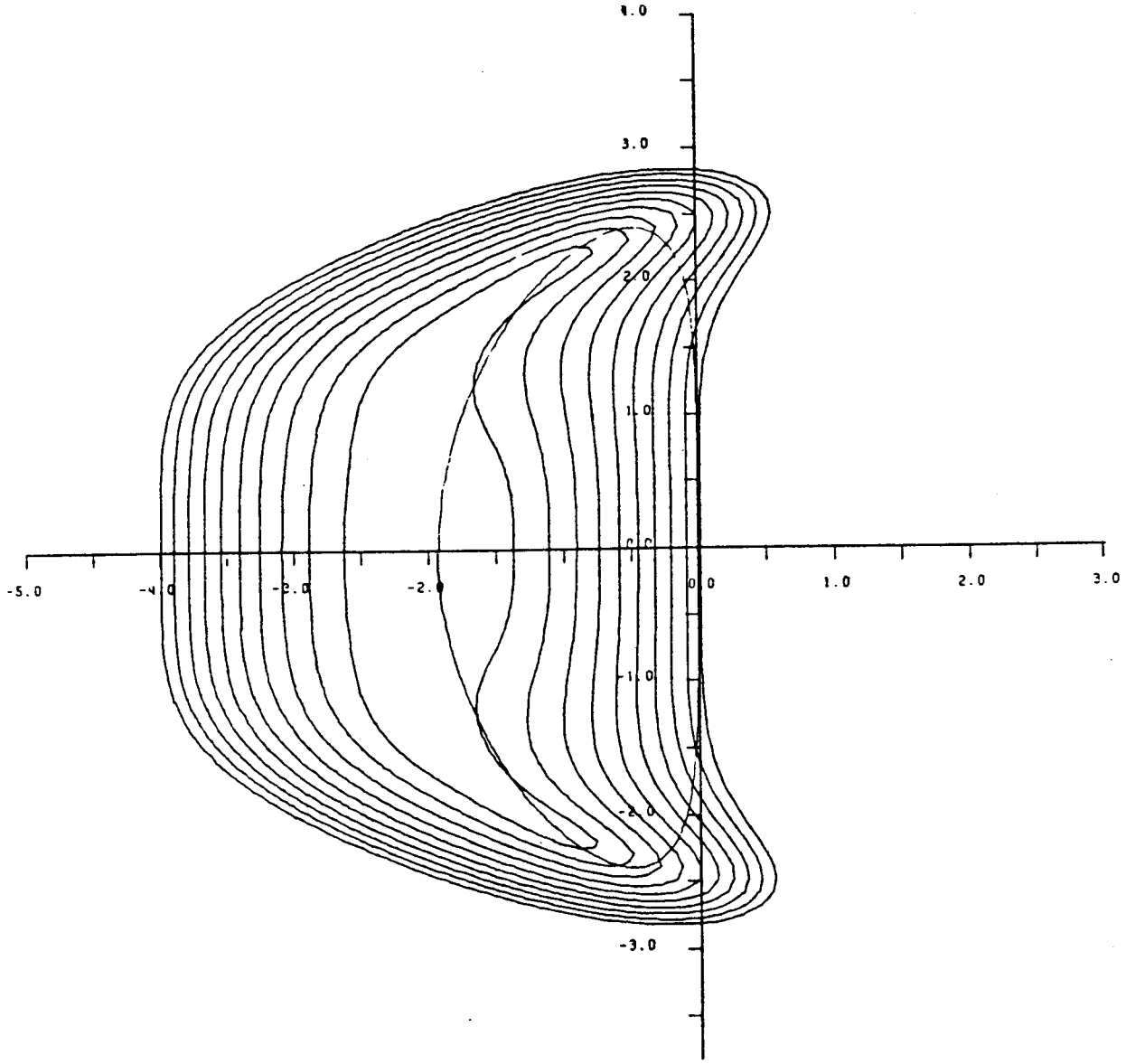

(a) Stability region of 4 stage scheme with two evaluations of dissipation Contour lines $|g| = 1., .9, .8, \ldots$ and locus of $z(\xi)$ for $\lambda = 2.4, \mu = 0.05$ Coefficients $\alpha_1 = 1/4, \alpha_2 = 1/3, \alpha_3 = 1/2, \beta = 1$

Figure 5.6:

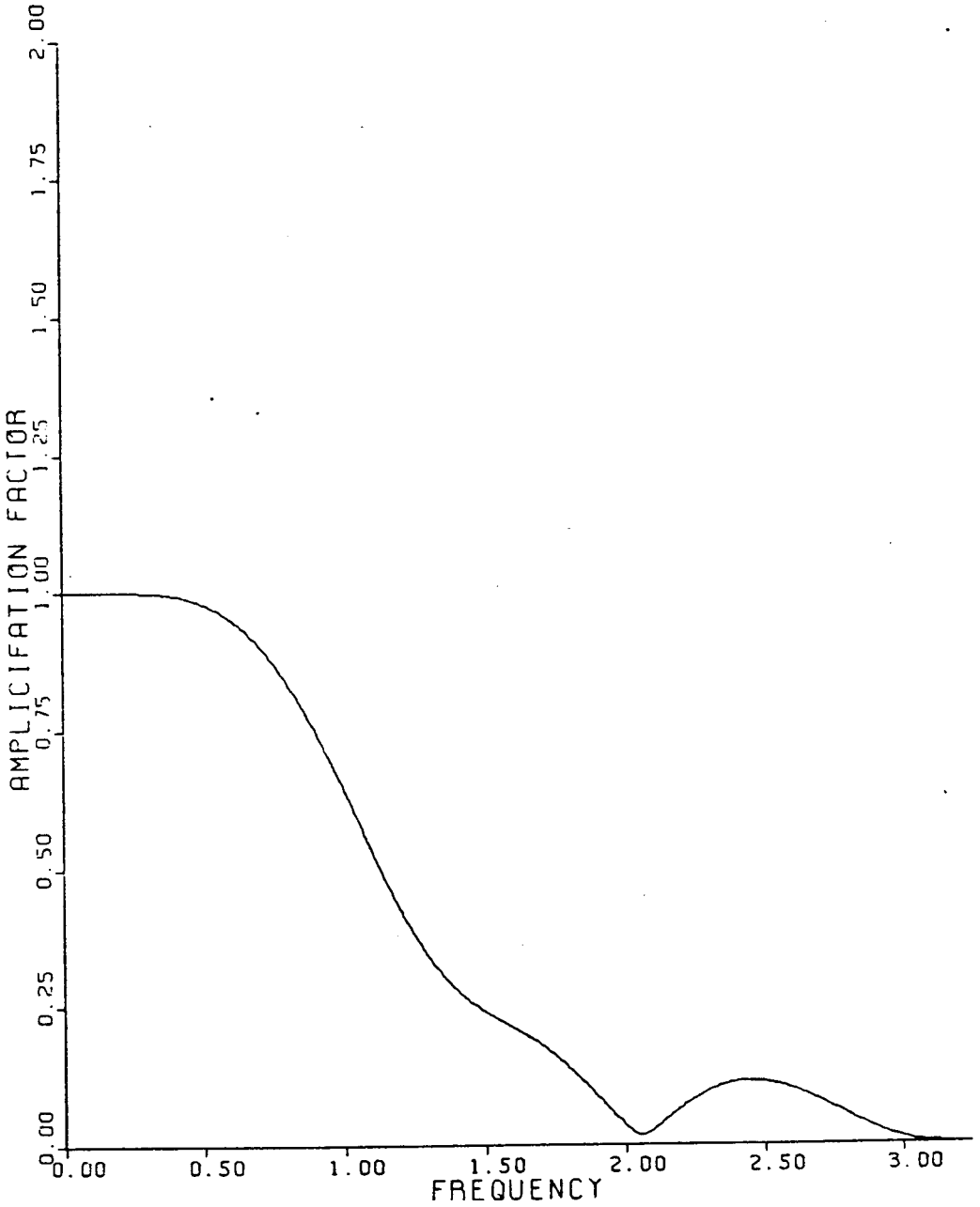

(b) Amplification factor 4 stage scheme with two evaluations of dissipation for $\lambda = 2.4, \mu = 0.05$ Coefficients $\alpha_1 = 1/4, \alpha_2 = 1/3, \alpha_3 = 1/2, \beta = 1$

Figure 5.6:

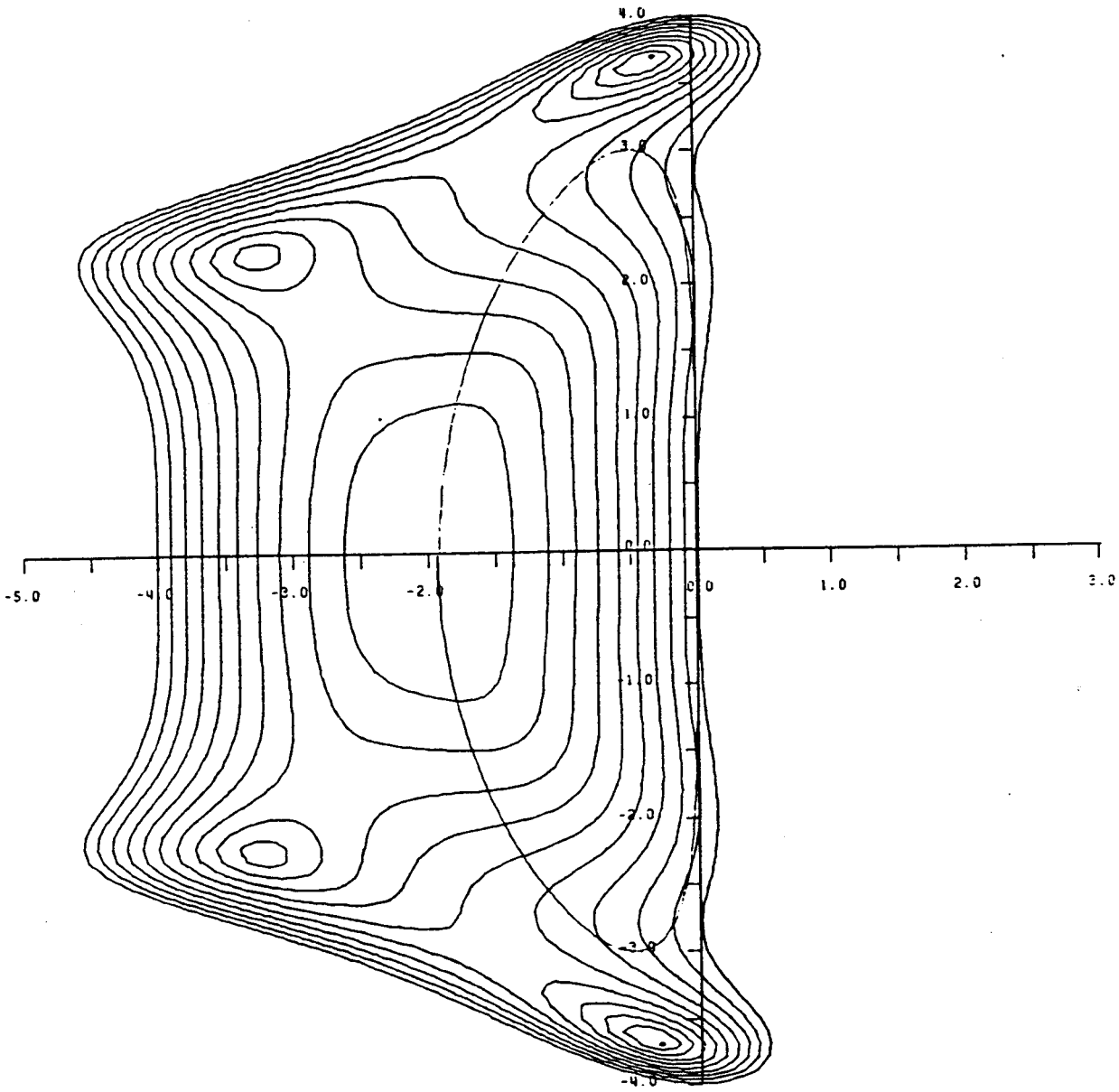

(a) Stability region of 5 stage scheme with two evaluations of dissipation Contour lines $|g| = .9, .8, .7 \ldots$ and locus of $z(\xi)$ for $\lambda = 3, \mu = 0.04$ Coefficients $\alpha_1 = 1/4, \alpha_2 = 1/6, \alpha_3 = 3/8, \beta = 1$

Figure 5.7:

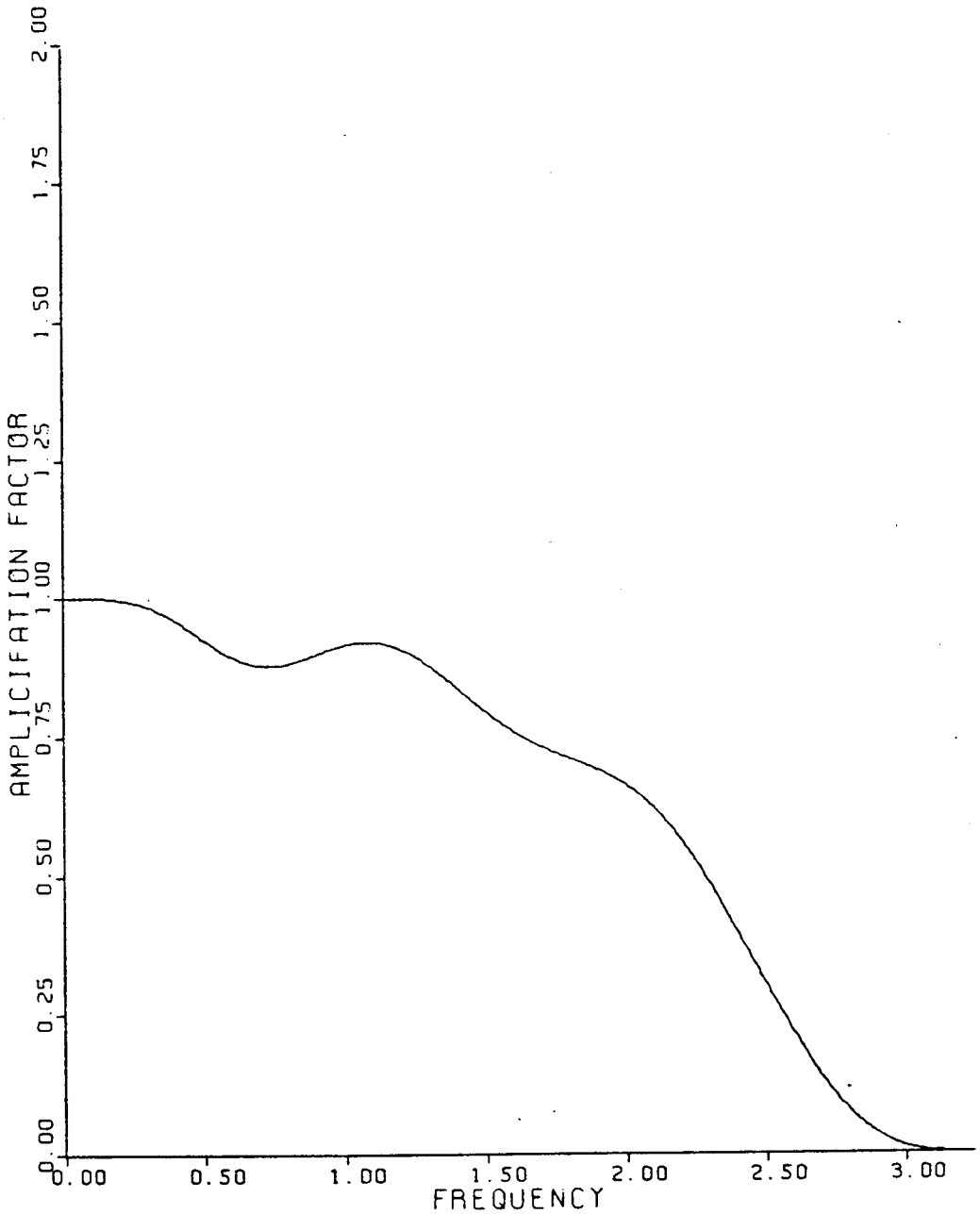

(b) Amplification factor 5 stage scheme with two evaluations of dissipation for $\lambda = 3, \mu = 0.04$ Coefficients $\alpha_1 = 1/4, \alpha_2 = 1/6, \alpha_3 = 3/8, \beta = 1$

Figure 5.7:

the results of some numerical experiments in which the multigrid multi-stage time stepping scheme was applied to initial data satisfying (5.52), to test its ability to recover a steady solution. The semi-discretization has the form

$$\frac{du_i}{dt} + \frac{1}{\Delta x}(f_{i+1/2} - f_{i-1/2} - d_{i+1/2} + d_{i-1/2}) = 0$$

where $f_{i+1/2}$ is the convective flux

$$f_{i+1/2} = 1/4(u_{i+1}^2 + u_i^2)$$

and $d_{i+1/2}$ is the artificial dissipative flux.

Several alternative forms of the dissipative flux were tested:

1) Adaptive Dissipation (Section 5e)

$$\begin{aligned} d_{i+1/2} &= \epsilon^{(2)}_{i+1/2}\alpha_{i+1/2}(u_{i+1} - u_i) \\ &\quad -\epsilon^{(4)}_{i+1/2}\alpha_{i+1/2}(u_{i+2} - 3u_{i+1} + 3u_i - u_{i-1}) \end{aligned}$$

where

$$\alpha_{i+1/2} = \frac{1}{4}|u_{i+1} + u_i| \text{ (scheme 1a)}$$

or

$$\alpha_{i+1/2} = \frac{1}{4}\{|u_{i+1}| + |u_i|\} \text{ (scheme 1b)}$$

Also $\epsilon^{(2)}_{i+1/2}$ and $\epsilon^{(4)}_{i+1/2}$ are determined by defining a sensor

$$\nu_i = \frac{|u_{i+1} - 2u_i + u_{i-1}|}{|u_{i+1}| + 2|u_i| + |u_{i-1}|}$$

Set

$$\bar{\nu}_{i+1/2} = \max(\nu_{i+2}, \nu_{i+1}, \nu_i, \nu_{i-1})$$

Then

$$\epsilon^{(2)}_{i+1/2} = \min(0, k^{(2)}, \bar{\nu}_{i+1/2})$$

and

$$\epsilon^{(4)}_{i+1/2} = \max(0, k^{(4)} - \bar{\nu}_{i+1/2})$$

By choosing $k^{(2)} = 1$ the scheme is locally TVD whenever $\nu_{i+1/2} \geq 1$

2) TVD Scheme (Section 5f)

$$\begin{aligned} d_{i+1/2} &= \alpha_{i+1/2}(u_{i+1}-u_i) - \tfrac{1}{2}(g_{i+1}+g_i) \\ &\quad + \tfrac{1}{2}|g_{i+1}-g_i|\text{sign}(u_{i+1}-u_i|) \end{aligned}$$

where

$$\alpha_{i+1/2} = \frac{1}{4}|u_{i+1}+u_i|$$

or

$$\alpha_{i+1/2} = \frac{1}{4}\{|u_{i+1}|+|u_i|\}$$

Also the anti-diffusive flux g_i is determined by

$$\tilde{g}_{i+1/2} = \alpha_{i+1/2}(u_{i+1}-u_i)$$

and

$$g_i = B(\tilde{g}_{i+1/2}, \tilde{g}_{i-1/2})$$

where $B(r,s)$ is the min-mod function (5.23). The choice of a $\alpha_{i+1/2}$ in schemes la and 2a allows a stationary shock with at most one interior point, but also allows a stationary expansion shock. The alternative form used in schemes lb and 2b excludes the stationary expansion shock, and still allows a discrete shock with no tail, but now with 2 interior points, as may be verified solving a quadratic equation.

Calculations were performed with a 3 stage time stepping scheme in which the dissipative terms were evaluated twice, as defined by equations (5.30) and (5.48), with the coefficients

$$\alpha_1 = .6, \quad \alpha_2 = .6, \quad \beta = .35$$

The stability region of this scheme is shown in Figure 5.8. The grid contained 128 cells, and 5 grid levels were used in the multigrid scheme.

Figure 5.9 shows a typical evolution using scheme la. Figure 5.9(a) shows the first 10 time steps, starting from the initial data at the bottom of the figure. It can be seen that by the completion of the 6th step the solution is indistinguishable from the final steady solution, illustrated in Figure 5.9(b). In this case the symmetry of the initial data results in a shock wave with no interior points. The convergence history measured by the average value of eau/ati is shown in Figure 5.9(c). Figure 5.10 shows a similar evolution with shifted initial data. The shock wave in the final steady state is displaced to the right and contains a single interior point, as a consequence of the choice of the viscosity coefficient $\alpha_{i+1/2}$. Figure 5.11 shows the first calculation repeated with scheme 1b. The final solution now has a shock wave with 2 interior points because of the additional dissipation introduced by the choice of an entropy satisfying viscosity coefficient. The TVD schemes 2a and 2b produced results which were essentially identical to those produced by schemes la and lb, but with a slower rate of convergence to a steady state.

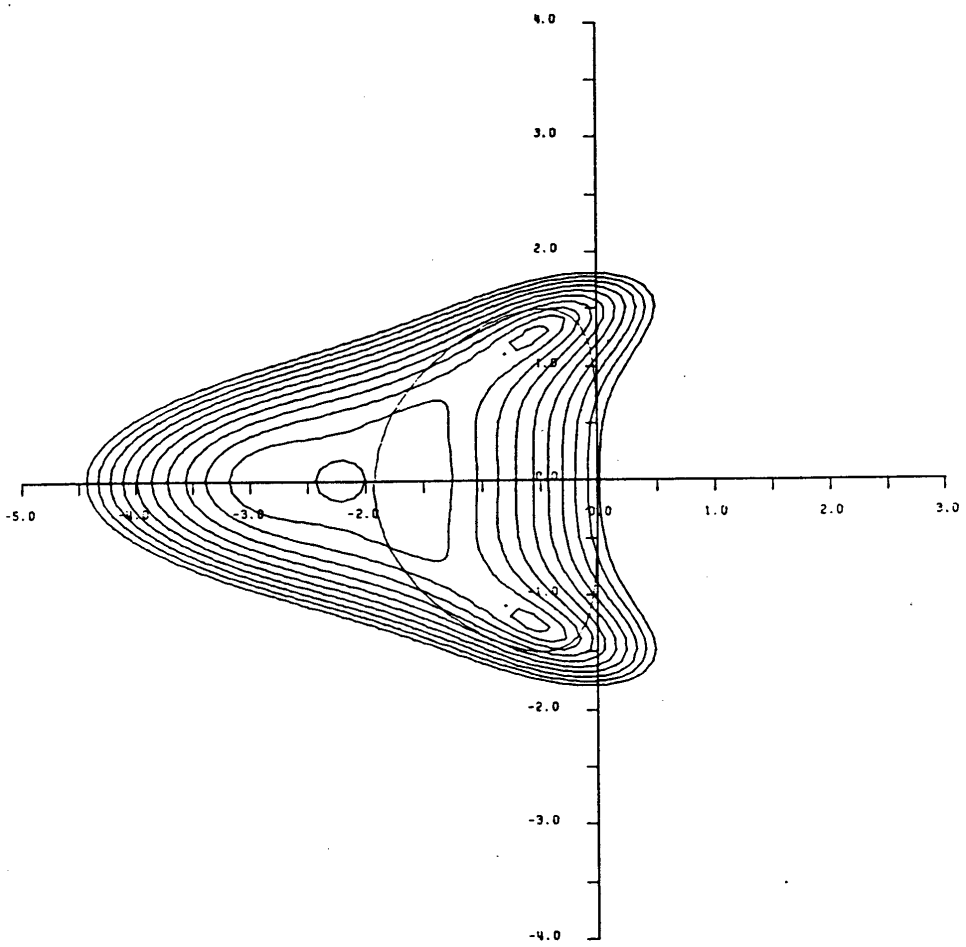

Figure 5.8: Stability region of 3 stage scheme with two evaluations of dissipation Contour lines $|g| = 1., .9, .8, \ldots$ and locus of $z(\xi)$ for $\lambda = 1.5, \mu = .08$ Coefficients $\alpha_1 = .6, \alpha_2 = .6, \beta = .625$

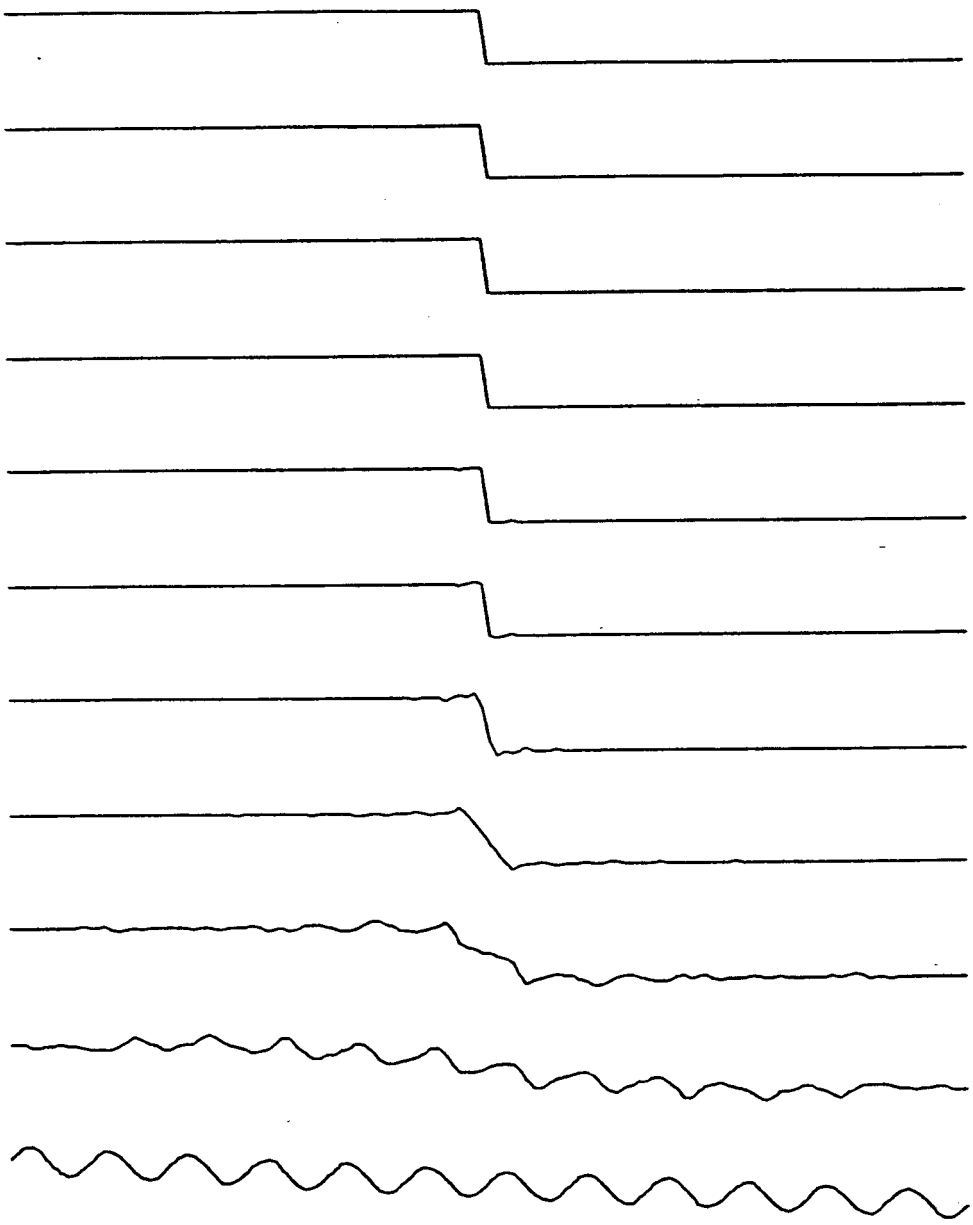

(a) Initial state and first 10 cycles in evolution of Burger's equation (reading upwards) Adaptive dissipation(scheme 1a) 128 cells 5 grids $\lambda = 2.0$

Figure 5.9:

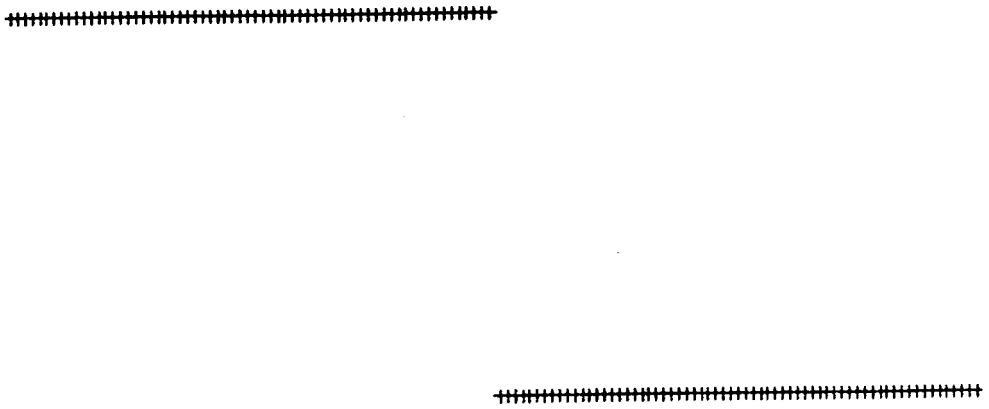

(b) Final state of Burger's equation after 20 cycles of the multigrid scheme Residual $.532710^{-8}$

Figure 5.9:

l) Results from the Euler Equations

This section presents some typical results of multigrid calculations of the Euler equations for two-dimensional flow. The 5 stage scheme defined by equation (5.50) was used in all the examples, and residual averaging was also used to allow steps corresponding to a Courant number of 7.5. Results are first presented for the standard scheme with adaptive dissipation as defined in Section 4.

The first example is the flow past a circular cylinder at Mach .50, calculated on a grid with 128 cells in the circumferential direction and 32 cells in the radial direction. The inner part of the grid is shown in Figure 5.12(a). The calculation was started from an initial condition of uniform flow. Figure 5.12(b) shows the final pressure distribution in terms of the pressure coefficient $c_p = (p - p_\infty)/1/2\rho_\infty q_\infty^2$. There is a shockwave of moderate strength slightly beyond the crest of the cylinder. Figure 5.12(c) shows the convergence history. One curve shows the decay of the logarithm of the error (measured by the root mean square rate of change of density on the fine grid): the mean rate of convergence is just under .8 per multigrid cycle. The other curve shows the build up of the number of grid points in the superzonic zone: it can be seen that the flow field is fully developed in about 30 cycles.

The next examples are transonic flows past airfoils. Figure 5.13 shows the result for the NACA 0012 airfoil at Mach .8 and an angle of attack a = 1.250, and Figure 5.14 shows the result for the Korn airfoil at Mach .75 and a = 00. An 0-mesh was used in these calculations with the outer boundary at a distance of about 50 chords. Each result was obtained with 50 cycles on an 80 x 16 mesh, followed by 50 cycles on a 160 x 32 mesh. This was sufficient for full development of the flow field. The flow past the NACA

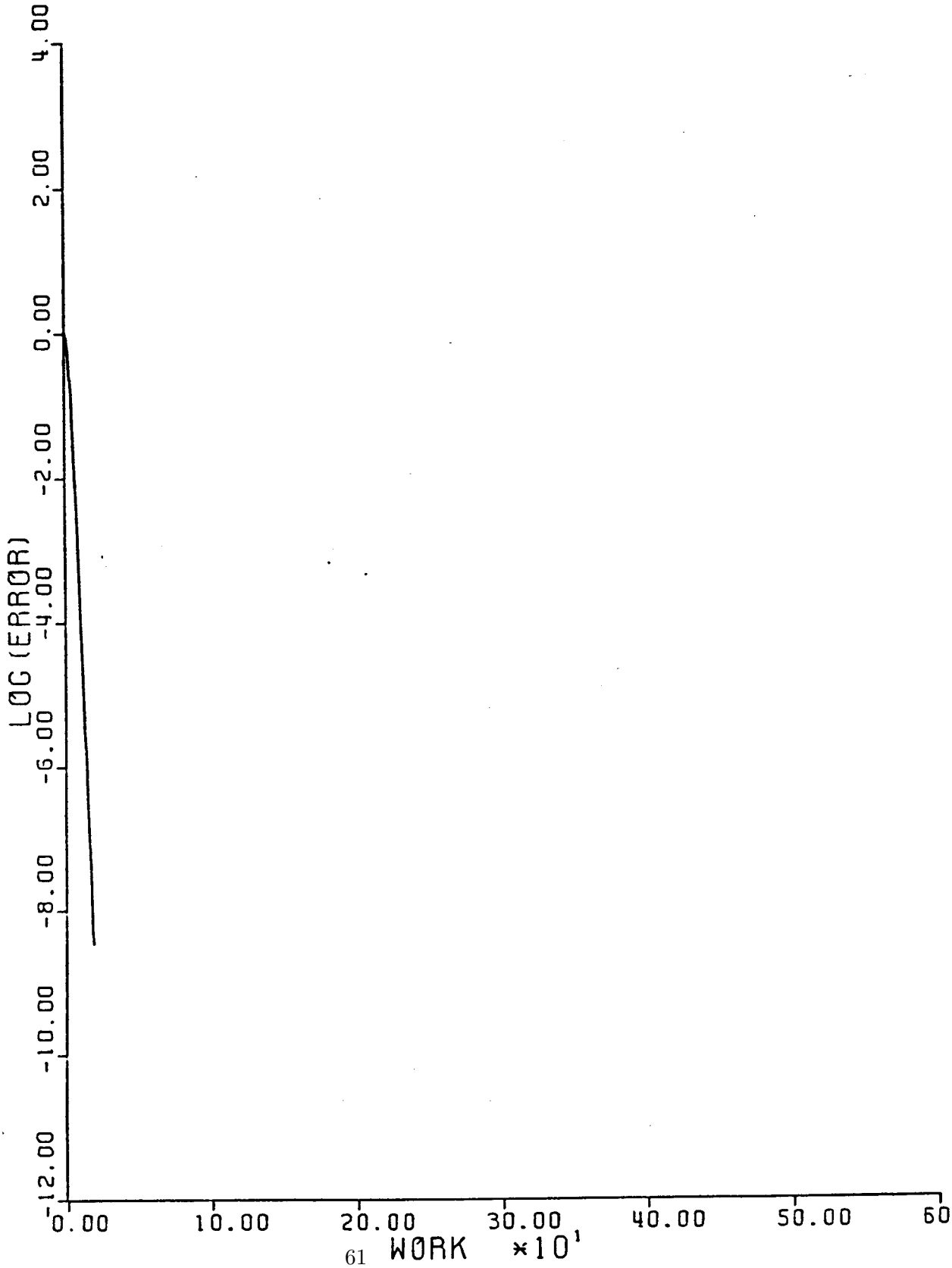

(c) Convergence history for Burger's equation Adaptive Dissipation (scheme 1a) 128 cells 5 grids $\lambda = 2.0$ Mean rate of reduction .3587 per cycle.

Figure 5.9:

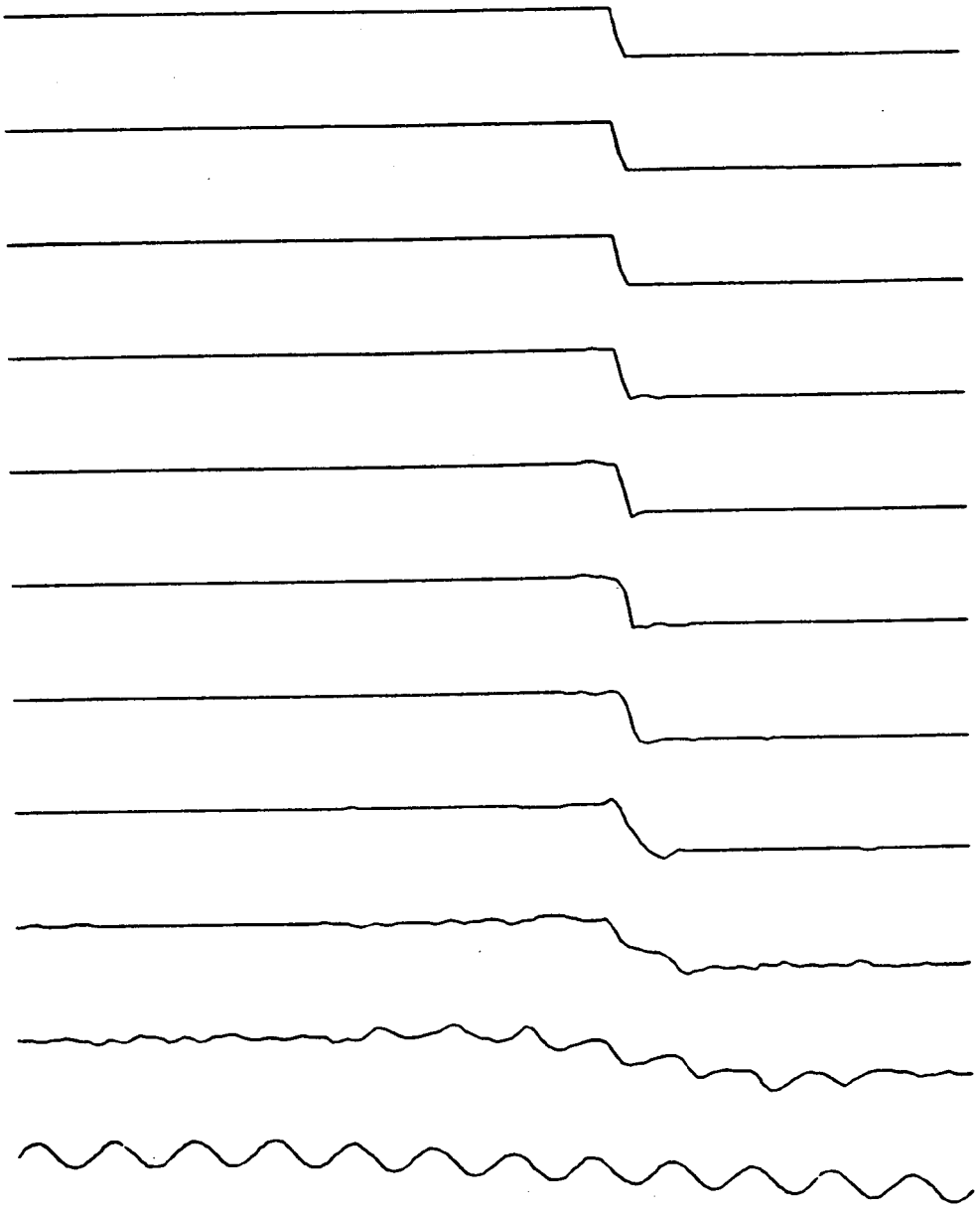

(a) Initial state and first 10 cycles in evolution of Burger's equation (reading upwards) Adaptive dissipation(scheme 1a) 128 cells 5 grids $\lambda = 2.0$

Figure 5.10:

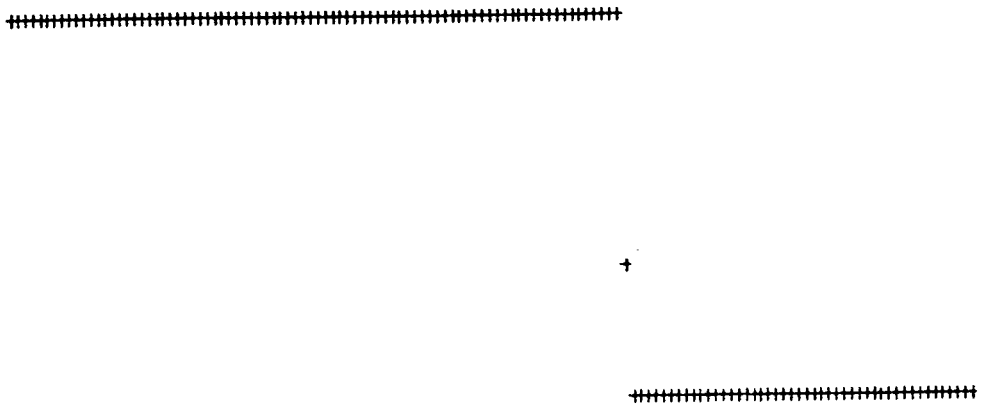

(b) Final state of Burger's equation after 20 cycles of the multigrid scheme Residual $.247610^{-6}$

Figure 5.10:

0012 airfoil contains a fairly strong shock wave on the upper surface, which is resolved in about 5 mesh cells, and a weak shock wave on the lower surface, which is quite smeared. The Korn airfoil is designed to be shock free at the given Mach number and angle of attack. The result of the Euler calculation is in close agreement with the result of the design calculation [89]. The drag should be zero in a shock free flow, and the calculated value of the drag coefficient $CD = .0005$ is an indication of the level of discretization error. Another measure of error is the entropy, which should also be zero. In this calculation the entropy, measured by $\frac{p}{\rho^\gamma} - \frac{p_\infty}{\rho_\infty^\gamma}$, is less than .001 everywhere in the flow field.

The final example shows the effect of replacing the scheme with adaptive dissipation by the TVD scheme for the case of the NACA 0012 airfoil at Mach .8 and $\alpha = 1.25^\circ$. The result is shown in Figure 5.15. It can be seen that sharper shock waves are obtained, with one interior cell. The entropy level ahead of the shock waves is much higher than in the calculation shown in Figure 5.12, however, and the stagnation enthalpy is no longer constant.

These results clearly demonstrate that the convergence of a time dependent hyperbolic system to a steady state can be substantially accelerated by the introduction of multiple grids. With the formulation here proposed, the steady state is entirely determined by the space discretization scheme on the fine grid. It is independent of both the time stepping scheme, and the discretization procedure used on the coarse grids. Either of these could be modified in any way which would improve the rate of convergence or reduce the computational effort. The existing scheme captures shocks fairly well using the adaptive dissipation of Section 5e. The shock resolution is improved by the use of the TVD scheme of Section 5f, at the expense of larger errors in the smooth part of the flow.

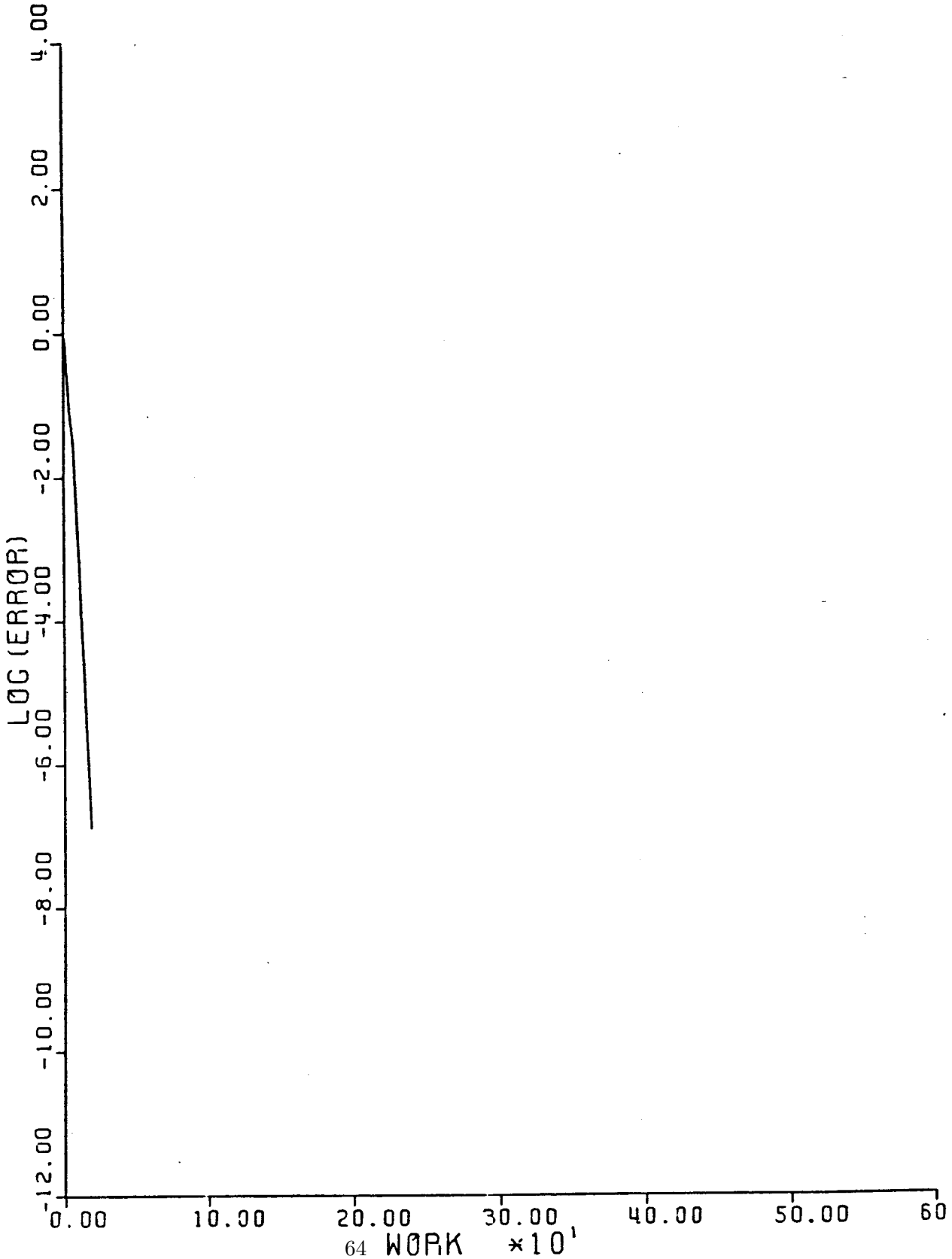

(c) Convergence history for Burger's equation Adaptive Dissipation (scheme 1a) 128 cells 5 grids $\lambda = 2.0$ Mean rate of reduction .4339 per cycle.

Figure 5.10:

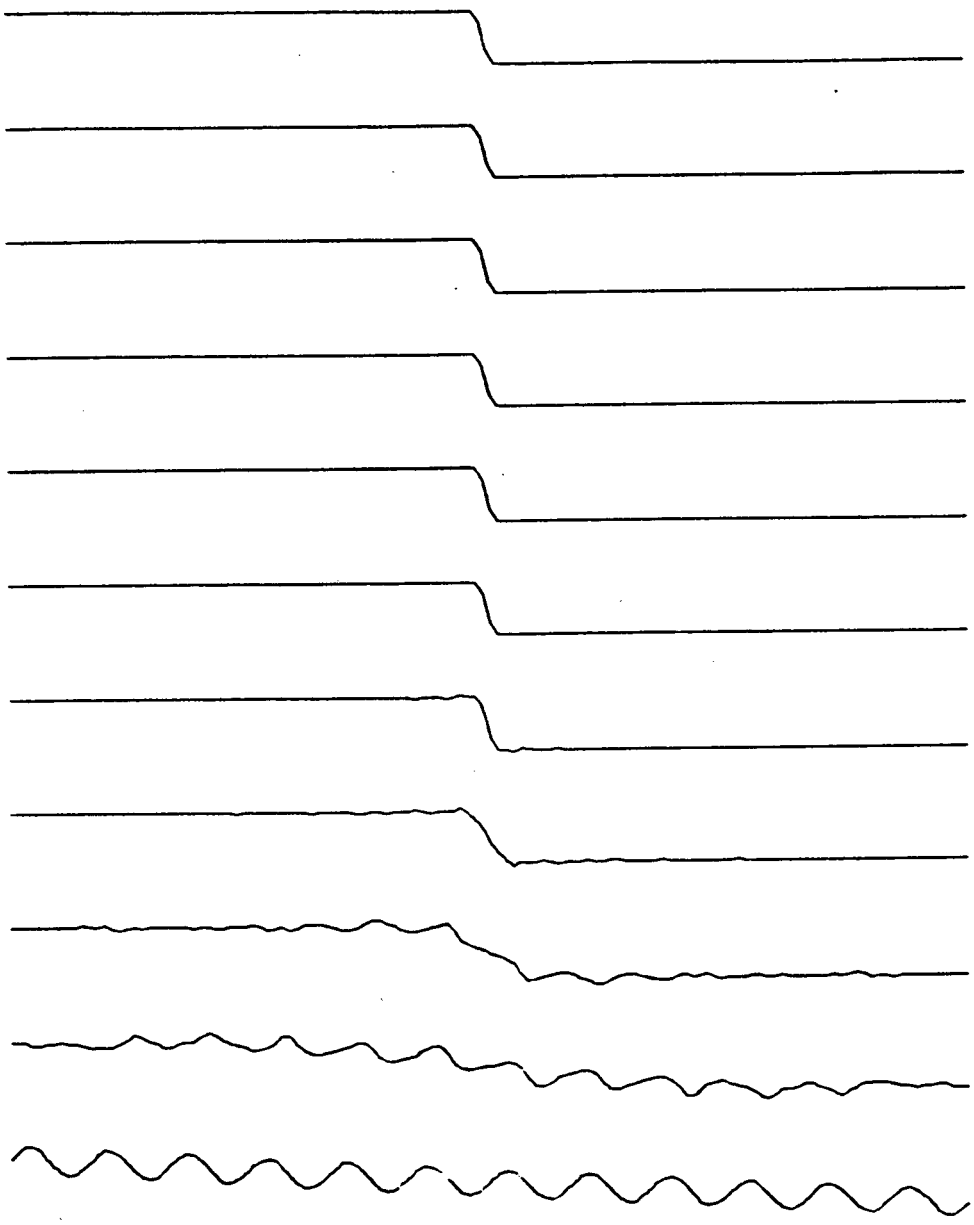

(a) Initial state and first 10 cycles in evolution of Burger's equation (reading upwards)
Adaptive dissipation(scheme 1b) 128 cells 5 grids $\lambda = 2.0$

Figure 5.11:

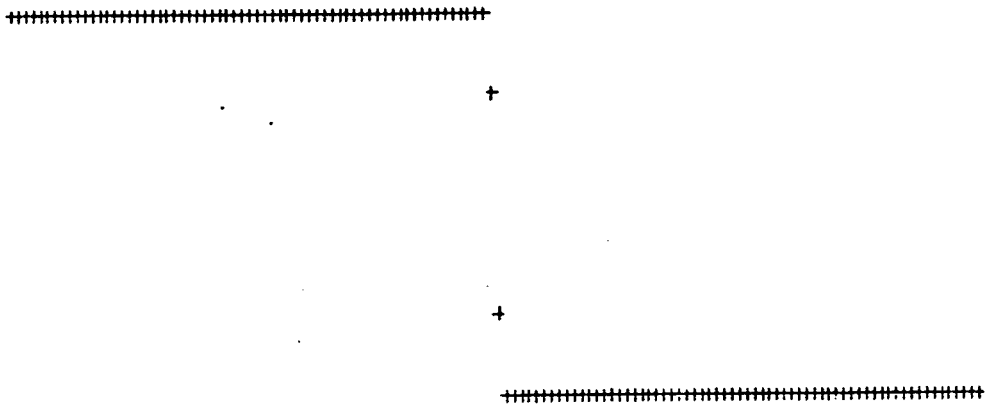

(b) Final state of Burger's equation after 20 cycles of the multigrid scheme Residual $.902810^{-8}$

Figure 5.11:

6 Viscous Flow Calculations

a) Boundary Layer Corrections

While it is true that the viscous effects are relatively unimportant outside the boundary layer, the presence of the boundary layer can have a drastic influence on the pattern of the global flow. This will be the case, for example, in the event that the flow separates. The boundary layer can also cause global changes in a lifting flow by changing the circulation. These effects are particularly pronounced in transonic flows. The presence of a boundary layer can cause the location of the shock wave on the upper surface of the wing to shift 20% of the chord.

While we must generally account for the presence of the boundary layer, the accuracy attainable in solutions of the Navier Stokes equations for complete flow fields is severely limited by the extreme disparity between the length scales of the viscous effects, and those of the gross patterns of the global flow. This has encouraged the use of methods in which the equations of viscous flow are solved only in the boundary layer, and the external flow is treated as inviscid. These zonal methods can give very accurate results in many cases of practical concern to the aircraft designer. The underlying ideas have been comprehensively reviewed in recent papers by Lock and Firmin [90], LeBalleur [91], and Melnik [92].

The general features of a zonal method are Illustrated in Figure 6.1. In the outer region the real viscous flow is approximated by an equivalent inviscid flow, which has to be matched to the inner viscous flow by an appropriate selection of boundary conditions. In most of the boundary layer the viscous flow equations may consistently be approximated by the boundary layer equations. This is sufficient in regions of weak interaction, in which

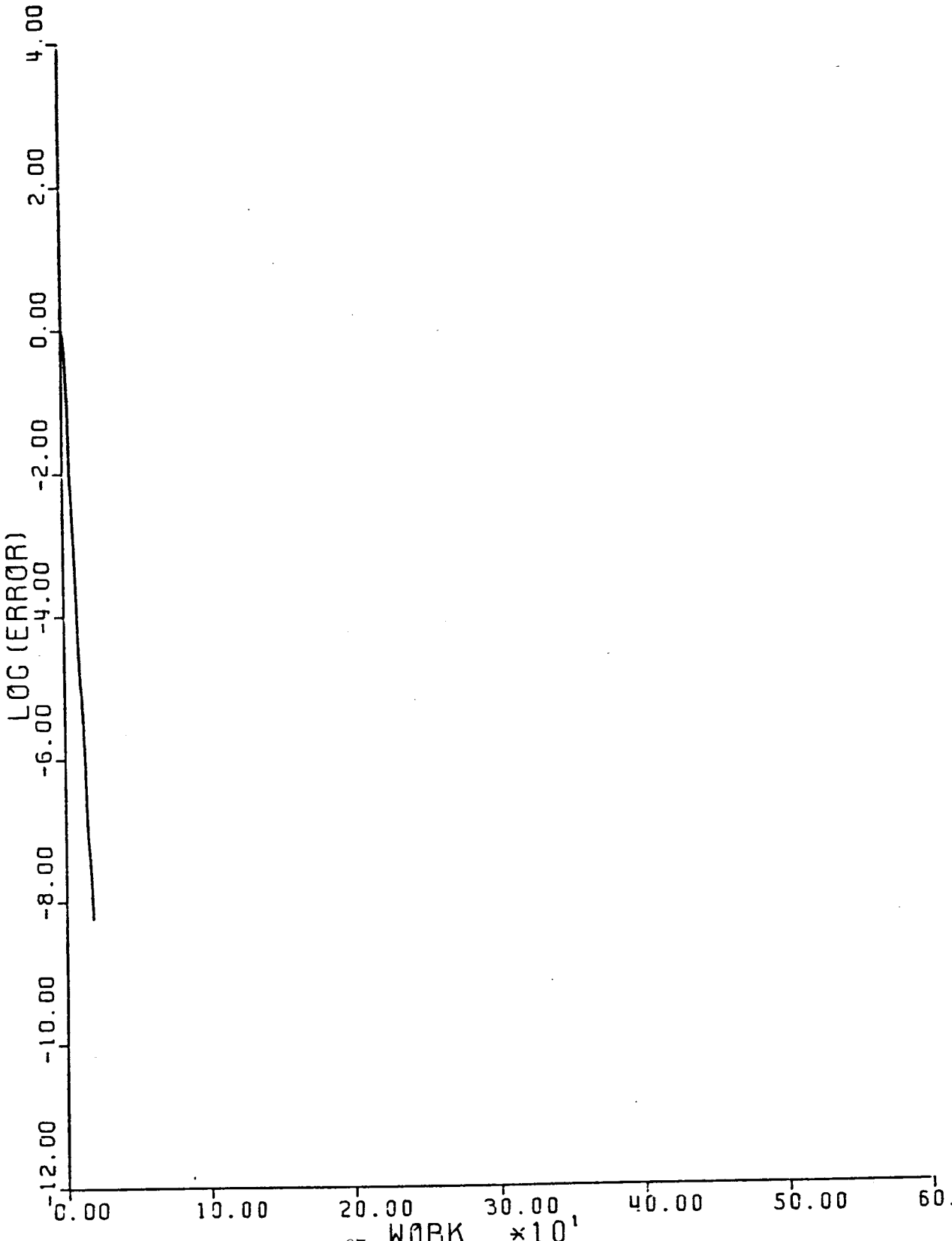

(c) Convergence history for Burger's equation Adaptive Dissipation (scheme 1a) 128 cells 5 grids $\lambda = 2.0$ Mean rate of reduction .3688 per cycle.

Figure 5.11:

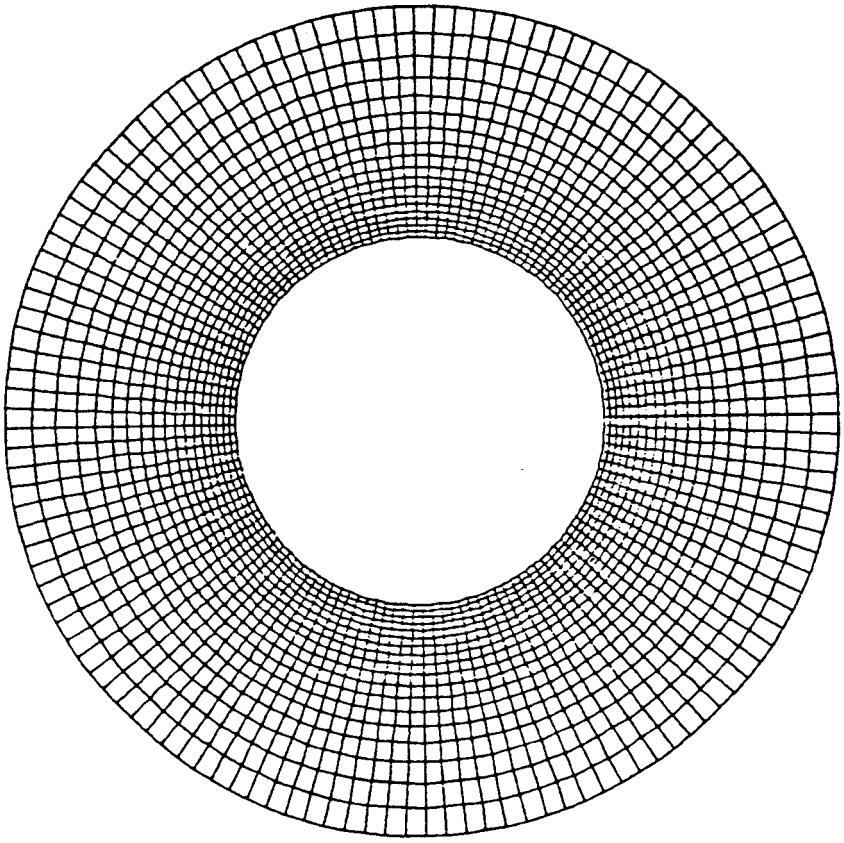

(a) Inner part of the grid for 128 X 32 cells

Figure 5.12:

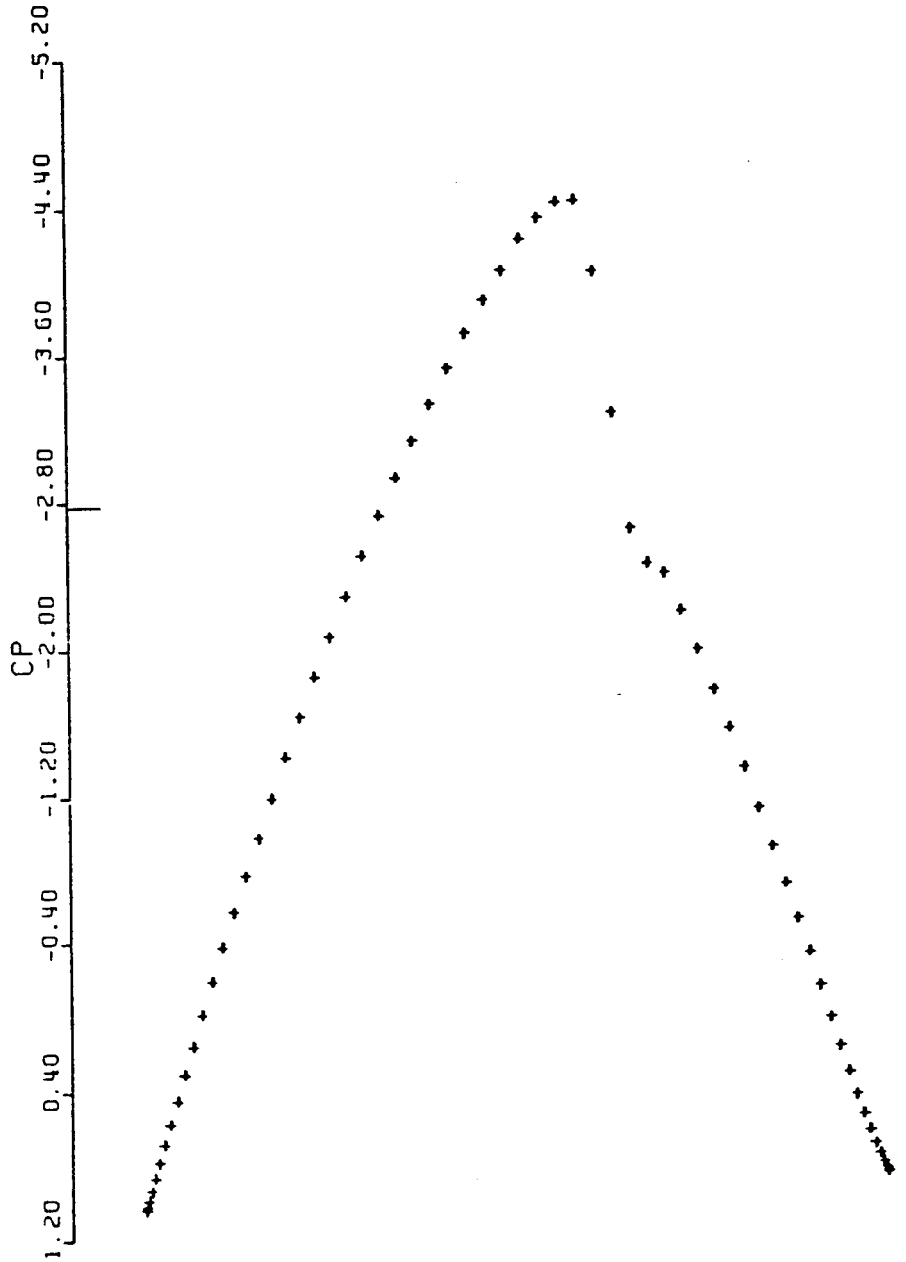

(b) Pressure distribution for circle Mach .450 CL 0. CD .0236 128X32 grid 100 cycles Residual $.77810^{-7}$

Figure 5.12:

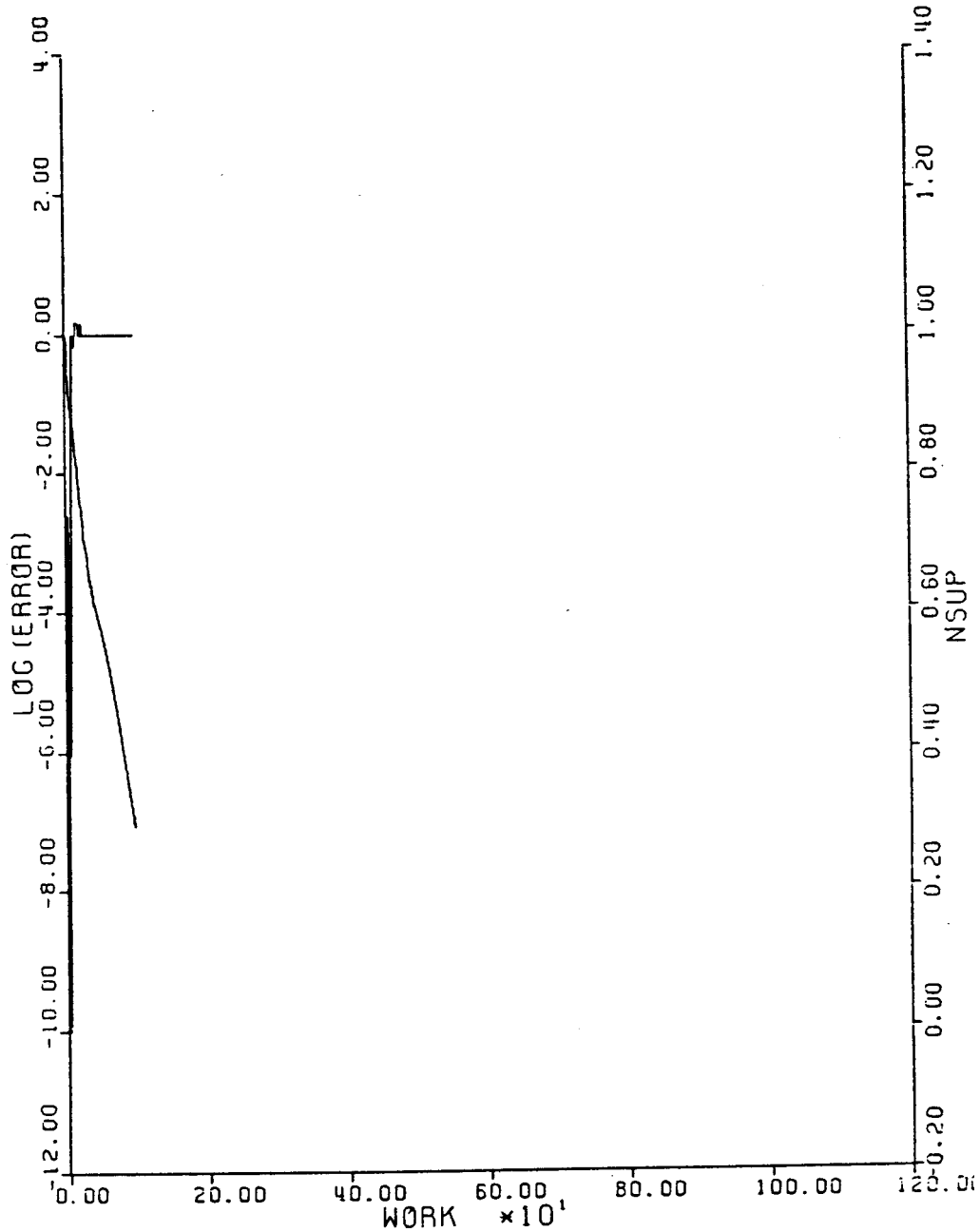

(c) Convergence history for circle Mach .450 CL 0. CD .0236 128X32 grid 100 cycles Residual $.77810^{-7}$ Mean rate of error reduction .8481 per cycle.

Figure 5.12:

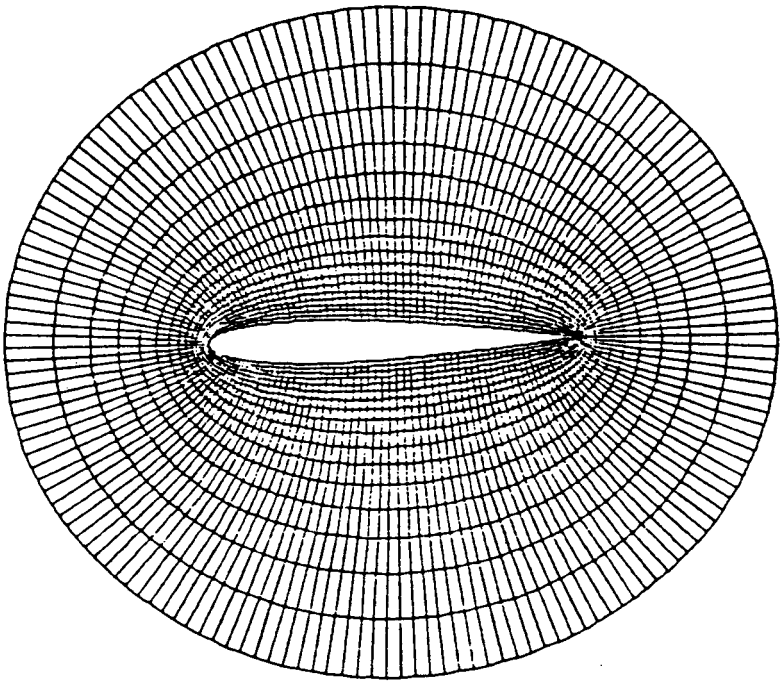

(a) Inner part of the grid for NACA 0012 160 X 32 cells

Figure 5.13:

the viscous effect on the pressure is small. There are, however, regions of strong interaction in which the classical boundary layer formulation fails, because of the appearance of strong normal pressure gradients across the boundary layer. Coupling conditions for the interaction between the inner viscous flow and the outer inviscid flow can be derived from an asymptotic analysis in which the Reynolds number is assumed to become very large. The two solutions could be patched at the outer edge of the boundary layer. It is often more convenient, however, to allow the equivalent inviscid flow to overlap the inner viscous region.

A complete analysis of the viscous flow over an airfoil should include the following principal effects:

1. The displacement effect of the boundary layer over the airfoil
2. The displacement effect of the wake
3. The wake curvature effect induced by the momentum defect in the wake
4. The Interaction of the boundary layer with the trailing edge
5. The interaction of the boundary layer with shock waves

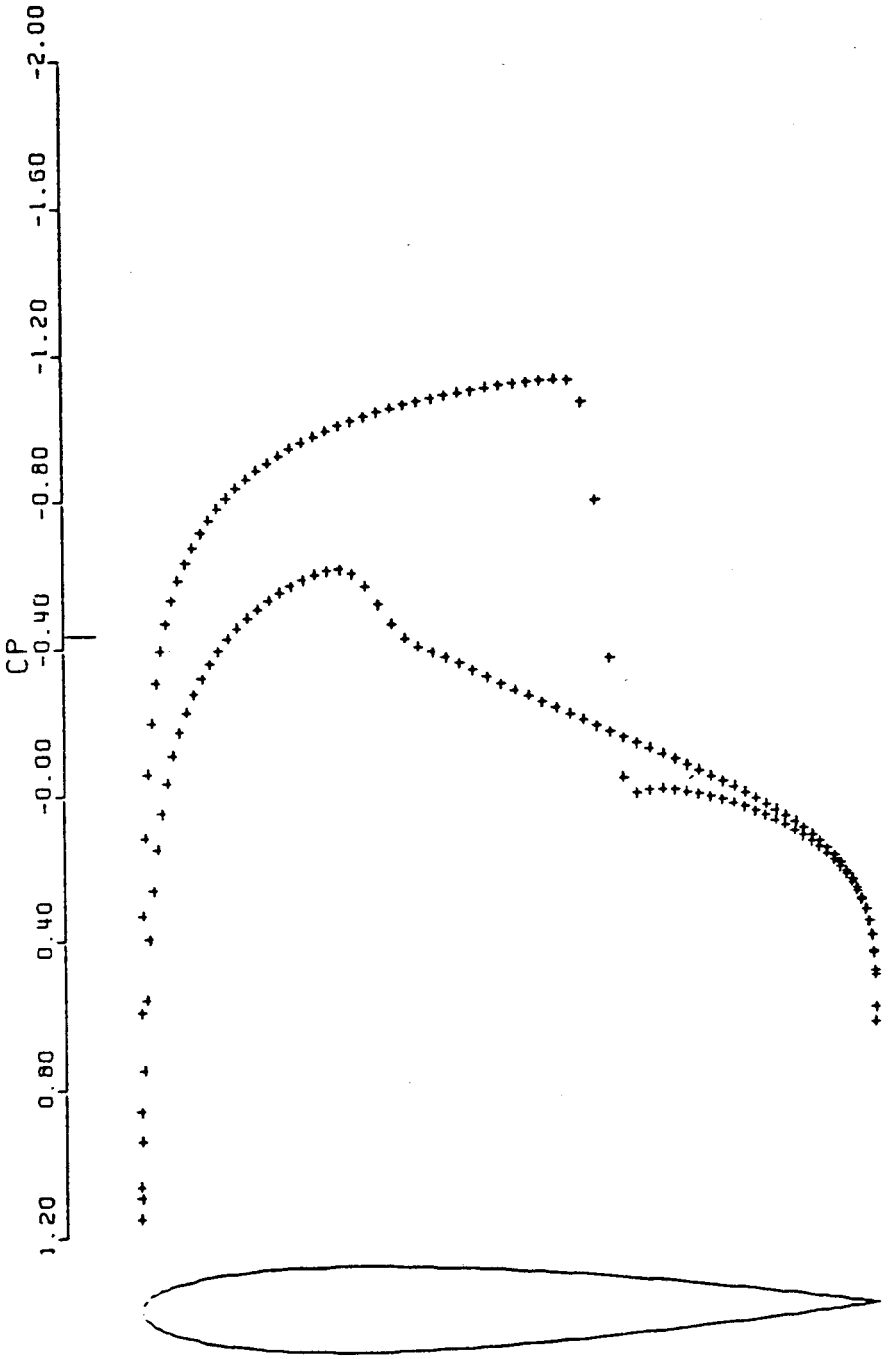

(b) Pressure distribution for NACA 0012 Mach .800 α1.25° CL .3504 CD .0227
160X32 grid 50 cycles Residual .15210^{-3}

Figure 5.13:

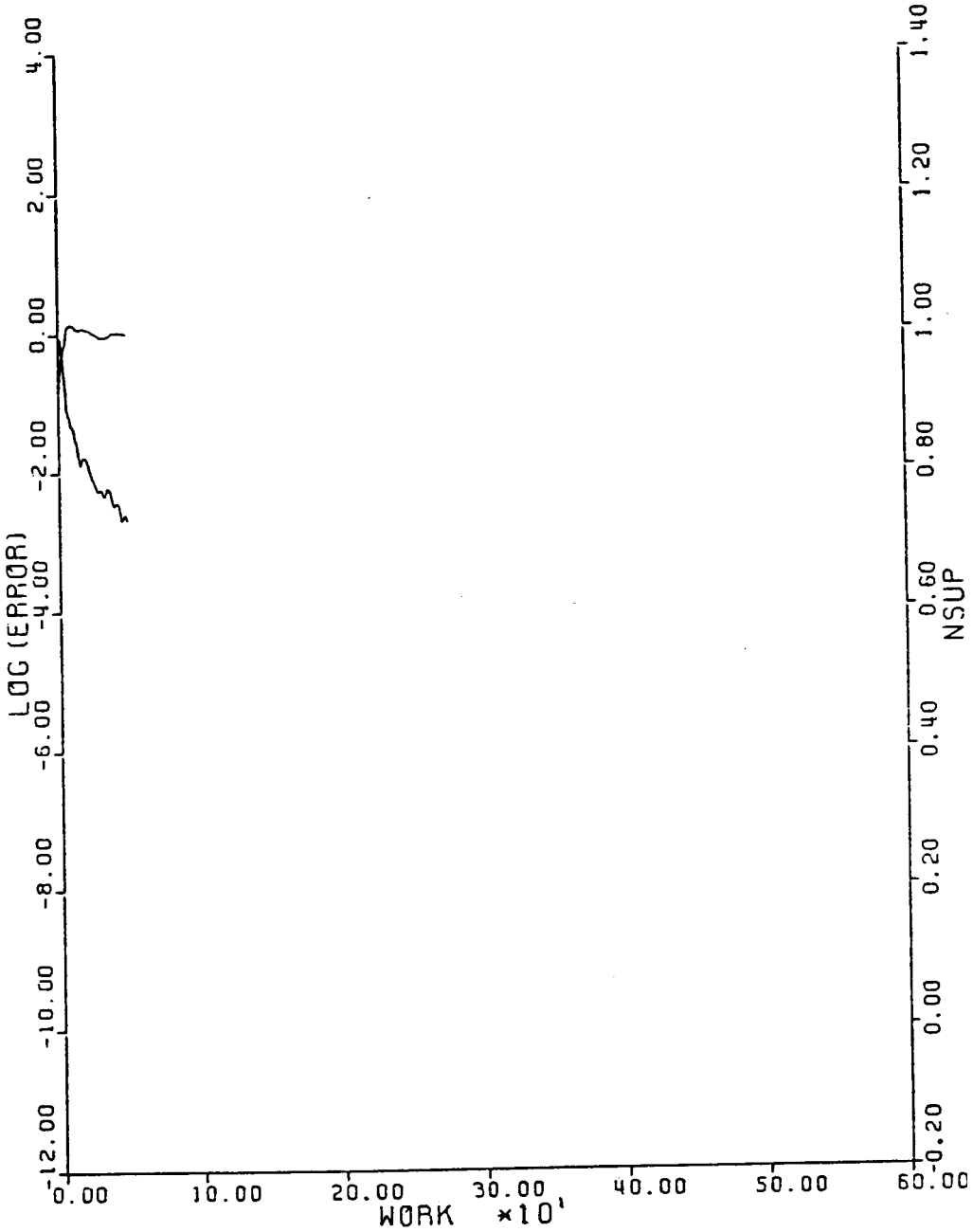

(c) Convergence history for NACA 0012 Mach .800 α1.25° CL .3504 CD .0227 160X32 grid 50 cycles Residual .15210^{-3} Mean rate of error reduction .8817 per cycle.

Figure 5.13:

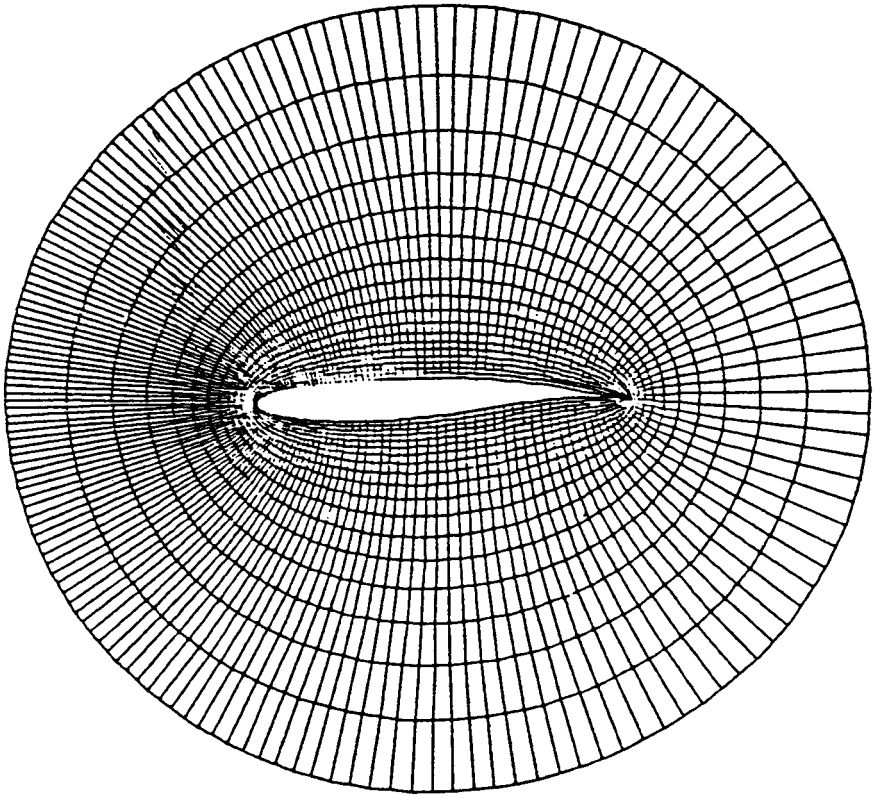

(a) Inner part of the grid of Korn airfoil 160 X 32 cells

Figure 5.14:

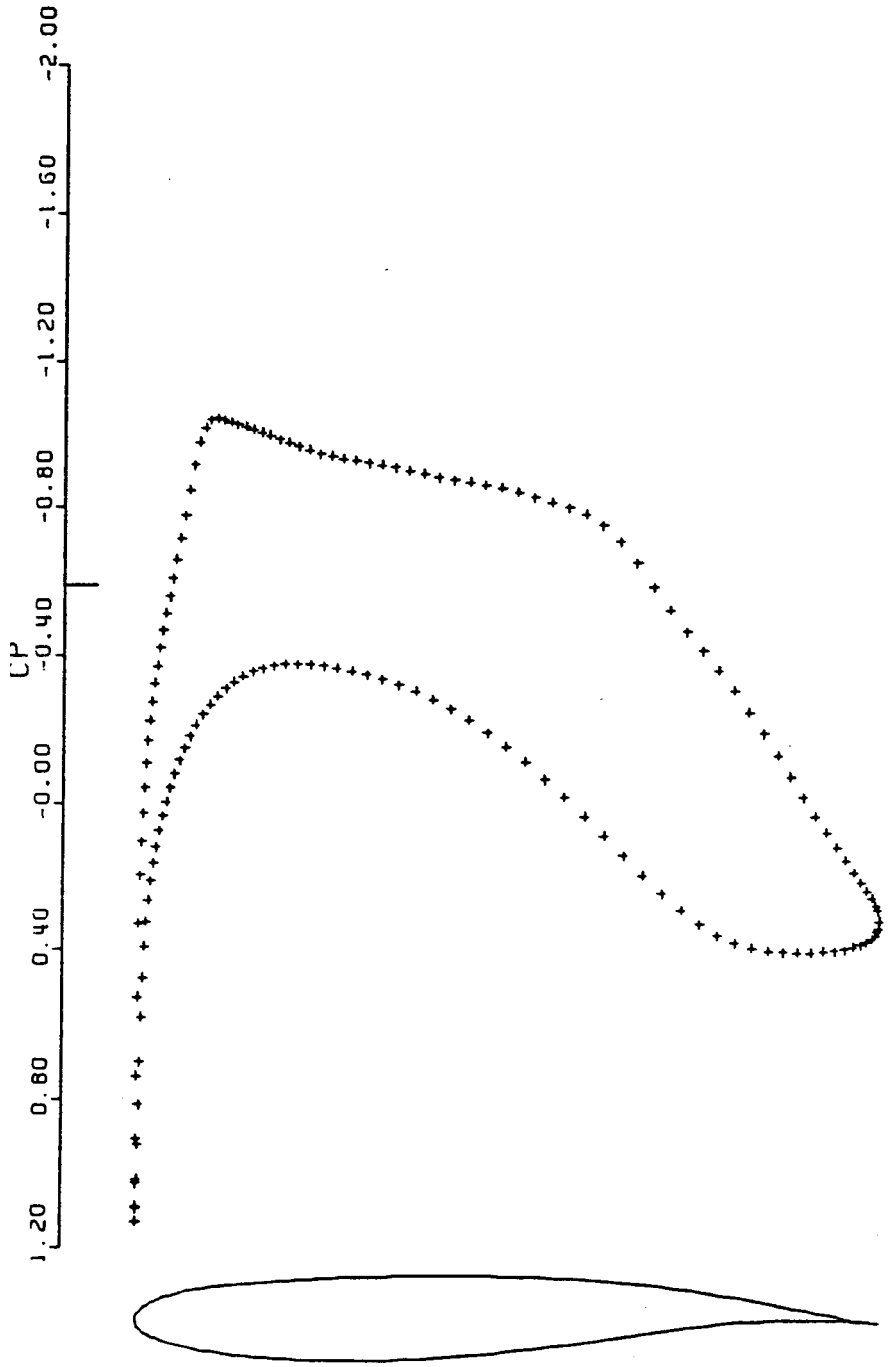

(b) Pressure distribution for Korn airfoil Mach .750 $\alpha 0^\circ$ CL .6254 CD .005 160X32 grid 50 cycles Residual $.11210^{-3}$

Figure 5.14:

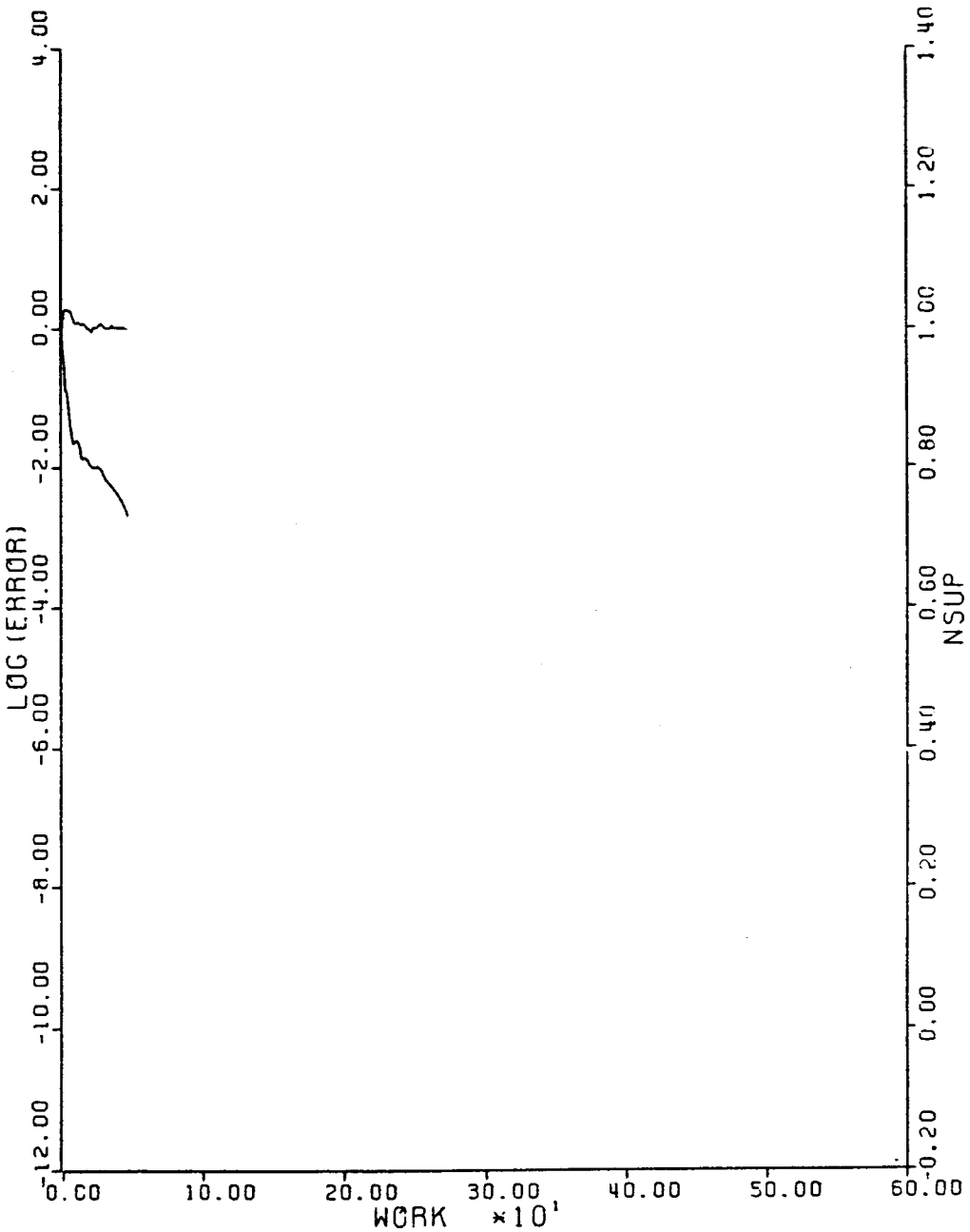

(c) Convergence history for Korn airfoil Mach .750 $\alpha 0^\circ$ CL .6254 CD .005 160X32 grid 50 cycles Residual $.11210^{-3}$ Mean rate of error reduction .8820 per cycle.

Figure 5.14:

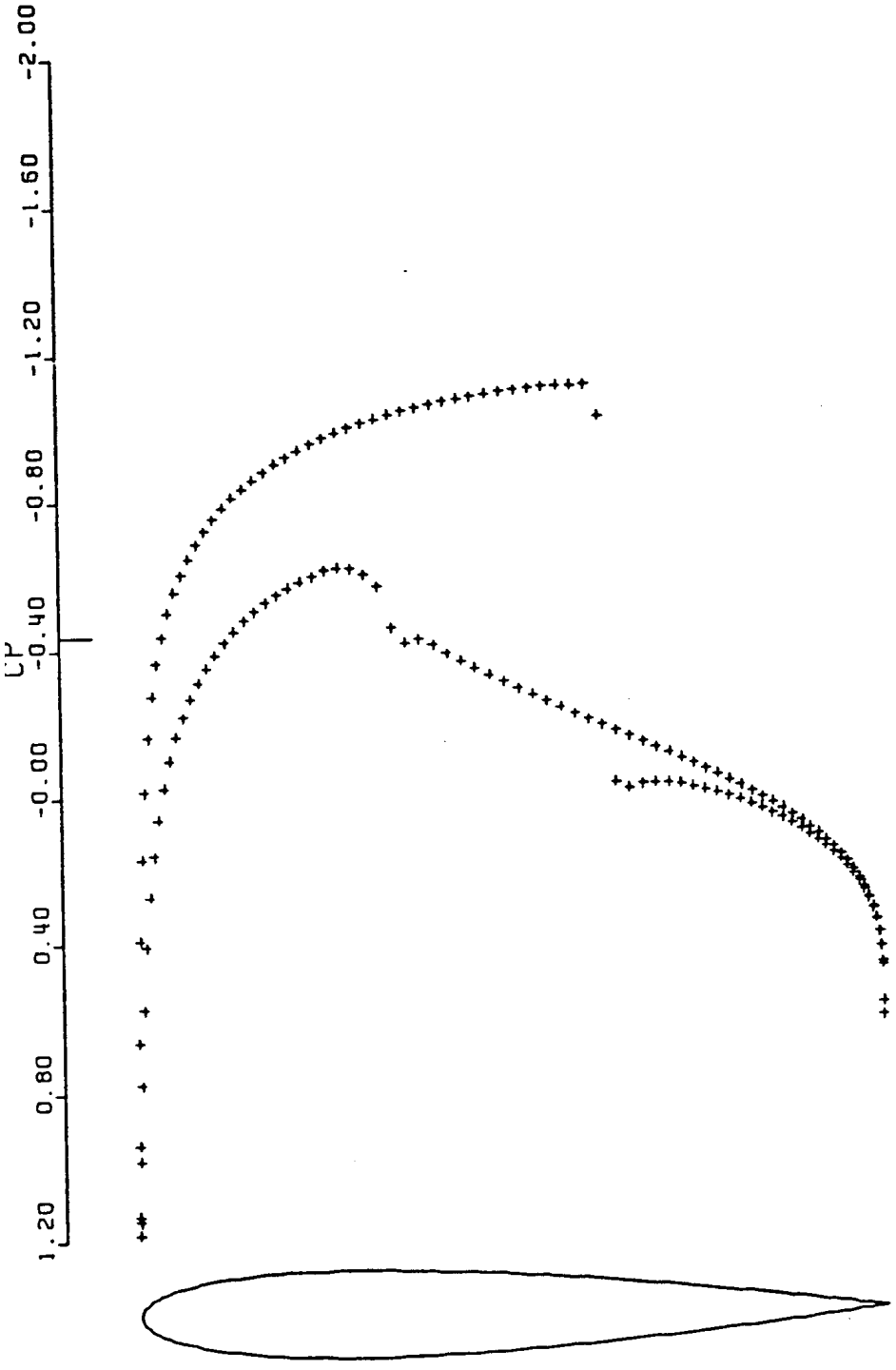

Figure 5.15: Pressure distribution for NACA 0012 Result using TVD scheme. Mach .800 α1.25° CL .3504 CD .0227 160X32 grid 500 cycles Residual $.86910^{-4}$

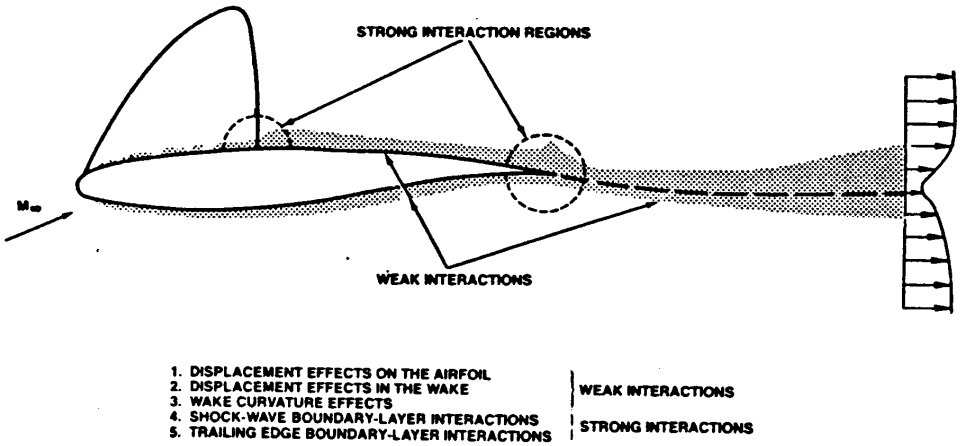

Figure 6.1: Viscid-Inviscid Interactions on Airfoils

The first three of these are weak Interactions, and the last two are strong interactions.

The displacement effect is caused by the outward displacement of the streamlines which results from the reduced mass flow in the boundary layer. This effect can be modeled by adding an equivalent thickness to the body, equal to the displacement thickness of the boundary layer, and applying the flow tangency condition at the surface of the modified body. An alternative formulation, discussed, for example, by Lighthill, is to extend the equivalent inviscid flow to the real body, and to apply a transpiration boundary condition [93]. This condition can be derived by considering the defect equation for the difference between the inviscid and viscous flows [90, 91]. By integrating the continuity equation across the boundary layer, and assuming that the inviscid and viscous flows match at the edge of the boundary layer, we find that

$$(\rho_i v_i)|_{\text{wall}} = \frac{d}{ds}\int_0^\delta (\rho_i u_i - \rho u) dn \tag{6.1}$$

where s and n are the streamwise and normal directions, δ is the boundary layer thickness, and the subscript i denotes the inviscid flow. This is the boundary condition that is now applied in the calculation of the equivalent inviscid flow. We can write it as

$$(\rho v)|_{\text{wall}} = \frac{dQ}{ds} \tag{6.2}$$

where Q is the mass flux defect defined by the integral in equation (6.1). If the outer inviscid flow is represented by the Euler equations, similar defect equations for the momentum and energy provide the additional boundary conditions that are needed to solve the Euler equations [94]. The displacement effect is usually more pronounced on the upper surface than it is on

the lower surface. This leads to an equivalent decambering of the airfoil which acts to reduce the lift.

There is also a displacement effect due to the wake behind the airfoil. The matching condition for the wake displacement effect is

$$[v]_{\text{wake}} = \frac{1}{\rho_w}\frac{dQ_w}{ds} \tag{6.3}$$

where $[v]$ is the jump in the normal velocity across the wake, ρ_w is the average of the densities in the Inviscid flow on the two sides of the wake, and Q_w is the total mass flux defect in the wake. The main result of the wake displacement effect is a reduction in the pressure near the trailing edge, and a corresponding increase in the drag.

The curvature of the wake induces an additional reduction of the lift. Because there is a momentum defect in the wake, it acts like a jet flap with a negative momentum coefficient. The deflection of the wake towards the direction of the outer stream requires a normal pressure gradient, with the result that the pressure at the trailing edge is larger on the upper surface than it is on the lower surface. The Kutta condition for the equivalent inviscid flow-must be modified to allow for this difference in the pressures. The matching condition for the wake curvature effect is

$$[p]_{\text{wake}} = C_w\kappa_w \tag{6.4}$$

where $[p]$ is the jump in the pressure across the wake, C_w is the total momentum defect in the wake and κ_w is the wake curvature. The magnitude of the wake curvature effect is formally of the same order as that of the displacment effect.

The analysis of the flow in regions of strong interaction is more complicated because of the breakdown of the boundary layer approximation. In the region of the trailing edge the flow in the boundary layer accelerates, and the boundary layer thickness decreases, because the retardation of the flow by skin friction suddenly ceases. Melnik has developed a consistent model of the strong interaction of an unseparated turbulent boundary layer with a cusped trailing edge, under the assumption that the Reynolds number is large [85]. As the flow passes through a shockwave, the sharp pressure rise at the foot of the shock wave causes a steep thickening of the boundary layer. As long as the shock wave is not too strong, it turns out, however, that the growth of boundary layer thickness through the shockwave is quite well predicted by boundary layer theory, although the local details of the flow are not accurately modeled. Consequently the coupling condition (6.1) can still be used to obtain the global flow.

The coupled viscous and inviscid equations are solved iteratively. The simplest procedure is a direct one. The inviscid flow is first solved without a boundary layer, and the boundary layer is calculated using the wall pressure

from the inviscid solution as a boundary condition. The inviscid flow is then recalculated with a boundary condition which accounts for the presence of the boundary layer, and the process is repeated until the solution converges. A linearized analysis of this procedure indicates that it will generally be necessary to under-relax the changes in the boundary conditions, and that it will become unstable near a separation point [90, 95].

This difficulty has led to the introduction of semi-inverse methods in which the transpiration boundary condition is prescribed in both the inviscid flow calculation and the boundary layer calculation [95, 96]. The inviscid flow calculation provides an estimate u_e, I of the speed at the edge of the boundary layer. An inverse boundary layer method is used to calculate a corresponding estimate u_e, V of the speed at the edge of the boundary layer from the boundary layer equations. In Carter's method, [95], the equivalent mass flux defect Q appearing in the transpiration boundary condition (**??**) is then multiplied by the correction factor

$$1 + \omega \left(\frac{u_e, V}{u_e, I} - 1 \right)$$

where ω is a fixed relaxation factor, and the process is repeated. Le Balleur uses a more complicated correction formula with a locally varying relaxation factor [96]. These methods converge for flows containing separated regions.

The method of Bauer, Garabedian, Korn and Jameson was the first to incorporate boundary layer corrections into the calculation of transonic potential flow [89]. This method only accounted for displacement effects on the airfoil, And modeled the wake as a parallel semi-infinite strip. Nevertheless, this simple model substantially improved the agreement with experimental data. More complete theoretical models including effects due to the wake thickness and curvature have been developed by Collyer and Lock [97], Le Balleur [98], and Melnik, Chow, Mead, and Jameson [99]. Recently Whitfield, Thomas, Jameson, and Schmidt have developed a method based on the use of the Euler equations for the inviscid flow [100]. Figure 6.2 shows the result of a calculation by the method of Melnik, Chow, Mead, and Jameson. It can be seen that the inclusion of the boundary layer correction shifts the inviscid result into close agreement with the experimental data.

b) Reynolds Averaged Navier Stokes Equations

The simulation of attached flows by zonal methods now rests on a firm theoretical foundation, and has reached a high level of sophistication in practice. The treatment of three-dimensional flows is presently limited by a lack of available boundary layer codes for general configurations. During the last few years there has also emerged the possibility of simulating flows with small separated regions by zonal methods. In cases of massive flow separation, where the flow is often observed to be unsteady, adequate zonal

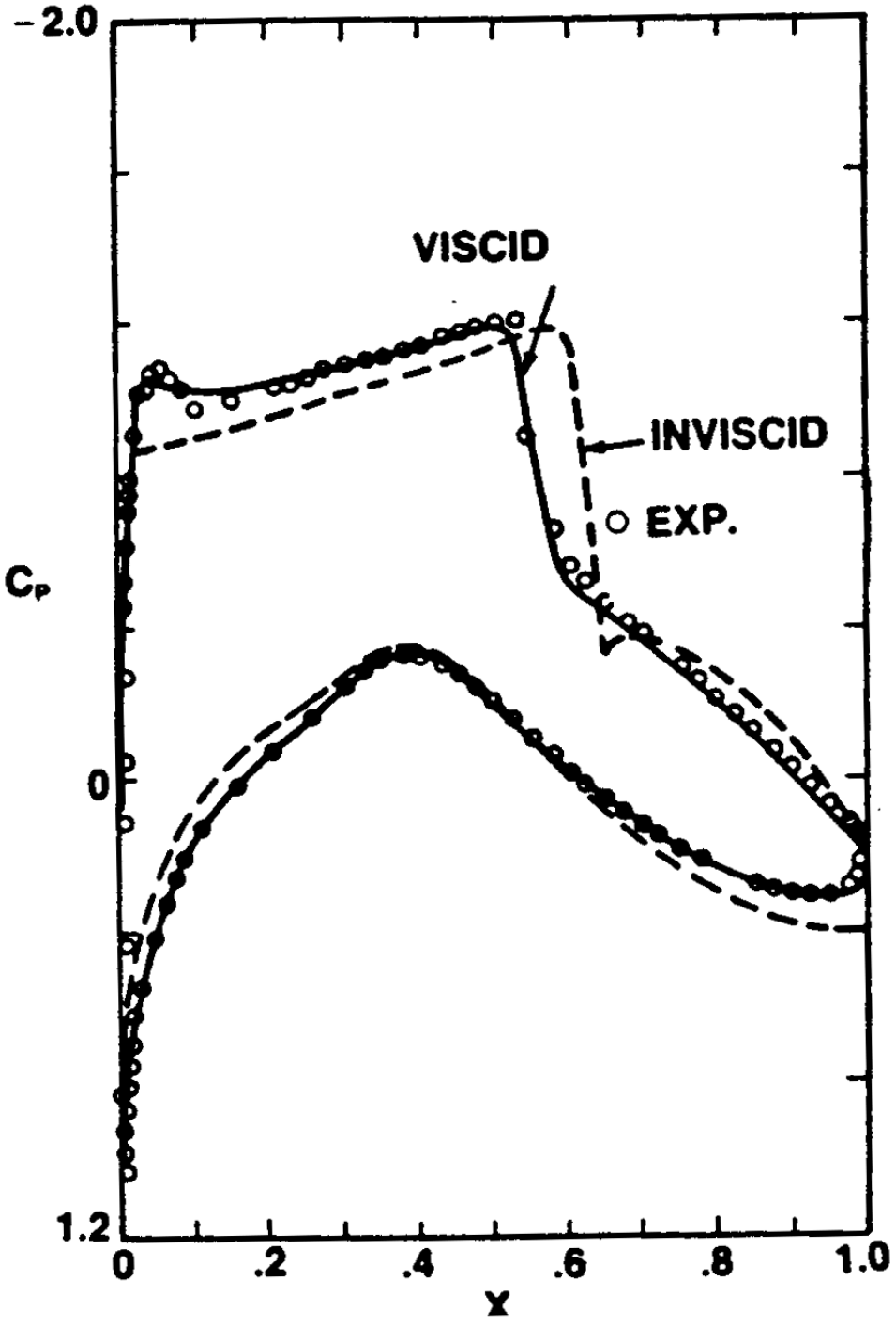

Figure 6.2: Comparisons Between the Viscid and Inviscid Solutions and Experimental Data RAE 2822 Airfoil, Mach .725, CL .743

models have yet to be developed. Zonal methods also have the disadvantage that extensions to more general configurations require a separate asymptotic analysis of each component region, such as the corner between a wing and a nacelle pylon, with the result that they can become unmanageable as the complexity of the configuration is increased.

For these reasons a continuing body of research is directed at the global solution of the Reynolds averaged Navier Stokes equations. The hope is that it will be possible to develop a fairly universal method, which will be able to predict separated flows where the present zonal methods fail, in particular, separated flows that are two-dimensional and unsteady, and three-dimensional separated flows, both steady and unsteady. The present state of the art has been very thoroughly reviewed by Mehta and Lomax [1011. During the past decade the Navier Stokes equations have been the subject of exploratory investigations aimed at establishing the feasibility of their solution, but the methods so far developed have been too expensive to permit their use in a routine production mode.

The principal requirements for a satisfactory solution of the Reynolds averaged Navier Stokes equations are:

1. The reduction of the discretization errors to a level such that any numerically introduced dissipative terms are much smaller than the real viscous terms.

2. The closure of the equations by a turbulence model which accurately represents the turbulent stresses.

The problem of sufficiently reducing the numerical errors Is particularly severe in regions of strong interaction, such as the foot of a shock wave, where it may not be possible to attain a high order of accuracy in the difference approximation. The use of a fine enough mesh to overcome this problem has so far been impeded by a lack of powerful enough computers.

The development of the necessary numerical methods is already quite well advanced. The methods described in the previous section can generally be carried over to the Navier Stokes equations. MacCormack has extended both his explicit scheme and his new implicit scheme to the treatment of viscous flows [102, 85]. Diewert has used MacCormack's explicit scheme in his path-finding calculations of viscous flows over airfoils [103], and Shang and Hankey have recently used the same scheme to calculate the flow past a hypersonic cruiser [104]. Beam and Warming have also made a corresponding extension of their alternating direction implicit scheme to treat viscous flows [105].

Rapid developments in the speed and memory of computers are steadily improving the prospect of useful simulations of the Reynolds averaged Navier Stokes equations. In the opinion of Mehta and Lomax, the development of reliable turbulence models is now the crucial pacing item [101]. No single

turbulence model has been found which can be used in the simulation of a variety of flows. At the present time not much is known about the behaviour of turbulence in separated regions [106], and this has impeded the development of turbulence models for complex three-dimensional flows. It appears that near term improvements in the computational simulation of turbulent flow will probably depend heavily on experimental inputs and checks.

7 Conclusion

Quite satisfactory methods are now available for the prediction of steady transonic flows using either the potential flow equation or the Euler equations as a mathematical model.

With the advent of a new generation of computers it will be entirely feasible to calculate solutions of the Euler equations for a complete aircraft. A code to solve the Euler equations for wing-body-tail-fin combinations is already operational [56]. The kind of configuration which can be treated is illustrated in Figure 7.1. The Cray 2, for example, is projected to be at least six times faster than the Cray 1, and will have 256 million words of memory. When a Cray 1 is used to perform calculations with the four-stage scheme described in Section 5c, three-dimensional Euler solutions on a 25000 point mesh can be advanced 200 steps in 150 seconds. Assuming that the multigrid acceleration procedure described in Section 5e is introduced, 200 steps should be ample for convergence. Using a grid with one million points, it should therefore be possible to calculate a solution in 20 minutes or less with a Cray 2. One million grid points should be enough for a reasonably accurate representation of an airplane, and the corresponding memory requirement, of the order of 40 million words, would not tax the new machines.

We can also anticipate the routine calculation of unsteady flows for the determination of structural loads. Looking further ahead, we can see on the horizon the increasingly real possibility of simulating the flow past a complete aircraft with the Reynolds averaged Navier Stokes equations.

Acknowledgment

I have had invaluable help from my friends in preparing this paper. I am particularly indebted to Robert Melnik for discussions of the problems of viscous flow calculations, and to Tim Baker for his assistance in correcting the complete manuscript.

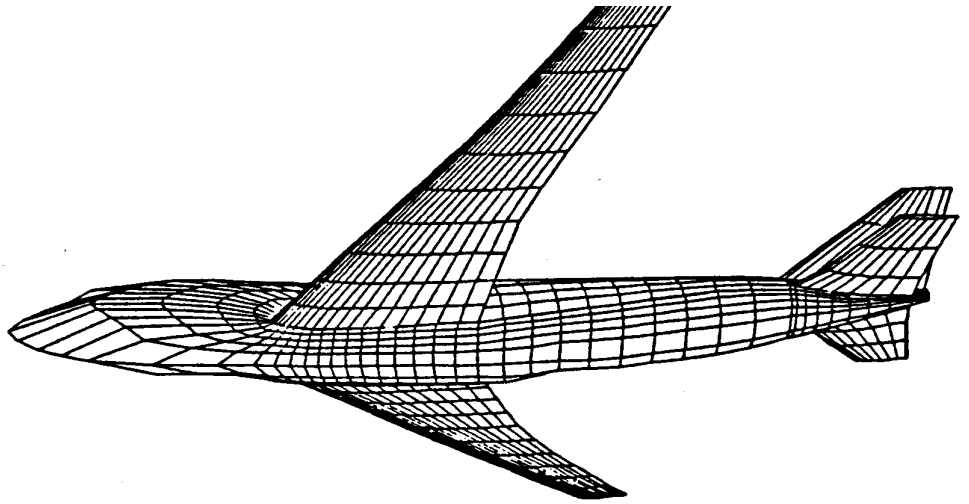

Figure 7.1: Transonic Glider

References

[1] Theodorsen, Theodore, "Theory of Wing Sections of Arbitrary Shape", NACA TR 411, 1931.

[2] Whitcomb, R. T., "A Study of the Zero Lift Drag-Rise Characteristics of Wing-Body Combinations Near the Speed of Sound", NACA TR 1273, 1956.

[3] Whitcomb, R. T., "Review of NASA Supercritical Airfoils", 9th ICAS Congress Haifa, Paper 74-10, 1974.

[4] Whitcomb, R. T., "A Design Approach and Selected Wind Tunnel Results at High Subsonic Speeds for Wing-Tip Mounted Winglets", NASA TN D8260, 1976.

[5] Morawetz, C.S., "On the Non-Existence of Continuous Transonic Flows Past Profiles", Comm. Pure. Appl. Math., 9, 1956, pp. 45-48.

[6] Chapman, D. R., "Computational Aerodynamics Development and Outlook", Dryden Lecture, 1979, AIAA Journal, 17, 1979, pp. 1293-1313.

[7] Hess, J. L. and Smith, A. M. 0., "Calculation of Non-Lifting Potential Flow About Arbitrary Three-Dimensional Bodies", Douglas Aircraft Report, ES 40622, 1962.

[8] Rubbert, P. E. and Saaris, G. R., "A general Three Dimensional Potential Flow Method Applied to V/STOL Aerodynamics, SAE Paper 680304, 1968.

[9] Hunt, B., "The Mathematical Basis and Numerical Principles of the Boundary Integral Method for Incompressible Potential Flow Over 3-D AerodynamicConfigurations", IMA Conference on Numerical Methods in Applied Fluid Dynamics, Reading, 1978, edited by B. Hunt, Academic Press, 1980, pp. 49-135.

[10] Murman, E. M. and Cole, J.D., "Calculation of Plane Steady Transonic Flows, AIAA Journal, 9, 1971, pp. 114-121.

[11] Jameson, Antony, "Iterative Solution of Transonic Flows Over Airfoils and Wings, Including Flows at Mach 1", Comm. Pure. Appl. Math, 27, 1974, pp. 283-309.

[12] Albone, C.M., "A Finite Difference Scheme for Computing Supercritical Flows in Arbitrary Coordinate Systems", RAE Report 74090, 1974.

[13] Murman, E.M., "Analysis of Embedded Shock Waves Calculated by Relaxation Methods," AIAA Journal, 12, 1974, pp. 626-633.

[14] Jameson, Antony, "Transonic Potential Flow Calculations in Conservation Form," Proc. AIAA 2nd Computational Fluid Dynamics Conference, Hartford, 1975, pp. 148-161.

[15] Eberle, A., "A Finite Volume Method for Calculating Transonic Potential Flow Around Wings from the Minimum Pressure Integral", NASA TM 75324, translated from MBB UFE 1407(0), 1978.

[16] Hafez, M., South, J.C. and Murman, E.M., "Artificial Compressibility Method for Numerical Solutions of Transonic Full Potential Equation", AIAA Journal, 17, 1979, pp. 838-844.

[17] Hoist, T. L. and Ballhaus, W. F., "Fast Conservative Schemes for the Full Potential Equation Applied to Transonic Flows", AIAA Journal, 17, 1979, pp. 145-152.

[18] Lock, R. C., "A Modification to the Method of Garabedian and Korn", ' Proc. GAMM Workshop on Numerical Methods for the Computation of Inviscid Transonic Flows with Shock Waves," Stockholm, 1979, edited by A. Rizzi and H. Viviand, Vieweg, 1981, pp. 116-124.

[19] Jameson, Antony, "Numerical Solution of the Nonlinear Partial Differential Equations of Mixed Type", Proc. SYNSPADE 1975, edited by B. Hubbard, Academic Press, 1976, pp. 275-320.

[20] Engquist, B. and Osher, S., "Stable and Entropy Satisfying Approximations for Transonic Flow Calculations", Math. Comp., 34, 1980, pp. 45-75.

[21] Goorjian, P., Meagher, M., and Van Buskirk, R., "Implicit Monotone Algorithms for the Small-Disturbance and Full Potential Equations Applied to Transonic Flows", AIAA Paper 83-0371, 1983.

[22] Jameson, Antony and Caughey, D. A., "A Finite Volume Method for Transonic Potential Flow Calculations", Proc. AIAA 3rd Computational Fluid Dynamics Conference, Albuquerque, 1977, pp. 35-54.

[23] Jameson, Antony, "Remarks on the Calculation of Transonic Potential Flow by a Finite Volume Method", Proc. IMA Conference on Numerical Methods in Applied Fluid Dynamics, Reading, 1978, edited by B. Hunt, Academic Press, 1980, pp. 363-386.

[24] Bristeau, M. 0., Pironneau, 0., Glowinski, R., Periaux, J., Perrier, P., and Poirier, G., "Application of Optimal Control and Finite Element Methods to the Calculation of Transonic Flows and Incompressible Viscous Flows," Proc. IMA Conference on Numerical Methods In Applied Fluid Dynamics, Reading, 1978, edited by B. Hunt, Academic Press, 1980, pp. 203-312.

[25] Bristeau, M. 0., Glowinski, R., Perlaux, J., Perrier, P., Pironneau, 0., and Poirier, G., "Transonic Flow Simulations by Finite Elements and Least Squares Methods", Proc. of 3rd International Conference on Finite Elements in Flow Problems, Banff, 1980, Vol. 1, edited by D. H. Norrie, pp. 11-29.

[26] Ballhaus, W. F., Jameson, A., and Albert, J., "Implicit Approximate Factorization Schemes for Steady Transonic Flow Problems", AIAA Journal, 16, 1978, pp. 573-579.

[27] Hoist, T. L., and Thomas, S. D., "Numerical Solution of Transonic Wing Flow Fields", AIAA Paper 82-0105, 1982.

[28] Baker, T. J., "Approximate Factorization Methods", Proc. IMA Conference on Numerical Methods in Aeronautical Fluid Dynamics, Reading, 1981, edited by P. L. Roe, Academic Press, 1982, pp. 115-141.

[29] Fedorenko, R. P., "The Speed of Convergence of One Iterative Process", USSR Comp. Math. and Math. Phys., 4, 1964, pp. 227-235.

[30] South, J. C. and Brandt, A., "Application of a Multi-Level Grid Method to Transonic Flow Calculations", Proc. of Workshop on Transonic Flow Problems in Turbomachinery, Monterey, 1976, edited by T. C. Adamson and M. F. Platzer, Hemisphere, 1977, pp. 180-206.

[31] Hackbusch, W., "On the Multi-Grid Method Applied to Difference Equations", Computing, 20, 1978, pp. 291-306.

[32] Jameson, Antony, "Acceleration of Transonic Potential Flow Calculations on Arbitrary Meshes by the Multiple Grid Method", Proc. AIAA 4th Computational Fluid Dynamics Conference, Williamsburg, 1979, pp. 122-146.

[33] Caughey, D. A., "Multigrid Calculation of Three-Dimensional Transonic Potential Flows", AIAA Paper 83-0374, 1983.

[34] Lax, P. D., "Weak Solutions of Nonlinear Hyperbolic Equations and Their Numerical Computation," Comm. Pure Appl. Math., 7, 1954, pp. 159-193.

[35] Lax, P. D. and Richtmyer, R. D., "Survey of the Stability of Linear Finite Difference Equations", Comm. Pure. Appl. Math., 9, 1956, pp. 267-293.

[36] Lax, P. D. and Wendroff, B., "Systems of Conservation Laws", Comm. Pure Appl. Math., 13, 1960, pp. 217-237.

[37] Lax, P. D. and Wendroff, B., 'Difference Schemes for Hyperbolic Equations with High Order of Accuracy", Comm. Pure. Appl. Math., 17, 1964, pp. 381-398.

[38] Richtmyer, R. D., and Morton K. W., "Finite Difference Methods for Initial Value Problems", InterScience, 1967.

[39] Kreiss, H. 0., "Stability Theory of Difference Approximations for Mixed Initial Boundary Value Problems", I, Math. Comp., 22, 1968, pp. 703-714.

[40] Gustaffson, B., Kreiss, H. 0., and Sundstrom, A., "Stability Theory of Difference Approximations for Mixed Initial Boundary Value Problems", II, Math. Comp., 26, 1972, pp. 649-686.

[41] Gustaffson, B., "The Convergence Rate for Difference Approximations to Mixed Initial Boundary Value Problems", Math. Comp. 29, 1975, pp. 396-406.

[42] Gustaffson, B., and Oliger, J., "Stable Boundary Discretiziations for a Class of Time Discretization of ut = ADO ux", Uppsala University Computer Science Report 87, 1980.

[43] Engquist, B., and Majda, A., "Absorbing Boundary Conditions for the Numerical Simulation of Waves", Math. Comp., 31, 1977, pp. 629-651.

[44] Bayliss, A., and Turkel, E., "Far Field Boundary Conditions for Compressible Flows", Proc. Symposium on Numerical Boundary Condition Procedures, NASA CP 2201, 1981.

[45] Moretti, Gino, "Calculations of Three Dimensional Inviscid Supersonic Flows", NASA CR 3573, 1982.

[46] Arlinger, B. G., "Computation of Supersonic Flow Around Three Dimensional Wings", Proc. 13th ICAS Congress, Seattle, 1982, Vol. 2, pp. 224-232.

[47] Veuillot, J. P., and Viviand, H., "Methodes Pseudo-Instationnaire pour le Calcul d'Ecoulements Transsoniques", ONERA Publication 1978-4, 1978.

[48] Jameson, Antony, "Transonic Aerofoil Calculations Using the Euler Equations", Proc. IMA Conference on Numerical Methods in Aeronautical Fluid Dynamics, Reading, 1981, edited by P. L. Roe, Academic Press, 1982, pp. 289-308.

[49] MacCormack, R. W., "The Effect of Viscosity in Hyper-Velocity Impact Cratering", AIAA Paper 69-354, 1969.

[50] MacCormack, R. W. and Paullay, A. J., "Computational Efficiency Achieved by Time Splitting of Finite Difference Operators", AIAA Paper 72-154, 1972.

[51] MacCormack, R. W. and Paullay, A. J., "The Influence of the Computational Mesh on Accuracy for Initial Value Problems with Discontinuous or Nonunique Solutions", Computers and Fluids, 2, 1974, pp. 339-360.

[52] Rizzi, A. W. and Schmidt, W., "Finite Volume Method for Rotational Transonic Flow Problems", Proc. 2nd GAMM Conference on Numerical Methods in Fluid Mechanics, edited by E. H. Hirschel and W. Geller, GAMM, 1977, pp. 152-161.

[53] Lerat, A. and Sides, J., "A New Finite Volume Method for the Euler Equations with Applications to Transonic Flows", Proc. IMA Conference on Numerical Methods in Aeronautical Fluid Dynamics, Reading, 1981, edited by P. L. Roe, Academic Press, 1982, pp. 245-288.

[54] Jameson, A., Schmidt, W., and Turkel, E., "Numerical Solution of the Euler Equations by Finite Volume Methods Using Runge-Kutta Time Stepping Schemes", AIAA Paper 81-1259, 1981.

[55] Schmidt, W., and Jameson, A., "Recent Developments in Finite Volume Time Dependent Techniques for Two and Three Dimensional Transonic Flows", Von Karman Institute Lecture Series 1982-04, 1982.

[56] Jameson, Antony, and Baker, Timothy J., "Solution of the Euler Equations for Complex Configurations", Proc. AIAA 6th Computational Fluid Dynamics Conference, Danvers, 1983, pp. 293-302.

[57] Courant, R., Isaacson, E., and Rees, M., "On the Solution of Nonlinear Hyperbolic Differential Equations", Comm. Pure. Appl. Math., 5, 1952, pp. 243-255.

[58] Steger, J. L., and Warming, R. F., "Flux Vector Splitting of the Inviscid Gas Dynamics Equations with Applications to Finite Difference Methods," J. Comp. Phys., 40, 1981, pp. 263-293.

[59] Lax, P. D., "Hyperbolic Systems of Conservation Laws and the Mathematical Theory of Shock Waves", SIAM Regional Series on Applied Mathematics, 11, 1973.

[60] Jameson, Antony, and Lax, Peter, D., "Conditions for the Construction of Multi-point Total Variation Diminishing Difference Schemes", Princeton University Report MAE 1650, 1984.

[61] Osher, S., "Riemann Solvers, The Entropy Condition, and Difference Approximations", To appear in SIAM Journal on Numerical Analysis.

[62] Harten, A., Hyman, J. M., Lax, P. D., and Keyfitz, B., "On Finite Difference Approximations and Entropy Conditions for Shocks", Comm. Pure Appl. Math., 29, 1976, pp. 297-322.

[63] Harten, A., "High Resolution Schemes for Hyperbolic Conservation Laws", New York University Report DOE/ER 03077-175, 1982.

[64] Roe, P. L., "Some Contributions to the Modelling of Discontinous Flows", Proc. AMS/SIAM Summer Seminar on Large Scale Computation in Fluid Mechanics, San Diego, 1983.

[65] Sweby, P. K., "High Resolution Schemes Using Flux Limiters for Hyperbolic Conservation Laws", to appear in J. Computational Physics.

[66] Osher, Stanley and Chakravarthy, Sukumar, "High Resolution Schemes and the Entropy Condition", ICASE Report NASA CR 172218.

[67] Boris, J. P., and Book, D. L., "Flux Corrected Transport, 1 SHASTA, A Fluid Transport Algorithm that Works", J. Computational Physics, 11, 1973, pp. 38-69.

[68] Zalesak, S. "Fully Multidimensional Flux Corrected Transport Algorithm for Fluids", J. Computational Physics, 31, 1979, pp. 335-362.

[69] van Leer, B., "Towards the Ultimate Conservative Difference Scheme. II Monotonicity and Conservation Combined in a Second Order Scheme," J. Computational Physics, 14, 1974, pp. 361-370.

[70] Goodman, J. B. and Leveque, R. J., "On the Accuracy of Stable Schemes for 2-D Scalar Conservation Laws", to appear in Math. Comp.

[71] van Leer, B., Flux Vector Splitting for the Euler Equations", Proc. 8th International Conference on Numerical Methods in Fluid Dynamics Aachen, 1982, edited by E. Krause, Springer, 1982, pp. 507-512.

[72] Godunov, S. K., "A Difference Method for the Numerical Calculation of Discontinous Solutions of Hydrodynamic Equations", Mat. Sbornik, 47, 1959, pp. 271-306, translated as JPRS 7225 by U.S. Dept. of Commerce, 1960.

[73] Roe, P. L., "The Use of the Riemann Problem in Finite Difference Schemes", Proc. 7th International Conference on Numerical Methods in Fluid Dynamics, Stanford 1980, edited by W. C. Reynolds and R. W. MacCormack, Springer, 1981, pp. 354-359.

[74] Roe, P. L., "Approximate Riemann Solvers, Parameter Vectors, and Difference Schemes", J. Computational Physics, 43, 1981, pp. 357-372.

[75] Van der Houwen, "Construction of Integration Formulas for Initial Value Problems", North Holland, 1977.

[76] Sonneveld, P., and van Leer, B., "Towards the Solution of Van der Houwen's Problems". To appear in Nieuw Archief voor Wiskunde.

[77] Roe, P. L., and Pike, J., "Restructuring Jameson's Finite Volume Scheme foi the Euler Equations", RAE Report, 1983.

[78] Beam, R. W., and Warming, R. F., "An Implicit Finite Difference Algorithm for Hyperbolic System in Conservation Form", J. Comp. Phys., 23, 1976, pp. 87-110.

[79] Rizzi, A., and Skollermo, G., "Semi-Direct Solution to Steady Transonic Flow by Newton's Method", Proc. 7th International Conference on Numerical Methods in Fluid Dynamics, Stanford, 1980, edited by W. C. Reynolds and R. W. MacCormack, Springer, 1981, pp. 349-353.

[80] Gourlay, A. R., and Mitchell, A. R., "A Stable Implicit Difference Method for Hyperbolic Systems In Two Space Variables", Numer. Math., 8, 1966, pp. 367-375.

[81] Briley, W. R. and MacDonald, H., "Solution of the Three Dimensional Compressible Navier-Stokes Equations by an Implicit Technique", Proc. 4th International Conference on Numerical Methods in Fluid Dynamics, 1974.

[82] Pulliam, T. H., and Steger, J. L., "Implicit Finite Difference Simulations of Three-Dimensional Compressible Flow", AIAA Journal, 18, 1980, pp. 159-167.

[83] Jameson, Antony, and Turkel, E., "Implicit Schemes and LU Decompositions", Math, Comp. 37, 1981, pp. 385-397.

[84] Buratynski, E. K., "A Lower-Upper Factored Implicit Scheme for the Numerical Solution of the Euler Equations Applied to Arbiratry Cascades", Cornell University Thesis, 1983.

[85] MacCormack, R. W., "A Numerical Method for Solving the Equations of Compressible Viscous Flows", AIAA Paper 81-110, 1981.

[86] Lerat, A, Sides, J., and Daru, V., "An Implicit Finite Volume Scheme for Solving the Euler Equations", Proc. 8th International Conference on Numerical Methods in Fluid Dynamics, Aachen, 1982, edited by E. Krause, Springer, 1982, pp. 343-349.

[87] Ni, R. H., "A Multiple Grid Scheme for Solving the Euler Equations", Proc. AIAA 5th Computational Fluid Dynamics Conference, Palo Alto, 1981, pp. 257-264.

[88] Jameson, Antony, "Solution of the Euler Equations by a Multigrid Method", Applied Mathematics and Computation, 13, 1983, pp. 327-356.

[89] Bauer, F., Garabedian, P., Korn, D., and Jameson, A., "Supercritical Wing Sections II, Springer, 1975.

[90] Lock, R. C. and Firmin, M. C. P., "Survey of Techniques for Estimating Viscous Effects in External Aerodynamics", Proc. IMA Conference on Numerical Methods in Aeronautical Fluid Dynamics, Reading, 1980, edited by P. L. Roe, Academic Press, 1982, pp. 337-430.

[91] Le Balleur, J. C., "Numerical Viscid-Inviscid Interaction in Steady and Unsteady Flows", Proc. 2nd Symposium on Numerical and Physical Aspects of Aerodynamic Flows, Long Beach, 1983.

[92] Melnik, R. E., "Turbulent Interactions on Airfoils at Transonic Speeds - Recent Developments", Proc. AGARD Conference on Computation of ViscousInviscid Interactions, Colorado Springs, 1980, AGARD CP 291, Paper No. 10.

[93] Lighthill, M. J., "On Displacement Thickness", J. Fluid Mechanics, 4, 1958, pp. 383-392.

[94] Johnston, W., and Sockol, P., "Matching Procedure for Viscous Inviscid Interactive Calculations", AIAA Journal, 17, 1979, pp. 661-663.

[95] Carter, J. E., "A New Boundary Layer Inviscid Iteration Technique for Separated Flow", Proc. AIAA 4th Computational Fluid Dynamics Conference, Williamsburg, 1979, pp. 45-55.

[96] Le Balleur, J. C. Peyret, R., and Viviand, H., "Numerical Studies in High Reynolds Number Aerodynamics", Computers and Fluids, 8, 1980, pp. 1-30.

[97] Collyer, M. R., and Lock, R. C., "Prediction of Viscous Effects in Steady Transonic Flow Past an Aerofoil", Aeronautical Quarterly, 30, 1979, pp. 485-505.

[98] Le Balleur, J. C., "Strong Matching Methods for Computing Transonic Viscous Flow Including Wakes and Separations - Lifting Airfoils, La Recherche Aerospatiale, 3, 1981.

[99] Melnik, R. E., Chow, R. R., Mead, H. R., and Jameson, A., "A Multgrid Method for the Computation of Viscid/Inviscid Interaction on Airfoils", AIAA Paper 83-0234, 1983.

[100] Whitfield, D. L., Thomas, J. L., Jameson, A., and Schmidt, W., "Computation of Transonic Viscous Inviscid Interacting Flow", Proc. 2nd Symposium on Numerical and Physical Aspects of Aerodynamic Flows, Long Beach, 1983.

[101] Mehta, Unmeel, and Lomax, Harvard, "Reynolds Averaged Navier Stokes Computations of Transonic Flow - the State of the Art", Proc. Transonic Perspectives Symposium, Moffett Field, 1979, edited by D. Nixon, AIAA, 1981, pp. 297-375.

[102] MacCormack, R. W., and Baldwin, B. S., "A Numerical Method for Solving the Navier Stokes Equations with Application to Shock Boundary Layer Interactions, " AIAA Paper 75-1, 1975.

[103] Deiwert, G. S., "Numerical Simulation on High Reynolds Number Transonic Flows,"AIAA Journal, 134, 1975, pp. 1354-1359.

[104] Shang, J. S., and Hankey, W. L., "Computation of Flow Past a Hypersonic Cruiser', Proc. 2nd Symposium on Numerical and Physical Aspects of Aerodynamic Flows, Long Beach, 1983.

[105] Beam, R., and Warming, R. F., "An Implicit Factored Scheme for the Compressible Navier Stokes Equations", AIAA Journal, 16, 1978, pp. 393-402.

[106] Bradshaw, P., "Structure of Turbulence in Complex Flows", AGARD LS 94, 1978.